

Metabolic dependencies of metastasis-initiating cells in breast cancer

Présentée le 13 octobre 2023

Faculté des sciences de la vie
Unité du Prof. Huelsken
Programme doctoral en approches moléculaires du vivant

pour l'obtention du grade de Docteur ès Sciences

par

Candice Megan T YOUNG

Acceptée sur proposition du jury

Prof. D. Constam, président du jury
Prof. J. Hülsken, directeur de thèse
Prof. N. Vannini, rapporteur
Prof. M. Knobloch, rapporteuse
Prof. D. Suter, rapporteur

ACKNOWLEDGEMENTS

There is simply no way for me to properly express in writing, how much gratitude and appreciation I have for the people who have helped me get through these few years, but I will try my best to do so here.

I, of course, first want to thank my advisor, Joerg, who (perhaps regrettably) accepted me and my ridiculousness to join his group. He taught me how to think like a scientist, he gave me the space and freedom to develop my project, and he gave me a little (a big) boost whenever things were going sideways. He was always there when I needed him, for both scientific and emotional support, and he always tried to never let my mediocrity get the best of me.

I want to then thank all of the new and old members of the lab. Angela, Lolo, Luisa, Mat, Maxim, and Paloma –it was always a pleasure coming to work even when experiments weren't cooperating, because they were all there to lighten the load. It was extremely fun to go through this PhD (almost in sync) with them and I can't imagine a better group of people to have gone on this journey with. Krishna, Laura, and Pablo, I'm thankful that they breathed new life into the lab. I only managed to finish what I needed to do because I could feed off of their energy. I also undoubtably want to thank Pierre and Fanny who saved my butt more times than I can count. Pierre not only took on some aspects of my project that I no longer had the mental capacity to deal with, but he also is a great life coach, and the number one reason why I still got to enjoy life outside of the lab, since he would show me all the best hiking routes in the area. Fanny also has always been super supportive and does not hesitate to offer her help for work, experiments, or simply surviving life here in Switzerland. I would not have managed to make it to the end without everyone's help and friendship.

I'm also thankful for all of the core facilities at EPFL (BIOP, FCCF, GECF, HCF, CPG) and AGORA (AIVC, CIF, FCF, IVIF, MEP, MPF) and the SIB for their expertise and patience in helping me do all the things that I couldn't have possibly done or even understood. I also want to thank my committee members, Profs. Constam,

Suter, Vannini, and Knobloch, for taking the time to evaluate and provide feedback on the presented work.

I want to express my gratitude to my friends since way back when, especially Jeanina and Cherie. It's been invaluable going through the same life stages with them despite being continents apart. They always know what to say to make me laugh and keep my head straight –I couldn't have asked for better lifelong friends.

I am also incredibly grateful for my family, as they have been a constant throughout everything I do. I am able to move from country to country and change the trajectory of my life fairly regularly because I know I have your confidence and your support, despite the distance. I want to especially thank my big sister, Ach, who has been my mentor, therapist, and cheerleader since forever. I only manage to do ok because I try to do as well as she does.

I want to thank my silly little girl, Lola, who hasn't been in my life for that long, but has certainly made it a whole lot brighter. Even if I think she only loves me for the food I provide, she always reminds me that no problem can't be solved with a little walk in the woods, a hike in the mountains, or the most bestest game, fetch.

Finally, I want to thank my life partner, Sébastien. I don't think there's any amount of appropriate vocabulary to encapsulate how much he's been there for me throughout this PhD --suffice to say I would not have come out of this as an almost fully functioning human being without him. He does so much to keep me going and most importantly, he makes me happy everyday even when I'm not.

ABSTRACT

Metastasis is the process by which cancer cells from the primary tumor travel through the blood stream to generate a secondary tumor site in a distant organ. Although very few cells are able to make this journey, the resulting effects are dire since most cancer fatalities are due to the presence of metastatic lesions. Therefore, understanding the mechanisms by which cells metastasize can help uncover vulnerabilities and facilitate the development of novel strategies for preventing and/or combatting metastatic cancer.

Here, we investigated the metabolic features of a rare population of plastic and stem-like cells in breast cancer called metastasis-initiating cells (MICs) that are highly efficient at colonizing distant organs. We found that endogenous MICs rely on mitochondrial metabolism, specifically the tricarboxylic acid cycle (TCA) and fatty acid usage. Sorting tumors cells based solely on mitochondrial activity or levels of neutral lipid stores is sufficient at identifying MICs. We determined that in MICs, the TCA cycle is important for generating citrate that is then exported out to the cytoplasm for the regeneration of acetyl-CoA and subsequent acetylation of H3K27. Blocking acetyl-CoA generating metabolic pathways and readers of H3K27ac reduced expression of epithelial-to-mesenchymal related genes, MIC frequency, and metastatic capacity. In contrast, supplying an exogenous source of acetyl-CoA, reverses these effects. In breast cancer patient cohorts, we also observe a correlation between heightened expression of our MIC-derived metabolic signature and acetyl-CoA generating enzymes with distant relapse-free survival or overall survival. These suggest that there is a complex interplay between metabolism and epigenetics that induces and maintains a pro-metastatic phenotype in breast cancer cells.

Metastasis is a systemic disease that arises from the confluence of optimally balanced multimodal inputs. It is therefore no surprise, that current efforts to target late-stage metastatic cancers with monotherapies leave much to be desired. It may therefore be worthwhile to determine an ideal synergistic combination of therapies that targets several MIC-dependencies simultaneously to effectively prevent or

eradicate metastatic disease and lower the chances of compensatory resistance mechanisms, while reducing the likelihood of toxic adverse effects.

Keywords

cancer, metastasis, metastasis-initiating cells, metabolism, epigenetics, acetyl-coa, breast cancer, histones, epithelial to mesenchymal transition, plasticity

ABSTRACT – FRENCH

Une métastase est le processus par lequel les cellules cancéreuses d'une tumeur primaire se déplacent à travers le système sanguin pour former un site de tumeur secondaire dans un organe distant. Même si très peu de ces cellules sont capables de réaliser ce voyage, les effets qui en résultent sont graves, car la plupart des décès dus au cancer sont causés par la présence de lésions métastatiques. Par conséquent, la compréhension des mécanismes de formation de métastase aide à identifier les vulnérabilités et faciliter le développement de nouvelles stratégies pour prévenir et/ou combattre les cancers métastatiques.

Dans cette étude, nous avons examiné les caractéristiques métaboliques d'une population rare de cellules plastiques. Celles-ci sont semblables à des cellules souches du cancer du sein, appelées cellules initiatrices de métastases (CIM), qui sont très efficaces pour coloniser des organes éloignés. Nous avons découvert que les CIM endogènes dépendent du métabolisme mitochondrial, en particulier du cycle de l'acide tricarboxylique (CAT) et de l'utilisation des acides gras. Le tri des cellules tumorales uniquement en fonction de leur activité mitochondriale ou de leurs réserves de lipides neutres permet d'identifier ces CIM. Nous avons déterminé que chez ces CIM, le CAT est important pour générer du citrate qui est ensuite exporté vers le cytoplasme pour régénérer de l'acétyl-CoA et ultérieurement acétyler H3K27. Le blocage des voies métaboliques génératrices d'acétyl-CoA et des lecteurs de H3K27ac réduit l'expression des gènes associés à la transition épithélium-mésenchymateuse, la fréquence des CIM, et leur capacité métastatique. En revanche, l'apport d'une source exogène d'acétyl-CoA inverse ces effets. Dans les cohortes de patients atteints de cancer du sein, nous observons également une corrélation entre l'expression accrue de notre signature métabolique dérivée des CIM et les enzymes génératrices d'acétyl-CoA, avec la survie sans rechute à long terme ou la survie. Cela suggère qu'il existe une interaction complexe entre le métabolisme et l'épigénétique qui induit et maintient un phénotype pro-métastatique chez les cellules cancéreuses du sein.

La formation de métastase qui résulte de la convergence d'entrées multimodales parfaitement équilibrées, est une maladie systémique. Il n'est donc pas surprenant

que les efforts actuels pour cibler les cancers métastatiques à un stade avancé avec des monothérapies sont peu efficaces. Il serait donc intéressant de déterminer une combinaison synergique idéale de thérapies qui ciblent simultanément plusieurs dépendances des CIM afin de prévenir efficacement la formation ou d'éliminer les métastases et de réduire les chances de mécanismes de résistance compensatoires, tout en diminuant la probabilité d'effets indésirables toxiques.

Mots Clés

cancer, métastase, cellules initiatrices de métastases, métabolisme, épigénétique, acétyl-CoA, cancer du sein, histones, transition épithéliale-mésenchymateuse, plasticité

ABBREVIATIONS

α KG – α -ketoglutarate
2HC – 2-hydroxyglutarate
ATP – adenosine triphosphate
BOHB – β -hydroxybutyrate
CR – caloric restriction
CCLE – cancer cell line encyclopedia
ECAR – extracellular acidification rate
ECM – extracellular matrix
EMT – epithelial to mesenchymal transition
ER – estrogen receptor
ETC – electron transport chain
FAO – fatty acid oxidation
FMD – fasting-mimicking diet
GEMM – genetically engineered mouse model
GFP – green fluorescent protein
HAT – histone acetyltransferase
HDAC – histone deacetylase
HER2 – human epidermal growth factor receptor 2
HFD – high fat diet
HMT – histone methyltransferase
KD – knockdown
LCFA – long chain fatty acid
LFD – low fat diet
MaSCs – mammary stem cells
MET – mesenchymal to epithelial transition
MIC – metastasis-initiating cell
MMP – mitochondrial membrane potential
NAM – nicotinamide
OCR – oxygen consumption rate
OS – overall survival
OXPHOS – oxidative phosphorylation
pEMT – partial epithelial to mesenchymal transition

PPP – pentose phosphate pathway
PR – progesterone receptor
PTM – post-translational modification
PyMT – MMTV-Polyoma Middle T
RFS – relapse-free survival
ROS – reactive oxygen species
SAH - s-adenosylhomocysteine
SAM - s-adenosylmethionine
TCA – tricarboxylic acid
TF – transcription factor
TNBC – triple negative breast cancer
TVI – tail vein injection

TABLE OF CONTENTS

ACKNOWLEDGEMENTS	2
ABSTRACT	4
Keywords	5
ABSTRACT – FRENCH	6
Mots Clés	7
ABBREVIATIONS	8
TABLE OF CONTENTS	10
FIGURES & TABLES	13
Figure List	13
Table List	13
Supplementary Figure List	14
Supplementary Table List	14
INTRODUCTION	15
Cancer Metastasis	15
I.I Metastatic Disease	15
I.II The Metastatic Cascade	16
I.III Metastasis-Initiating Cells	17
I.III.i Key Features of MICs	18
I.III.ii Origins of MICs	21
I.III.iii. Methods to Assay for and Identify MICs	22
A Primer on Epigenetics	26
Cancer Metabolism	30
III.I Metabolism during the Metastatic Cascade	32
III.II Influence of Metabolism over Cellular Phenotypes	33
Breast Cancer	37
OBJECTIVES OF THE RESEARCH	39
RESULTS – PRESENTED AS A MANUSCRIPT	40
Abstract	42
Introduction	42
Results	44
Metastasis-initiating cells show increased mitochondrial activity	44
Metastasis initiating cells are dependent on enhanced fatty acid flux and usage	49

Modulating acetyl-CoA generation and availability alters metastatic capacity	56
MICs show enhanced requirement for acetyl-CoA supply to control histone acetylation	60
Increased acetylation on H3K27 induces expression of genes for epithelial-to-mesenchymal transition	64
Human breast cancer cell lines exhibit a similar dependence on mitochondrial activity and acetyl-CoA for metastasis	69
Additional Results	75
Discussion	77
Conflict of Interest	81
Acknowledgements	81
BRIEF SUMMARY OF RESULTS	82
Addressing Aim 1: Identifying metabolic dependencies of MICs	82
Addressing Aim 2: How MIC metabolism contributes to MIC function	83
Addressing Aim 3: Confirmation in human models	83
DISCUSSION & OUTLOOK	84
Current state of related metabolic and epigenetic therapies	89
CONCLUSION	95
SUPPLEMENTARY DATA	96
EXPERIMENTAL PROCEDURES	110
Mice	110
Cell lines	110
Tumor cell isolation from spontaneous PyMT tumors	110
In vitro treatments	111
Flow Cytometry	111
Seahorse Assays	113
Proliferation Assay	113
Metabolomics Measurements	114
Western Blotting	114
RNA Isolation and Sequencing	115
Real time qPCR	116
Lentivirus Production for miR-mediated KDs	118
ChIP-Seq	118
Lipid Droplet Measurements	119
Experimental Metastasis Assay	120

Orthotopic Experiments _____	120
CCL4 Dataset Analysis _____	121
Kaplan-Meier _____	121
Statistical Analysis and Data Availability _____	121
REFERENCES _____	122
CURRICULUM VITAE _____	147

FIGURES & TABLES

Figure List

Fig. 1: The metastatic cascade.	17
Fig. 2: Spectrum of phenotypes across the epithelial to mesenchymal transition. ...	19
Fig. 3: Some example methods used to assay for MIC activity in vivo.	24
Fig. 4: Sites on histone tails that can be methylated, acetylated, or phosphorylated.	27
Fig. 5: Metabolic contributions to aspects of cell physiology outside of bioenergetics, focusing on the major fuel sources, glucose, glutamine, and fatty acids.	31
Fig. 6: The contribution of metabolic pathways to histone methylation and acetylation.	35
Fig. 7: Activity modulation of epigenetic modifiers by metabolite availability.	36
Fig. 8: Heightened mitochondrial activity is a key feature of MICs.	47
Fig. 9: MICs rely on fatty acid turnover and usage.	53
Fig. 10: MICs rely on pathways that generate acetyl-CoA.	57
Fig. 11: Metabolism supports histone acetylation to facilitate metastatic capacity in MICs.	63
Fig. 12: Metabolism-induced histone acetylation enables expression of EMT-related genes.	67
Fig. 13: Metabolic dependencies for mitochondrial activity and acetyl-CoA define metastatic activity in human breast cancer cell lines.	72
Fig. 14: Canonical vs. non-canonical TCA cycle adapted from Arnold et al. (2022) ²⁶⁶	86
Fig. 15: Acetyl-CoA at the nexus of vital cellular processes.	90

Table List

Table 1: Non-exhaustive list of identified endogenous MICs in primary human specimens and autochthonous mouse models.	25
Table 2: Common epigenetic modifications and their associated transcriptional output.	28

Supplementary Figure List

Supplementary Fig. 1: MICs have heightened mitochondrial activity 49

Supplementary Fig. 2: MICs specifically rely on fatty acid usage for metastasis and not for proliferation 54

Supplementary Fig. 3: MICs have enhanced lipid droplet dynamics 56

Supplementary Fig. 4: Dependence on acetyl-CoA generation pathways are not due to ATP or proliferation 60

Supplementary Fig. 5: Blocking acetyl-CoA generation and writing and reading of H3K27ac reduces metastasis without affecting proliferative capacity 63

Supplementary Fig. 6: Additional data showing increased EMT gene expression mediated by acetyl-CoA generating pathways and histone acetylation..... 67

Supplementary Fig. 7: Similar dependence on mitochondrial activity and acetyl-CoA generation in human cell lines and patient cohorts..... 74

Supplementary Fig. 8:..... 76

Supplementary Table List

Supplementary Table 1:..... 96

Supplementary Table 2:..... 104

Supplementary Table 3:..... 106

INTRODUCTION

Cancer Metastasis

1.1 Metastatic Disease

The main cause of cancer mortality is metastatic disease, where cells from the primary tumor have spread and grown into new tumors in distant organs. These metastatic nodules disrupt the homeostatic functions of the tissues and organs in which they reside causing the interruption of vital physiological processes such as breathing and digestion. Patients that are diagnosed at a late stage, where metastatic disease is present, can have up to a 9-fold reduction in 5-year survival rate in comparison to those that are diagnosed at an early stage, where the cancer is still localized to the tissue-of-origin¹.

In the last 10 years, survival rates for those diagnosed at a late stage have seen only modest improvements, such as in breast cancer, where the 5-year survival rate increased just 20% (23.3% to 30.6%) from 2004 to 2014¹. Recent estimates have even predicted that the incidence of metastatic disease will increase in the coming years, particularly for those cancers originating from the esophagus, pancreas, kidney, skin, and breast². Although late stage metastatic disease can be treated, the majority of treatments only combat comorbid symptoms and improve quality of life^{3,4}. In other words, there is currently little that can be done to substantially increase life expectancy and cure metastatic disease. It is therefore of value to better elucidate the mechanisms of metastasis and uncover actionable vulnerabilities to both prevent and target metastatic cancers.

I.II The Metastatic Cascade

For metastasis to form, cells from the primary tumor must pass through a rigorous selection process and successfully complete a series of steps to colonize a distant organ –this is called the metastatic cascade^{5,6} (**Fig. 1**):

- 1) Invasion– Cells invade through the local stroma by firstly becoming more motile, where they adopt a more mesenchymal or amoeboid⁷ phenotype by rearranging their cytoskeleton and expressing adhesive proteins on their surface that allow them to migrate⁸. They also secrete extracellular matrix (ECM) remodelling proteins that enable them to either loosen up the stroma⁹ and/or rearrange the ECM to induce migration¹⁰ and create linear and directional “highways” towards the blood vessels¹¹.
- 2) Intravasation—Cells must then interact with^{12,13} endothelial cells to cross¹⁴ and/or enzymatically disrupt¹⁵ the endothelial cell barrier that makes up the blood vessels to enter the blood stream. Alternatively, cells can also intravasate through existing avenues created by immune cells¹⁶.
- 3) Survival in Circulation—In circulation, cells have to survive low attachment conditions¹⁷, withstand shear forces^{18,19}, counteract the induction of increased reactive oxygen species (ROS)^{20,21}, and avoid immune recognition and attack²².
- 4) Extravasation—Circulating tumor cells eventually become trapped in certain capillary beds which is largely dictated by blood circulation patterns²³, remain and survive there²⁴, or extravasate (cross the endothelial cell wall again) and reside in the destination tissue close to the luminal wall^{25–28}.
- 5) Outgrowth and Colonization—Finally, cells must continue to survive at this foreign site^{29,30}, avoid immune recognition and attack^{31–33}, reverse their mesenchymal phenotype^{34,35}, and create a secondary niche that is conducive for growth and proliferation^{36,37}.

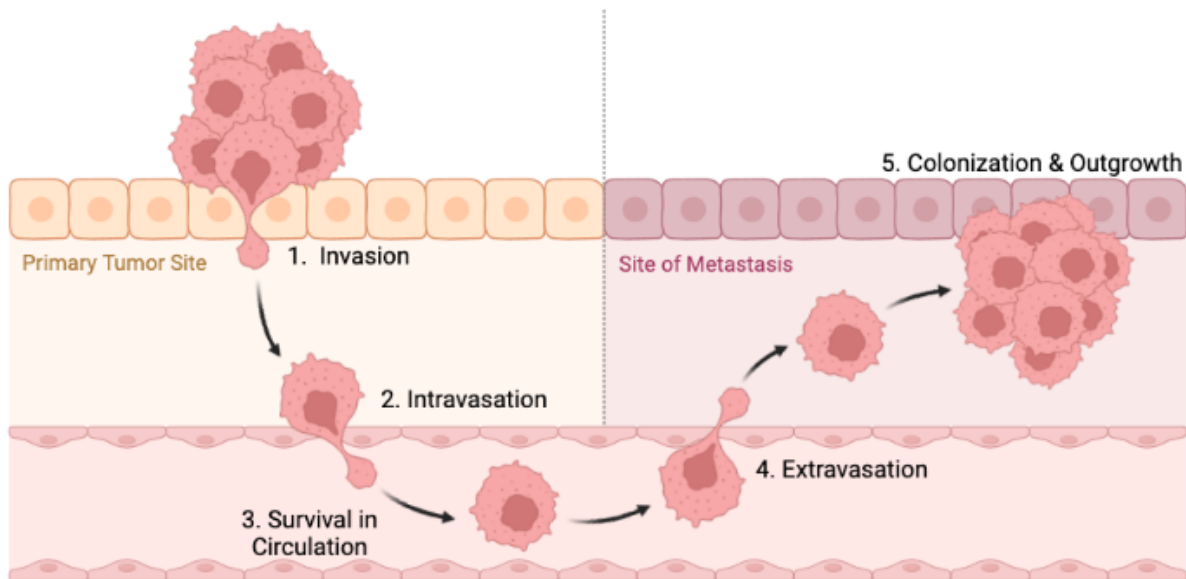


Fig. 1: The metastatic cascade.

Cells must successfully invade through the basement membrane, intravasate into the blood vessels, survive in circulation, exit the blood vessels, and seed and proliferate at a distant site to form metastasis. Figure was created in BioRender.com.

Completion of all the steps of the metastatic cascade is a highly inefficient process, as it requires precise orchestration of multiple cellular processes that can often be opposing. While this presents multiple opportunities to intervene and cease metastatic spread, it is estimated that less than 0.02% of cancer cells that leave the primary tumor are able to colonize distant organs^{38,39}. It is therefore crucial to identify and characterize these rare cells that have the unique capacity to complete the metastatic cascade for the development of novel targeted therapies and treatment regimens.

I.III Metastasis-Initiating Cells

Metastasis-initiating cells (MICs) are a rare population of cells within the heterogenous tumor mass that have a high propensity to seed and colonize distant organs. They are highly metastatic due to their stem-like and plastic phenotype that enables efficient and dynamic morphological and cellular changes to adapt to the varied challenges of the metastatic cascade.

I.III.i Key Features of MICs

Plasticity in normal stem cells connotes the ability of a cell to alter its phenotype and move up and down the differentiation hierarchy, for example, from stem cell to differentiated cell to stem cell⁴⁰. In metastatic cancer, it connotes the ability of MICs to shape-shift into advantageous phenotypes for survival, proliferation, and dissemination. One of the more prominent manifestations of MIC plasticity is the ability to undergo the epithelial to mesenchymal transition (EMT). EMT is a biological process whereby cells with an epithelial phenotype lose their cell-cell junctions, alter their cytoskeletal architecture to become more fibroblastic and motile, switch from an apical-basal polarity to a front-back polarity, increase expression of ECM adhesion proteins to assist with migration, and initiate the secretion of ECM remodelling enzymes for migration and invasion⁴¹. In non-cancer settings, EMT (and its reverse process, the mesenchymal to epithelial transition, MET) occurs during development and wound healing, where cells can undergo several rounds of EMT and MET to (re)generate specialized epithelial tissues⁴². In the cancer setting, EMT is co-opted not only to facilitate migration and invasion, but also to endow tumor cells with stem-like characteristics that increase their tumorigenicity⁴³, resistance to therapy^{44–46}, and immune suppression^{47,48}.

In recent years, it has become evident that MICs do not undergo EMT or MET to adopt a binary epithelial or mesenchymal phenotype, rather, they take on varying degrees of epithelial and mesenchymal features that fall along a partial EMT (pEMT) spectrum^{44,49,50} (**Fig. 2**). Several studies show that only cells in pEMT are able to metastasize efficiently, having up to 5-fold increase in metastatic capacity in comparison to their parental line^{44,49–51}. Partial EMT MICs are highly plastic, enabling the regeneration of a heterogenous tumor mass that can likely easily adapt to changing environments^{51,52}. The retention of both epithelial and mesenchymal features also enables the maintenance of cell-cell contacts as they disseminate and undergo collective migration to seed in clusters^{44,50,52}, which has been shown to increase metastatic potential up to 50-fold¹⁷. If tumor cells are prevented from assuming this pEMT state, the number of resulting metastases are significantly reduced⁴⁴. Lastly, features associated with pEMT, such as gene signatures⁵⁰ and heterogeneity scores⁵¹, predict poorer patient outcomes.

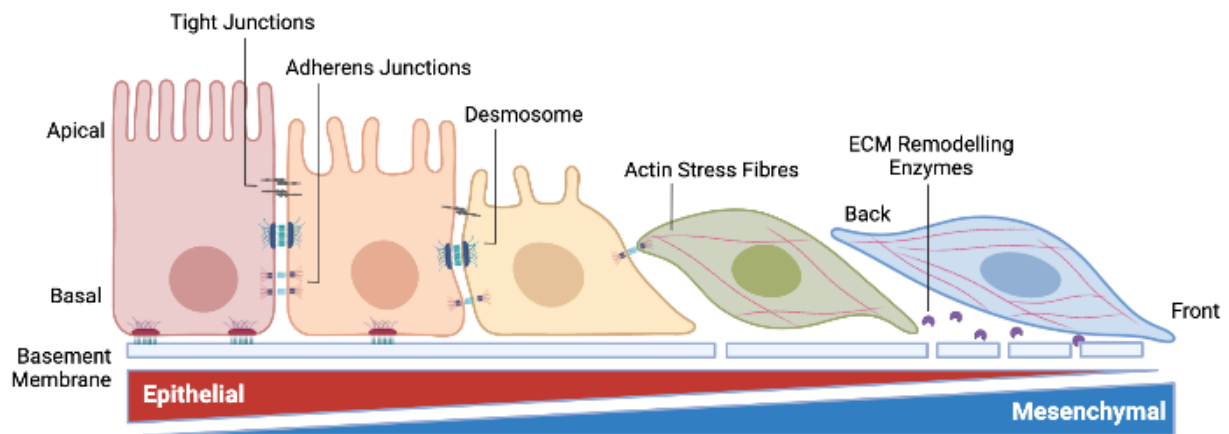


Fig. 2: Spectrum of phenotypes across the epithelial to mesenchymal transition. Epithelial cells express tight junctions, adherens junctions, and desmosomes to create an apical-basal polarity and enable cell-cell contacts that generate an epithelial barrier. They are also tethered to the basement membrane by hemidesmosomes. As they become more mesenchymal, these junctions and desmosomes are lost and cells start to reorganize their cytoskeleton and express contractile actin fibres for motility and to adapt a front-back polarity. Cells also start to secrete ECM remodelling proteins for invasion into the stroma and eventual escape from the primary tumor. Adapted from Dongre & Weinberg (2018)⁵³. Figure was created in BioRender.com.

Hand-in-hand with plasticity is stemness. Stemness is a term used to describe the ability of normal stem cells to self-renew or generate the whole spectrum of differentiated progeny. In metastatic cancer, it is also used to describe the ability of MICs to withstand environmental stressors and proliferate/survive independently from their original niche. Prior to or during arrival at a distant site, MICs must create new environments that are suitable for their outgrowth. This so-called (pre-)metastatic niche is important for anchorage, survival, protection, and proliferation⁵⁴. Tumor derived factors have been shown to alter the distant site by remodelling the ECM⁵⁵, inducing a leaky vasculature⁵⁶, and facilitate the activation³⁷ and accumulation³⁶ of pro-survival and pro-proliferative growth factors. One example is that melanoma and rhabdosarcoma cells cause perivascular cells to produce increased fibronectin that facilitates MIC anchorage, extravasation, and proliferation⁵⁷. Another example from work in our lab has shown that breast cancer MICs both express and induce the expression of the stromal ECM protein, POSTN, in the lungs to act as an anchor for WNT ligands³⁶, which are evolutionarily conserved signals that are essential for proper development and stem cell activity⁵⁸.

Abolishment of POSTN expression does not alter normal mammary gland development or tumor initiation, but only affects metastatic seeding³⁶.

MICs must then be able to self-renew and regenerate what is essentially a new tumor. These properties are, again, reminiscent of both embryonic and normal adult stem cells. Mammary stem cells (MaSCs), for example, are responsible for the generation of all of the differentiated cell lineages in the mammary gland during embryonic development and puberty and for the mammary gland's expansion and remodelling during the various stages of pregnancy⁵⁹. In more extreme experimental cases, one single MaSC can give rise to an entire mammary gland⁶⁰. It is therefore not unexpected that the expression of transcription factors that are essential to the identity of MaSCs can confer stem-like properties that are constituent to the MIC phenotype. A prime example is that the co-expression of *SOX9* and *SNAI2*, both of which are EMT transcription factors (TFs), has been shown to be sufficient to convert not only differentiated normal mammary cells into MaSCs, but also non-metastatic cells into MICs⁶¹. In the intestinal setting, the expression of *LGR5* denotes the normal intestinal stem cell which is capable of regenerating all of the cell types in the gut epithelium⁶². Although it has been observed that during metastasis, it is primarily *LGR5*- cells that accomplish the first four steps of the metastatic cascade, from invasion to extravasation, if *LGR5*- cells fail to gain plasticity and adopt a *LGR5*+ phenotype, they will ultimately fail to generate metastatic lesions⁶³.

Finally, MICs must also be able to evade immune recognition and killing at every stage of the metastatic cascade. MICs have been observed to downregulate ligands that are recognized by both the innate^{64,65} and adaptive immune system⁶⁶ to avoid attack. Conversely, MICs upregulate ligands like "don't eat me" signals (e.g. *CD47*⁶⁷) and immune checkpoints (e.g. *PD-L1*⁶⁸) that suppress immune activation. MICs can also alter their microenvironment to create physical barriers via the ECM to shield themselves from immune cells⁶⁹ or by secreting signals, like *TGFβ* that generates a hostile environment for antitumor immune cells like *CD4*⁺⁷⁰ and *CD8*⁺⁷¹ T cells but a permissive environment for protumor immune cells like regulatory T cells⁷².

I.III.ii Origins of MICs

Analysis of single nucleotide variations and copy number alterations⁷³ and lineage tracing experiments^{39,74} show that the cells comprising metastases stem from certain subpopulations that are already present in the primary tumor. In addition, comparisons of the genome sequences of paired primary and metastases show that there are very few differences in mutational burden⁷⁵⁻⁷⁸, suggesting that MICs don't arise due to the activation of a metastasis-specific oncogene. It is therefore likely that the differences between non-MICs and MICs are driven by differences in epigenetic modifications and transcription that result in altered phenotypes.

To support this, targeted transcriptomics analysis revealed higher expression of EMT and stem-related genes in micrometastatic lesions (which are enriched for MICs³⁶) in comparison to their respective primary tumors and late macrometastases⁷⁹. This was corroborated by another study that observed similar outcomes when examining circulating tumor cells in comparison to the primary tumor and resulting metastases⁸⁰. Profiling of accessible chromatin regions in metastases vs. primary tumors showed that there is a higher accessibility of gene regions in metastases in comparison to primary tumors, and that this can be necessary and sufficient to generate metastasis⁸¹. Although this study could suggest that major alterations to chromatin are required for metastatic potential, it has also been shown that a single histone mark change can be necessary and sufficient for EMT^{82,83}. Further, some non-MICs are known to maintain key genes in a poised chromatin state (where both active and repressive histone marks are present at the loci), so that they can easily dedifferentiate into MICs upon stimulation from the microenvironment⁸⁴. These examples support the notion that epigenetic modifications serve as the mechanism by which cells embody plasticity, as it can dynamically activate the biological processes needed to adapt to the various steps of the metastatic cascade⁸⁵. (See Section II for a Primer on Epigenetics)

In addition to the tumor-intrinsic mechanisms discussed, there may also be contributions from the environment that add to the MIC-phenotype. One recent example shows that heightened stress, in the form of glucocorticoids, increases metastatic capacity in breast cancer cells via activation of a protumor kinase,

ROR1⁸⁶. A clinical trial also observed that reduction of systemic inflammation by daily aspirin intake significantly reduced the risk of metastasis⁸⁷. In addition to these macroenvironment contributors, interactions with other cells during the metastatic cascade can also induce MICs. Platelets in circulation have been observed to increase metastasis by inducing EMT via TGF β signaling⁸⁸. Similar observations have been made from cancer-associated fibroblasts at the primary site⁸⁹. In relation to immune evasion, TNF α , which can be produced by various immune and stromal cells, has been shown to increase expression of the “don’t eat me signal”, CD47, via epigenetic mechanisms downstream of NF κ B activation⁹⁰. Finally, there’s also important contributions of non-MIC cells to the MIC phenotype. Cells expressing EMT-TFs were found to induce MIC activity in neighboring cells via GLI activation⁹¹. Additionally, distinct tumor subpopulations that were non-metastatic on their own were able to transform into MICs upon co-culture and co-transplantation, likely due to pro-MIC paracrine signaling and cooperation⁹².

To summarize, it is still unclear how exactly endogenous MICs arise and what exactly is the relative contribution of each of these influences on metastatic competency. It is unlikely that there is a singular definitive route to making a MIC, but regardless, there are some commonalities to their dependencies and these are crucial starting points for determining strategies for their identification, characterization, and elimination.

I.III.iii. Methods to Assay for and Identify MICs

Due to its complex nature, there have been several *in vitro* and *in vivo* assays that are used to assay for MIC activity. Commonly used *in vitro* assays make use of Boyden chambers, which are porous plastic inserts that are suspended above a cell culture dish. To measure migration, cells are typically placed in the top part of the chamber and are assayed at different time points to determine the speed and efficiency at which they move through the fixed-size pores towards a chemoattractant, commonly fetal bovine serum. There are numerous variations of this assay such as the addition of ECM and/or endothelial cells on top of the porous membrane to simulate invasion and/or intravasation. Another commonly used assay is the tumorsphere or colony forming unit assay, where cells are seeded at low

densities in suspension, or soft agar to assay for the ability to self-renew and proliferate in low attachment conditions. Particularly for breast cancer, mammospheres have been a standard read-out for stem cell activity in both normal mammary cells and tumor cells, as they have been shown to be enriched for stem-like populations^{93,94}. Although these assays are relatively easy to work with and can correlate with metastatic capacity^{95,96}, they are limited in their microenvironmental complexity and their exclusive use may not translate to the *in vivo* setting⁹⁷.

To experimentally assay for MICs *in vivo*, there are two commonly used methods: spontaneous or experimental metastasis assays (**Fig. 3**). In spontaneous metastasis assays, metastatic lesions are detected after tumor cells are transplanted at a primary site (orthotopically or subcutaneously). Because some metastatic outgrowths require more time to be detectable, tumors may need to be surgically excised to prevent excessive primary tumor growth, ensure sufficient time for the metastasis to proliferate, and for the survival of the recipient host. As an example, to verify that CD36⁺ cells were MICs in oral squamous cell carcinoma, Pascual et al. orthotopically injected serial dilutions of luciferase expressing CD36⁺ and CD36⁻ cells and monitored the mice over the course of 6 weeks to score for metastasis formation in both the lymph nodes and the lungs. They observed that despite being able to form primary tumors with the same speed and efficiency, only CD36⁺ cells were able to metastasize to the lymph nodes and lungs⁹⁸. Another group used a genetically engineered mouse model (GEMM) that labelled LMO2 expressing cells with green fluorescent protein (GFP) in an autochthonous model of breast cancer, the MMTV-Polyoma Middle T (PyMT), while all other cells remained red by TdTomato expression. They then orthotopically injected these cells into the mammary fat pad of the mice, and waited until tumors reached a humane end point to sacrifice the mice, dissociate the lungs, and measure the frequency of GFP⁺ or TdTomato⁺ cells. Because they observed an over 10-fold discrepancy in the frequency of GFP⁺ cells and TdTomato⁺ cells in the lungs, it was concluded that LMO2⁺ cells are the MICs⁹⁹. Although these experiments can very closely recapitulate all of the hurdles of metastatic colonization, the frequency of metastatic events can be very low (in these examples, they either only score for presence or absence of metastasis or number of cells in the lungs, not number of independent

metastatic seedings). Further, it is technically challenging, laborious, and time-consuming (experiments typically take up to 6 months).

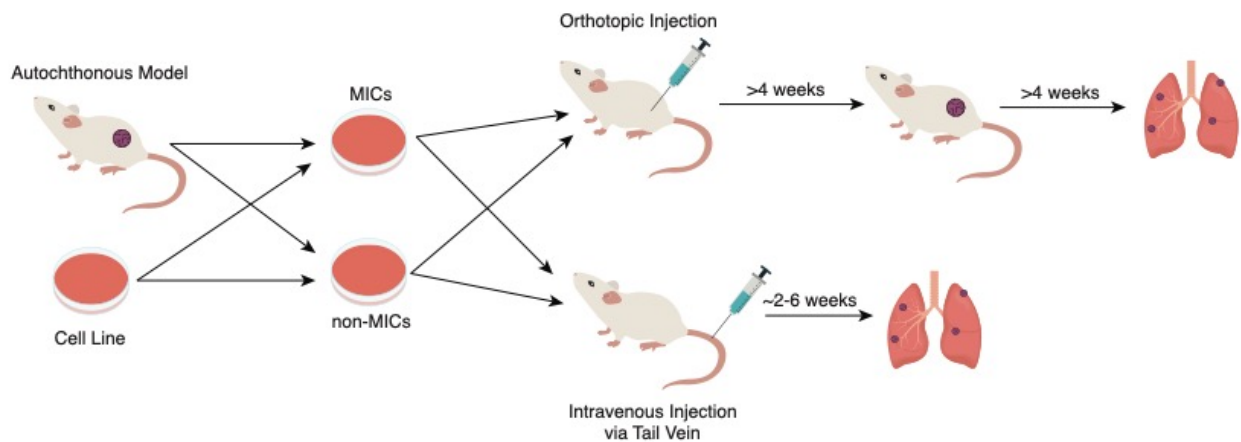


Fig. 3: Some example methods used to assay for MIC activity in vivo. Cells are taken from spontaneous tumors from an autochthonous GEMM model or an established cell lines. Cells can be sorted for cell specific markers and either plated or directly injected into recipient mice. Cells can then be injected into the orthotopic site for a spontaneous metastasis assay. The injected cells will develop a primary tumor, and once it reaches a certain size, the tumor can be removed to enable growth of any micrometastatic lesions. After a certain timepoint, the lungs (or whichever desired organ) can be analyzed for number of macrometastases formed. Cells can also be directly injected into the circulation for an experimental metastasis assay. Typically, cells are injected into the tail veins to assay for metastasis to the lungs. After 2-6 weeks, lungs can be analyzed for number of metastatic nodules.

Alternatively, cells can be directly introduced into circulation via three commonly used routes: intrasplenic injections, intravenous tail vein injections (TVIs), and intracardiac injections. These routes are specifically used depending on desired site of metastasis –the liver, lung, or systemic, respectively. As an example, CD90+ cells were identified to be MICs in the PyMT GEMM by performing TVIs on sorted CD90+ vs. CD90- cells. CD90+ were observed to generated metastatic lung nodules 10x more efficiently than their CD90- counterparts³⁶. Although this method bypasses the first two steps of the metastatic cascade (invasion and intravasation), it is less time-consuming, it is targeted, there is a higher frequency of metastatic events, and the number of metastatic events can be more easily quantified.

Crucial to all of this is the choice of cancer cell models. Autochthonous tumor models that attempt to model all features of human cancers from initiation to metastasis can be a good source for metastatic cancer cells¹⁰⁰. These cells display intratumor

heterogeneity, have appropriate interactions with the microenvironment, and are a close representation of the cell and tissue architecture of human cancers. The drawback of these cells are they are short-lived *ex vivo* and can vary from tumor to tumor, which makes mechanistic studies and genetic manipulation challenging. In contrast, cell lines are most commonly used as they are widely available, well-documented, and easy to manipulate. Although decades in artificial cell culture conditions select for certain clones that thrive in these artificial settings¹⁰¹, the lack of heterogeneity also makes mechanistic investigations simpler to conduct and interpret.

Although there's no one ideal method for assaying MIC activity, the use of a combination of these methods have been successful in identifying MICs in a variety of tissues. As mentioned in a few examples, MICs have now been identified in several tumor types including breast cancer^{36,99,102}, pancreas cancer¹⁰³, colorectal cancer¹⁰⁴, and oral squamous cell carcinoma⁹⁸. Each of these are identified with the use of cell-specific surface markers (**Table 1**) and have been validated as endogenously occurring MICs with enhanced metastatic capacity.

Table 1: Non-exhaustive list of identified endogenous MICs in primary human specimens and autochthonous mouse models.

Experimental metastasis assays refer to direct injection of cells into circulation while spontaneous metastasis assays refer to the detection of metastasis arising from implanted tumors at a primary site.

Tissue	Species	Markers	Metastasis Assay
Breast ³⁶	Mouse	CD45- CD31- Ter119- CD24+ CD90+	Experimental
Breast ¹⁰²	Human	CD45- CD31- CD3- CD64- CD10- CD20- GPA- CD24- CD44+	Spontaneous
Breast ⁹⁹	Human Mouse	CD45- CD31- Ter119- LMO2+	Spontaneous
Pancreas ¹⁰³	Human	CD45- CD31- CD133+ CXCR4+	Spontaneous
Colon ¹⁰⁴	Human	CD133+ CXCR4+	Experimental Spontaneous
Oropharynx ⁹⁸	Human	CD44br CD36+	Experimental Spontaneous

A Primer on Epigenetics

Although all cells harbor the same DNA blueprint, cells can exhibit vast variation in their gene expression patterns. The exact mechanisms underlying when, where, and how genes are differentially expressed are still under intense investigation; however, what is emerging is that there are several elements that comprise what is termed the “*cis*-regulatory code” that collectively instruct how genetic information is converted into phenotypes in a context-dependent, complex, and quantitative manner¹⁰⁵.

One of the main elements of the *cis*-regulatory code is the interaction of transcription factors to regulatory regions on the DNA, such as promoters and enhancers.

Promoters are located upstream of transcription start sites and thus, defines where transcription of a gene begins. Once a TF binds to this region, TFs initiate the formation of the transcription initiation complex which includes RNA polymerase, which will copy the DNA template into pre-messenger RNA. Enhancers, on the other hand, can be located upstream or downstream, proximal or distal to the gene-of-interest, and there also can be several enhancers that additively or redundantly influence the expression of a single gene. TFs and cofactors bind to enhancers, and bring this complex in proximity via DNA looping to promoters or even other enhancers¹⁰⁶ to increase the number of transcriptional machineries^{107,108} in the vicinity of the gene-of-interest, thus enabling enhancement of transcriptional initiation and elongation and ultimately, gene expression. In cancer, enhancers are exploited to increase the expression of tumor-promoting genes¹⁰⁹. A classic example is the translocation of the *MYC* oncogene close to the enhancer of the transcriptionally active IGH locus which increases the expression of *MYC* by 2-5 fold and thus drives neoplastic transformation to Burkitt Lymphoma^{110,111}.

DNA is hierarchically organized and compacted into the nucleus as chromatin by being wrapped and coiled around histone proteins. A nucleosome is the most basic packaged unit of chromatin, where 147 bp of DNA is wrapped around 8 histone proteins (the histone octamer). Each octamer consists of two copies of the histone proteins, H2A, H2B, H3, and H4. These histone proteins all consist of a structured globular domain and an unstructured tail of 25-40 residues, the latter being located on the N-termini (and the C-terminus of H2A) and having sequences unique from

each other but also highly evolutionarily conserved. Histone tails harbor multiple residues that can be post-translationally modified (**Fig. 4**), and these so-called epigenetic modifications play an important role in regulating gene transcription by two main mechanisms¹¹². First is by modifying the electrostatic interaction between histones and DNA. As DNA is negatively charged and histones are positively charged, there is an electrostatic interaction that maintains their tight association with each other. For gene transcription to occur, this tight association must be loosened, so to speak, to enable the access and recruitment of specific TFs and other members of the transcriptional machinery to the regulatory sequences for transcription. Phosphorylation and acetylation both reduce the charge on the histone proteins which consequently weakens their electrostatic attraction to DNA¹¹³; thus, the presence of these modifications is typically associated with increased gene expression. Second is by acting as docking sites for the recruitment of either transcriptional activators or repressors. For example, bromodomain-containing proteins like the BET family specifically bind to acetylated lysines to “read” these histone modifications¹¹⁴ and recruit factors for transcriptional initiation¹¹⁵. Some histone modifications can also increase transcription by preventing transcriptional repressors from binding such as H3K4me3¹¹⁶. In contrast, marks like H3K27me3 recruit transcriptional repressors and are thus associated with gene silencing¹¹⁷.

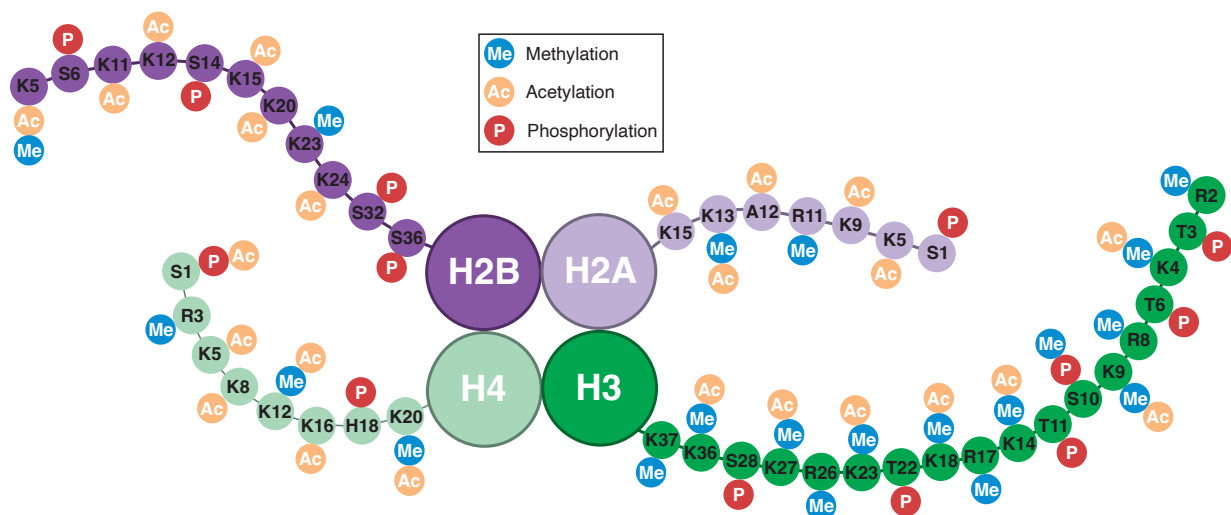


Fig. 4: Sites on histone tails that can be methylated, acetylated, or phosphorylated. Amino acid residues on histone tails can be post-translationally modified to carry epigenetic marks. These marks are added on by writers, recognized by readers, and are removed by erasers. Adapted from Torres-Perez et al (2021)¹¹⁸.

As such, these histone modifications form a language, termed the histone code, that describes and dictates transcriptional output^{119,120}. Many marks, such as the examples above, have been identified to be highly correlated and/or directly cause or prevent gene transcription. Some commonly studied histone modifications and their associations with gene transcription are outlined in **Table 2**.

Table 2: Common epigenetic modifications and their associated transcriptional output

Mark	Output
H3K4me3 ^{121,122}	Activation
H3K9me3 ^{123,124}	Repression
H3K27me3 ^{125,126}	Repression
H3K36me3 ¹²⁷	Activation
H3K9ac ¹²⁸	Activation
H3K27ac ^{129–131}	Activation

There are three main groups of proteins that regulate the histone code:

- 1) Writers are responsible for placing the modifications on histones. For example, specific histone acetyltransferase (HAT) complexes transfer the acetyl group from acetyl-CoA to conserved lysines, such as that of GCN5/PCAF to H3K9¹³² on promoters and CBP/P300 to H3K27 on enhancers¹³¹. Histone methyltransferases (HMT) that transfer the methyl group from s-adenosylmethionine (SAM) to lysines are also similarly site-specific.
- 2) Readers are responsible for binding to these histone modifications and act as effector proteins by recruiting all the necessary accomplices to elicit transcriptional repression or activation. The BET family of proteins mentioned above is one example of an epigenetic reader.
- 3) Erasers are responsible for removing modifications on histones. Histone deacetylases¹³³ and demethylases¹³⁴ remove acetyl and methyl groups, respectively, with a broader specificity than writers.

Because cancer is a “disease of deregulated gene expression”¹³⁵, epigenetics plays a pivotal role in executing the activation of gene programs that sustain tumor

progression. Large scale sequencing studies have found that epigenetic factors are frequently mutated or overexpressed across almost all cancer types¹³⁶, and some have even been identified as driver mutations. As an example, EZH2 is the catalytic subunit of the polycomb repressive complex 2 which is responsible for methylating H3K27 to promote gene silencing. It has been identified to drive several cancer types including lymphoma¹³⁷, melanoma¹³⁸, breast¹³⁹, and prostate¹⁴⁰ cancer primarily by silencing tumor suppressors and differentiation programs and thereby promoting stemness, EMT, and proliferation¹⁴¹.

Epigenetic marks are reversible and some of these occur over a relatively short time span. For example, the half-lives of histone acetylation and phosphorylation are within 15 minutes to 40 minutes and that of histone trimethylation occurs within 1 to 3 days. As such, cancers also exploit epigenetics for phenotypic switching across the temporal spectrum. Trimethylation on H3K27 (H3K27me3) placed by EZH2 can instruct where DNA methylation (and thus, gene silencing) should occur¹⁴². Because DNA methylation is a relatively stable mark (which is employed for tissue-specification during development¹⁴³), this induces a more permanent aggressive phenotype that, for example, can resist anti-androgen therapies in prostate cancer¹⁴⁴. Another example was mentioned earlier where in breast cancer cells, ZEB1 is maintained in this poised or bivalent chromatin state, which is characterized by the presence of both H3K4me3, an active mark, with H3K27me3, a repressive mark. Upon microenvironmental stimulation, in this case by TGF β , the removal of H3K27me3 induced the expression of EMT factors and a transition to a stem-like state that is associated with high tumorigenicity and metastasis⁸⁴. These examples suggest that epigenetics can provide MICs a way to assume different phenotypic states and enable dynamic adaptation to the many challenges of the metastatic cascade^{145,146}.

Cancer Metabolism

Although it was early last century when Otto Warburg first observed deregulated cellular bioenergetics in cancer¹⁴⁷, only in the second edition published in 2011 was metabolism recognized as one of the Hallmarks of Cancer¹⁴⁸. In essence, metabolism comprises the chemical reactions that occur in order to sustain life –a typical example is the breakdown of food into the three main macromolecules, carbohydrates (glucose), protein (glutamine) and fat (lipids) to generate energy in the form of adenosine triphosphate (ATP). However, in the last 20+ years, there has been an influx of evidence that metabolism not only sustains the bioenergetics of cells, but also exerts influence over cellular phenotypes at multiple levels of regulation. So much so that cancers exploit metabolism in several additional aspects^{149,150} (**Fig. 5**):

- 1) Support their unconstrained proliferative potential through anabolic reactions. For example, the building blocks of lipid membranes¹⁵¹ and nucleotides¹⁵² come from glucose and the import or generation of some amino acids depend on glutamine metabolism¹⁵³.
- 2) Combat ROS for survival. Cancer cells generally have higher levels of ROS, and although ROS can act as an important signal transducer, excessive amounts cause cell death¹⁵⁴. Cancer cells therefore rely on glucose and glutamine, which are major precursors for antioxidant generation^{21,155}. On the other hand, excessive lipids are vulnerable to chain peroxidation reactions which can eventually lead to ferroptosis¹⁵⁶.
- 3) Alter signaling networks. ROS also serves as an important signaling molecule where it has been found to oxidize the catalytic cysteines on phosphatases¹⁵⁷ which consequently affects protein function, such as the inactivation of tumor suppressors like PTEN¹⁵⁸. Lipid droplets are also well established as synthesis sites of inflammatory signalling¹⁵⁹ that can induce protumoral signaling such as induction of cell proliferation by PGE2¹⁶⁰.
- 4) Modulate gene expression. Several metabolites are co-factors, substrates, and allosteric regulators for epigenetic, post-transcriptional, and post-translational modifications (PTMs). In fact, 3 identified “oncometabolites” exert their neoplastic function by allosteric inhibition of histone and DNA

demethylases which then causes global gene expression changes that drive cancer initiation and progression^{161–163}.

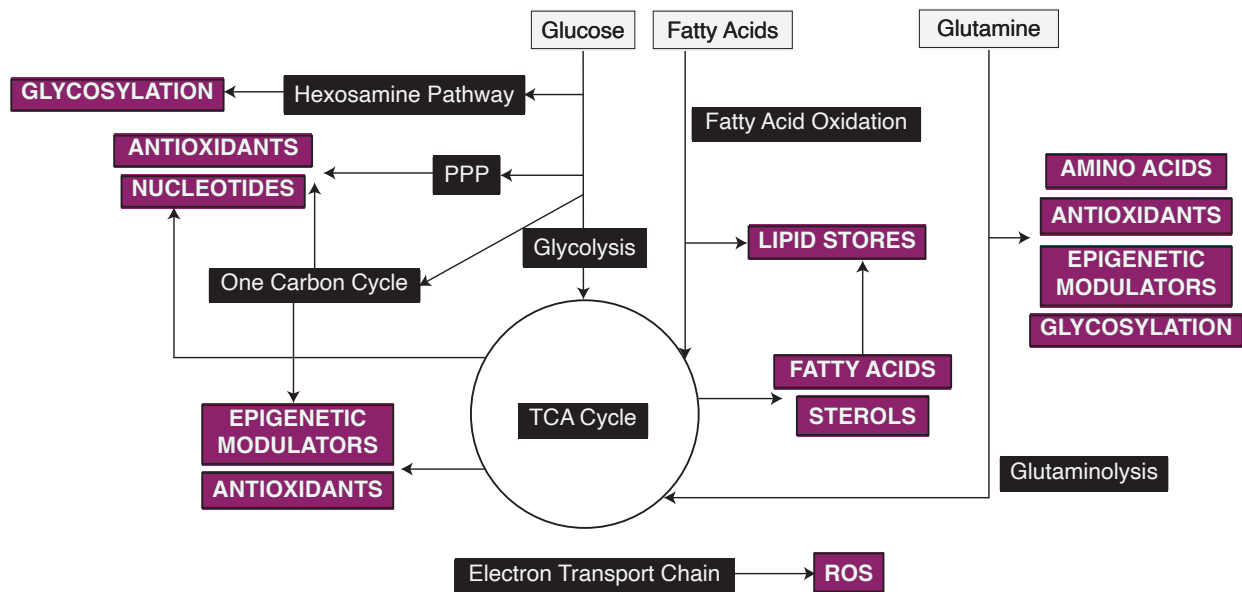


Fig. 5: Metabolic contributions to aspects of cell physiology outside of bioenergetics, focusing on the major fuel sources, glucose, glutamine, and fatty acids. Glucose¹⁶⁴ supplies precursors for nucleotide synthesis, epigenetic modifiers, antioxidant generation, and glycosylation through the pentose phosphate pathway (PPP), the one carbon cycle, and the hexosamine pathway. Glutamine¹⁶⁵ supplies precursors for amino acid synthesis, antioxidant generation, epigenetic modifiers, and nucleotide synthesis. Fatty acids¹⁶⁶ can be sequestered in lipid stores to prevent lipid peroxidation and serve as inflammatory signaling hubs. The electron transport chain and NOX enzymes (not in figure) are the main sources of ROS which can function as both a pro- and antitumor signal¹⁶⁷. All three fuel sources contribute to the TCA cycle for the generation of epigenetic modifiers, antioxidants, and precursors to sterol and lipid synthesis.

Because of the pleiotropic effects of metabolism, many oncogenes and (loss of) tumor suppressors have now been identified to drive cancer, at least in part through the induction of metabolic alterations¹⁶⁸. What is interesting is that preventing the assumption of certain metabolic characteristics can blunt neoplastic transformation and cause cell death, despite keeping all other signaling functions untouched. KRAS, the driver oncogene for pancreatic and lung adenocarcinomas and frequently mutated in other cancer types such as colorectal cancer, has been shown to increase glucose flux for ribose biogenesis¹⁵², to cause addiction to autophagy to maintain energy production¹⁶⁹, and to rely on glutamine-dependent antioxidant generation¹⁷⁰. Inhibition of just one of any of these metabolic pathways results in

significant delays in tumor initiation and growth, which exemplifies the evidence that metabolic alterations are essential for oncogenesis.

III.I Metabolism during the Metastatic Cascade

Just as cancer cells rely on metabolism to support their unlimited proliferative potential, MICs are increasingly found to depend on certain metabolic pathways to support their arduous journey from primary to secondary site.

As MICs move from the primary site to a distant site, there exists not only a different signaling niche, but also a different metabolic niche, where nutrient availability may vary substantially. The liver for example, is a highly hypoxic environment due to its compartmentalized metabolic activities that require varying oxygen gradients. On the other hand, the lung harbors excess amounts of oxygen because of its respiratory role. It has been shown that breast cancer cells that preferentially metastasize to the liver upregulate genes related to glycolysis in contrast to those that preferentially metastasize to the lung which upregulate genes related to oxidative phosphorylation (OXPHOS). In addition, they showed that metastasis to the liver, but not the lung, depends on PDK1 which is important for enforcing anaerobic glycolysis¹⁷¹. This suggests that there also exists a selection process for cells that either can adapt their metabolic phenotype or have a compatible metabolic phenotype for their target organ.

AMPK is a metabolic sensor which becomes activated during times of cellular stress –this is typically from low levels of ATP in relation to adenosine monophosphate or adenosine diphosphate, but it can also become activated due to oxidative, genotoxic, or xenobiotic stress. AMPK switches the cell's metabolic status by shutting down all anabolic processes, such as fuel storage and fat or protein synthesis to catabolic processes such as glycolysis, fatty acid oxidation, and autophagy¹⁷². It has been shown that AMPK is necessary for metastasis to the lungs in breast cancer by shuttling glucose through the tricarboxylic acid (TCA) cycle (which increases ATP output in contrast to anaerobic glycolysis) and simultaneously reducing ROS levels (ROS is known to increase during substrate detachment²⁰), which both contribute to cell survival upon departure from the primary site. Consequently, silencing AMPK

causes a drastic reduction of metastatic capacity¹⁷³, showing that being able to respond to multiple stressors and ensuring metabolic fitness are crucial to metastasis.

Outside of satisfying nutritional requirements, certain metabolic inputs are required to generate “tools” for metastasis. Pyruvate-derived α KG has been shown to be an allosteric modulator of P4HA. P4HA is the enzyme responsible for stabilizing (via hydroxylation) the collagen fibres that are deposited by MICs. Blocking the uptake of pyruvate causes the collagen fibres to be more vulnerable to matrix metalloproteinases which then prevents breast cancer cells from generating a suitable ECM, and thus reducing the number of metastatic nodules they can form¹⁷⁴. Similarly, it was found that circulating MICs and early metastatic lesions tend to downregulate PHGDH, an enzyme that shuttles glucose derived carbon towards the serine and glycine generation. It was found that loss of PHGDH activates generation of glycosylation precursors that increase the ability of MICs to invade and migrate. Thus, loss of PHGDH increases metastatic capacity and low levels or heterogenous expression of PHGDH is associated with higher probability of lymph node metastasis in patients¹⁷⁵.

III.II Influence of Metabolism over Cellular Phenotypes

It is important to underscore that not only does metabolism support cancer growth and proliferation, but it is directly intertwined with cellular phenotypes through pleiotropic mechanisms.

HIF-1 α is a metabolically-activated TF that is normally degraded in normoxia; but when cells experience hypoxia (such as in the core of a tumor mass), HIF-1 α is stabilized and activates a broad transcriptional program which includes increasing angiogenesis by increasing expression of VEGF and ANGs¹⁷⁶ and activating EMT by directly binding to promoters and causing transcription of EMT-TFs^{177,178}. As a consequence, HIF-1 α can induce non-stem-like cells to adopt a stem-like phenotype across several tissue types¹⁷⁹ and has also been identified to fuel cancer aggression and metastasis in a number of tissues^{180–182}.

It has also been observed that the availability of certain amino acids influences the ability of cancer cells to resist therapies. Dietary methionine restriction was found to sensitize cancer cells to 5-fluorouracil and radiation therapy due to its reduced input into the one carbon cycle which is responsible for generating nucleotides and antioxidants. As the two treatments cause disruption to nucleic acid synthesis and increased ROS, withdrawal of methionine exacerbated their efficacy and reduced tumor growth¹⁸³. In contrast, increased histidine catabolism sensitizes tumors to methotrexate by draining the pool of tetrahydrofolate, a folic acid derivative that methotrexate-treated cells were reliant on. Dietary supplementation of histidine increased sensitivity to methotrexate leading to increased tumor necrosis and reduced tumor growth¹⁸³.

Aside from metabolic TFs activating certain cell phenotypes and certain metabolites altering sensitivities to treatments, more and more metabolites are also being discovered to directly regulate gene expression. As mentioned, many metabolic intermediates involved in discrete and diverse metabolic pathways are cofactors, allosteric regulators, and substrates for epigenetic marks and PTMs¹⁸⁴ (**Fig. 6**). Because the Michaelis constant values of HATs and HMTs, for example, hover around the physiological concentration range of their substrates, the abundance or depletion of these metabolic substrates contributes to control the activity of these enzymes. This is in stark contrast to for example, kinases which are always in excess of their substrate, ATP, and are thus instead controlled by upstream signals¹⁸⁵ (**Fig. 7**).

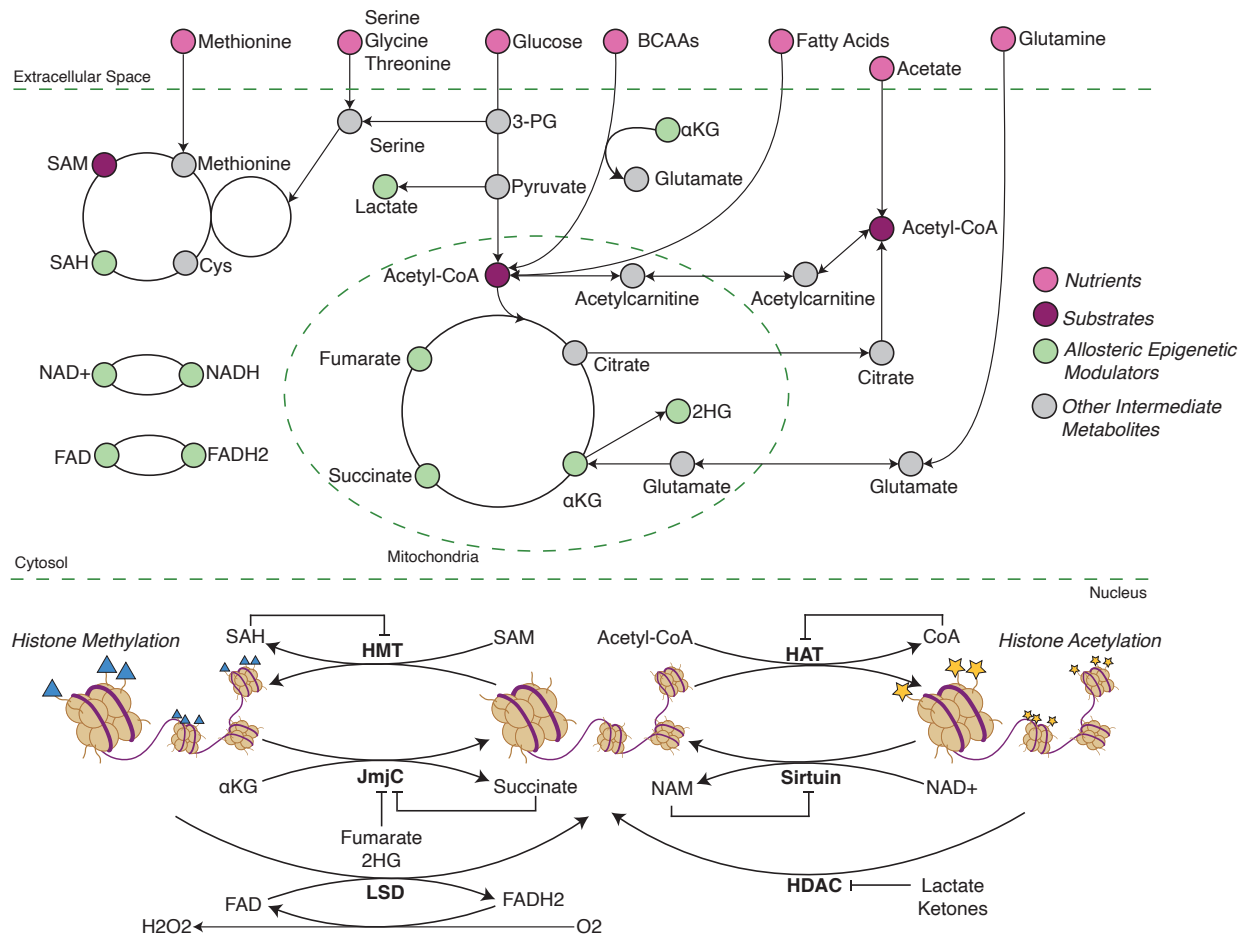


Fig. 6: The contribution of metabolic pathways to histone methylation and acetylation.

Macronutrients like methionine, serine, glycine, threonine, and glucose enter the one carbon cycle to generate SAM, which contributes a methyl group for histone methylation by HMTs, and SAH, which allosterically inhibits the activity of HMTs. Glucose, branched chain amino acids (BCAAs), fatty acids, and acetate all generate acetyl-CoA, which contributes an acetyl group for histone acetylation by HATs. Reductive glutamine carboxylation and the TCA cycle generates α KG, which is a cofactor for histone demethylases (e.g. JmjC, LSD), and fumarate, succinate, and sometimes 2HG, which allosterically inhibits histone demethylases. NAD⁺ which is derived from nicotinamide (NAM) or NADH oxidation (from the electron transport chain (ETC)) acts as a cofactor for sirtuins, which are histone deacetylases. On the other hand, lactate and ketone bodies like β -hydroxybutyrate (BOHB) allosterically inhibit histone deacetylases. Finally, FAD, which is generated by FADH₂ oxidation (from the ETC) serves as a cofactor for histone demethylases. Adapted from Reid et al. (2017)¹⁸⁵.

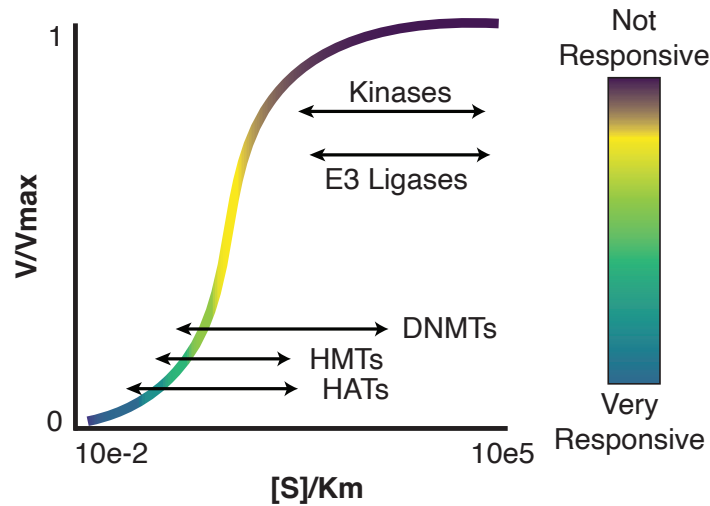


Fig. 7: Activity modulation of epigenetic modifiers by metabolite availability. In contrast to kinases and E3 ligases whose activity is not controlled by the local concentrations of their substrates (ubiquitin and ATP), DNA methyltransferases (DNMTs), histone methyltransferases (HMTs), and histone acetyltransferases (HATs) are more or less active depending on the concentrations of their cofactors, substrates, or allosteric regulators. Adapted from Reid et al. (2017)¹⁸⁵

Many examples of this have been shown in embryonic and pluripotent stem cells. Elevated levels of metabolites like α KG and acetyl-CoA were shown to be important for histone demethylation¹⁸⁶ and acetylation¹⁸⁷, respectively, to maintain expression of genes that sustain pluripotency like OCT4 and thus the ability to self-renew. Similar dependencies on metabolism-derived epigenetic modifications were then found to exist in cancer. NNMT is an enzyme that catalyzes the transformation of SAM (a methyl donor) into s-adenosylhomocysteine (SAH). When NNMT is overexpressed (as observed in many aggressive cancers), the absolute concentrations of SAH increase, which causes a reduction in the SAM:SAH ratio, and consequently reduced histone methylation on EMT-related genes such as *SNAI2* and *TGFB2*¹⁸⁸. Moreover in a separate study, the reduction or abundance of methionine (the precursor to SAM), even from dietary intake, alters the levels of histone methylation, which in turn can influence the expression of cancer related genes¹⁸⁹.

All of these underline the importance and scope of metabolism in influencing the outcome of cancer cells that attempt to complete the metastatic cascade.

Breast Cancer

Breast cancer is the most diagnosed cancer in women, where there are over 2.3 million new diagnoses and over 680,000 deaths annually. In the next few years, these statistics are predicted to increase to approximately 3 million and 1 million, respectively, due to the both growing and aging population¹⁹⁰. While the 5-year survival rates for patients diagnosed with breast cancer hover around 90%, if patients are diagnosed at a late stage when metastatic lesions are clinically detectable, their survival probability drops to under 30%¹. It is of note that about 20% of all breast cancer cases have been estimated to be attributed to modifiable risk factors, such as obesity, physical inactivity, and alcohol use³. Each of these has similarly been correlated with increased probability of metastasis^{191–193}. Currently, there is no cure for metastatic breast cancer.

There are four intrinsic breast cancer subtypes that are used to determine best course of treatment for patients: HER2-enriched, luminal A, luminal B, and triple negative breast cancer (TNBC)^{194,195}. Subtyping is typically accomplished by immunohistochemical staining with antibodies against four marker proteins, estrogen receptor (ER), progesterone receptor (PR), human epidermal growth factor receptor 2 (HER2, also known as ERBB2), and Ki67. HER2-enriched tumors have increased expression levels of HER2, typically due to genetic amplification events. In addition to HER2 amplification, they also frequently harbor TP53 mutations. Luminal A and B denote tumors that retain expression of the two hormone receptors, ER and PR, but luminal B tumors express these hormone receptors at a lower degree and express higher levels of Ki67 (a proliferation marker). Luminal tumors are called as such since they retain many markers of the luminal subpopulation of normal mammary glands –these are the cells that line the apical surface and differentiate into hormone or milk producing cells during puberty and/or pregnancy. On the other hand, TNBC does not express or expresses only very low levels of any of the three mentioned receptors, are likely to carry TP53 mutations, are typically undifferentiated, are heterogeneous, have a high proliferative index, and are typically associated with visceral organ metastases (lung, liver, brain)¹⁹⁶. TNBC is also frequently called basal or basal-like breast cancer because they tend to express markers of basal myoepithelial cells, which are the cells that line the basal surface of the mammary

ducts. Not only do they serve contractile functions during lactation, but they also are important organizers of the mammary epithelium as they significantly contribute to the ECM (and therefore patterning) of the basement membrane¹⁹⁷. It is also of note that MaSCs have been shown to reside within the basal subpopulation⁶⁰.

Development of endocrine and anti-HER2 therapies have been shown to improve outcomes for luminal¹⁹⁸ and HER2¹⁹⁹ breast cancers, respectively, however, there is still no targeted treatments for TNBC aside from chemotherapy²⁰⁰. This is especially concerning since TNBC is the most aggressive of all subtypes, where patients with TNBC have the lowest overall survival (OS) and relapse-free survival (RFS), regardless of whether they diagnosed at an early or late stage¹⁹⁶. In line with this, there is a higher expression of both stem-related signatures and frequency of MIC-like cells in TNBC compared to the other subtypes^{201–203}. Further, TNBC has been observed to be dependent on a number of metabolic pathways for tumor-initiation^{204,205} and therapy resistance^{206–208}

OBJECTIVES OF THE RESEARCH

As metastatic disease continues to be a challenge to treat and prevent, it is crucial to better understand the mechanisms by which MICs successfully complete the metastatic cascade for the development of MIC-specific therapies that are both efficacious and tolerable.

Metabolism has recently emerged as a crucial regulator of cancer progression, where it not only supports, but also drives tumor initiation, progression, and therapy resistance through pleiotropic mechanisms. Recent work has shown how different metabolic pathways support distinct stages of the metastatic cascade through generation of crucial proteins and enzymes, activation of key signaling networks, and sustaining survival. Further, metabolic alterations are heavily intertwined with gene expression and cellular phenotypes, as several metabolic intermediates regulate the activity of epigenetic modifiers.

It is also important to note that with the advent of single-cell technologies, it is evident that there not only exists intratumoral heterogeneity on a transcriptional level^{209,210}, but also on an epigenetic²¹¹ and metabolic level²¹². It is therefore likely that MICs differ from non-MICs in all three of these aspects to orchestrate their cell functions for successful metastatic colonization of distant organs.

With that being said, the primary aim of the project is to identify the metabolic dependencies unique to TNBC MICs in comparison to their non-MIC counterparts. To do that, we examined an endogenous MICs population from the PyMT model that our lab had previously identified³⁶ and also in a secondary metastatic murine TNBC line, the 4T1 model. The secondary aim of the project is to determine how these metabolic dependencies influence the MIC phenotype. The third and final aim of the project is to determine if these results can be recapitulated in the human setting. Throughout the project, we focused to validate all of the findings *in vivo* when possible, in an attempt to ensure the biological significance of the results.

RESULTS – PRESENTED AS A MANUSCRIPT

The results are presented in a form of a manuscript that has been submitted and revised for Nature Communications. Here, we investigate the metabolic dependencies of MICs in TNBC and identify how these influence gene expression and metastatic capacity. We use *in vivo* models to confirm our hypotheses and further validate our findings in human cell line models.

We also included an “Additional Results” section to report data that were not included in the final manuscript; thus, the experimental procedures were moved to the end of the thesis to accommodate methods used to generate the additional results.

In brief, we identified that MICs preferentially funnel fuels through the TCA cycle for acetyl-CoA generation. MICs depend on metabolic pathways that generate acetyl-CoA; blocking these results in reduced metastatic capacity and supplying additional acetyl-CoA increases metastatic capacity. We determined that MICs have endogenously higher levels of H3K27ac and inhibition of acetyl-CoA generation reduces this. H3K27ac is crucial for activating EMT gene programs, and blocking either epigenetic readers of H3K27ac or acetyl-CoA generating pathways dampens EMT gene expression. We therefore elucidate the links among metabolism, gene expression, and metastasis formation that is crucial to TNBC MICs.

Title: Metabolic dependencies of metastasis-initiating cells in female breast cancer

Authors: Young C. Megan^{1,2,3}, Beziaud Laurent^{1,2,3}, Dessen Pierre^{1,2,3}, Madurga-Alonso Angela^{1,2,3}, Santamaria-Martínez Albert^{1,3,4}, and Huelsken Joerg^{1,2,3,4}.

Author Affiliations:

¹Ecole Polytechnique Fédérale de Lausanne (EPFL), ISREC (Swiss Institute for Experimental Cancer Research), Lausanne 1015, Switzerland.

²Agora Cancer Research Center, Bugnon 25A, 1011 Lausanne, Switzerland.

³ Swiss Cancer Center Lèman, Switzerland.

⁴co-corresponding authors: albert.santamariamartinez@epfl.ch,
joerg.huelsken@epfl.ch

Author Contributions:

C.M.Y: Conceptualization, Methodology, Investigation, Formal analysis, Writing - Original Draft, Visualization; L.B: Investigation; P.D.: Methodology, Investigation; A.M.A.; Investigation; A.S.M.: Conceptualization, Writing - Review & Editing; J.H.: Conceptualization, Supervision, Funding acquisition, Writing - Review & Editing.

Detailed Description of Doctoral Candidate's Contribution:

CMY conceptualized the project and optimized and designed all the experiments presented here. CMY analyzed all the results, generated the figures, wrote the manuscript, and addressed reviewer comments.

Abstract

Understanding the mechanisms that enable cancer cells to metastasize is essential in preventing cancer progression. Here we examine the metabolic adaptations of metastasis-initiating cells (MICs) in female breast cancer and how those shape their metastatic phenotype. We find that endogenous MICs depend on the oxidative tricarboxylic acid cycle and fatty acid usage. Sorting tumor cells based upon solely mitochondrial membrane potential or lipid storage is sufficient at identifying MICs. We further identify that mitochondrially-generated citrate is exported to the cytoplasm to yield acetyl-CoA, and this is crucial to maintaining heightened levels of H3K27ac in MICs. Blocking acetyl-CoA generating pathways or H3K27ac-specific epigenetic writers and readers reduces expression of epithelial to mesenchymal-related genes, MIC-frequency, and metastatic potential. Exogenous supplementation of a short chain carboxylic acid, acetate, increases MIC frequency and metastasis. In patient cohorts, we observe that higher expression of oxidative phosphorylation related genes is associated with reduced distant relapse-free survival. These data demonstrate that MICs specifically and precisely alter their metabolism to efficiently colonize distant organs.

Introduction

Cancer cells exhibit altered biosynthetic and energy requirements which result in heightened and biased fuel uptake and utilization. Blocking required metabolic alterations such as increased glucose and/or amino acid utilization can effectively blunt transformation by inhibiting proliferation and causing cell death^{170,213,214}. Metabolism not only has supportive and enabling functions, but it can also directly influence cellular phenotypes. For example, hypoxia can induce cancer invasion¹⁷⁸ and the availability of certain amino acids can alter drug response^{183,215}. This demonstrates that changes in metabolism are essential in both supporting and driving cancer progression.

Metastatic disease causes the majority of cancer deaths and there are still very few therapeutic options for patients that are diagnosed at this late stage. Thus, understanding mechanisms for metastatic dissemination and progression can

uncover actionable vulnerabilities and potentially improve therapy. In many tumor types, metastasis is caused by a rare population of stem-like cells in the heterogenous tumor mass that are highly plastic. During metastasis formation, these metastasis-initiating cells (MICs) are required to undergo sequential, partially opposing phenotypic changes that enable them to invade into the surrounding tissue, enter and survive in the bloodstream, and generate a new tumor at a distant site²¹⁶. MICs have been identified in a variety of solid tumors, such as breast cancer^{36,102}, pancreas cancer¹⁰³, colorectal cancer¹⁰⁴, and oral squamous cell carcinoma⁹⁸, and their frequency has been shown to be correlated with poor prognosis.

In addition, comparisons of genome sequences between MICs and their non-MIC counterparts show a high degree of concordance^{217,218}, suggesting that the ability to metastasize to distant organs is not likely due to the accumulation of metastasis-specific driver mutations, but rather due to epigenetic modifications that enable reversible transitions in cell phenotype during the course of metastasis. In line with this, alterations in certain histone marks have recently been shown to be necessary and sufficient for cell state changes such as the epithelial-to-mesenchymal transition (EMT)^{82,83}. Some non-MICs are even able to dedifferentiate into MICs by maintaining key genes in a poised chromatin state⁸⁴, demonstrating that epigenetic modifications endow cells with the plasticity to adapt to various requirements during the metastatic cascade⁸⁵.

Metabolic alterations have been linked to each step of metastasis. For example, reductive glutamine metabolism is required to generate antioxidants for combatting reactive oxygen species under low attachment conditions, such as when traveling through the bloodstream²¹, and pyruvate is essential for generating sufficient levels of alpha ketoglutarate for collagen stabilization at the metastatic site for efficient tissue colonization¹⁷⁴. This raises the possibility that the metabolic phenotype of MICs is constituent for its metastatic potential.

Metabolism and epigenetics are inextricably linked. In contrast to kinases whose activity is controlled by upstream signaling pathways and not the abundance of its substrate, ATP, the activity of various epigenetic enzymes is influenced by the concentrations of certain metabolites which can be cofactors, substrates, or allosteric

regulators for these enzymes¹⁸⁵. Reduced availability of s-adenosyl methionine for example, has been shown to reduce histone methylation and increase subsequent transcription of genes in oncogenic signaling pathways^{188,189}.

Here we aim to investigate the metabolic differences between MICs and non-MICs and whether that may influence the transcription of gene programs in MICs that enable them to generate metastatic lesions. To do this, we utilize tumors deriving from the autochthonous breast cancer model, MMTV-Polyoma Middle T (PyMT), since this is where we had previously identified endogenous MICs that are exclusively capable of generating metastasis³⁶. We also validate and extend these findings in a second mouse model using the highly metastatic, triple negative breast cancer (TNBC) cell line 4T1. We uncover that MICs rely on fatty acid oxidation (FAO) and the oxidative tricarboxylic acid (TCA) cycle, and that these contribute to acetyl-CoA generation and the acetylation of histones on EMT-related genes. Blocking either the metabolic pathways that generate acetyl-CoA or acetylation reactions can reduce MIC frequency and metastatic potential *in vivo*.

Results

Metastasis-initiating cells show increased mitochondrial activity

Considering the conflicting evidence in the literature for the role of mitochondrial activity during metastasis^{219,220}, we sorted 4T1 breast cancer cells for varying levels of mitochondrial activity based on a fluorescent stain that preferentially accumulates in mitochondria with high mitochondrial membrane potential (MMP). High MMP cells have increased intracellular ATP than their low MMP counterparts²²¹ (**Supplementary Fig. 1a**). Tail vein injections (TVIs) revealed that the cells with high MMP generate 10x and 5x more metastatic nodules in the lungs compared to their low and medium counterparts, respectively (**Fig. 8a**), despite having similar proliferation rates (**Supplementary Fig. 1b**). We observe a similar MMP phenotype in 4T1 MICs that are ALDH bright compared to ALDH dim non-MICs²²² (**Fig. 8b**, **Supplementary Fig. 1c**). To confirm this phenotype in another model, we utilized the MMTV-Polyoma Middle T (PyMT) breast cancer model where we had previously identified MICs as Lin⁻CD24⁺CD90⁺³⁶. Using the same mitochondrial stain, we

observed that PyMT MICs have an almost 2-fold increase of MMP compared to their non-MIC counterparts (Lin⁻CD24⁺CD90⁻; **Fig. 8c**, **Supplementary Fig. 1d**), even when normalizing for mitochondrial mass (**Supplementary Fig. 1e**). RNA-sequencing of sorted PyMT MICs and non-MICs revealed increased expression of gene sets related to oxidative phosphorylation (OXPHOS) and mitochondrial metabolism (**Fig. 8d**), in addition to the expected increased expression of gene sets related to EMT and partial EMT⁵⁰ (**Supplementary Fig. 1f**). These data suggest that in metastatic cells, fuels may be preferentially utilized in mitochondria. To test this hypothesis, we measured oxygen consumption rate (OCR) and extracellular acidification rate (ECAR) in a Seahorse mitochondrial stress test. It was not possible to use sorted populations for this since we observed poor metabolic health and up to three-fold reduction of OCR in sorted cells (**Supplementary Fig. 1g**). Instead, we used tumorsphere- and monolayer-grown cells, since tumorspheres are known to be enriched for highly tumorigenic stem-like cells⁹⁴. When only glucose was provided as a fuel source, we observed that tumorspheres have a higher maximal respiratory capacity (**Fig. 8e**) and conversely lower glycolytic capacity (**Fig. 8f**), confirming our hypothesis. We also observed that tumorsphere-derived cells have a higher MMP compared to their monolayer counterparts (**Supplementary Fig. 1h**). Driving monolayer grown cells to undergo OXPHOS by replacing glucose in the cell culture media with galactose, which does not yield ATP through glycolysis and thereby forces the use of OXPHOS, increased MIC frequency in PyMT cells (**Fig. 8g**) and metastatic capacity in 4T1 cells (**Fig. 8h**). The increase of MICs we observed is not due to preferential death of non-MICs under nutrient stress as measured by Annexin V and propidium iodide staining (**Supplementary Fig. 1i**), or preferential increase in proliferative capacity of MICs as measured by reduction of CellTrace Violet staining (**Supplementary Fig. 1j**), but rather due to the maintenance of the MIC phenotype and/or the conversion of non-MICs to MICs (**Supplementary Fig. 1k**). Collectively, these data show that metastatic cells exhibit higher mitochondrial activity which directly affects their ability to colonize distant organs.

Figure 8

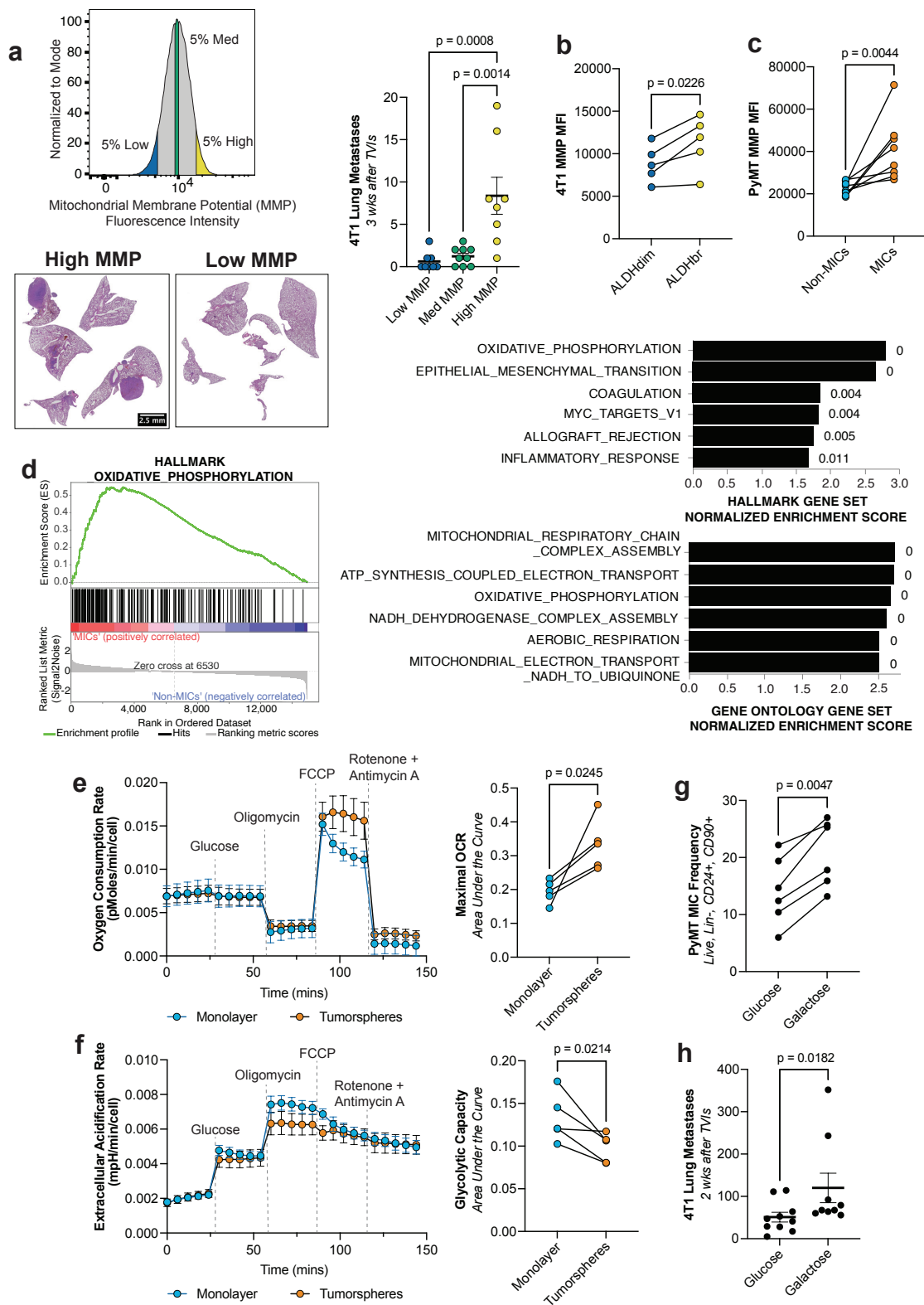
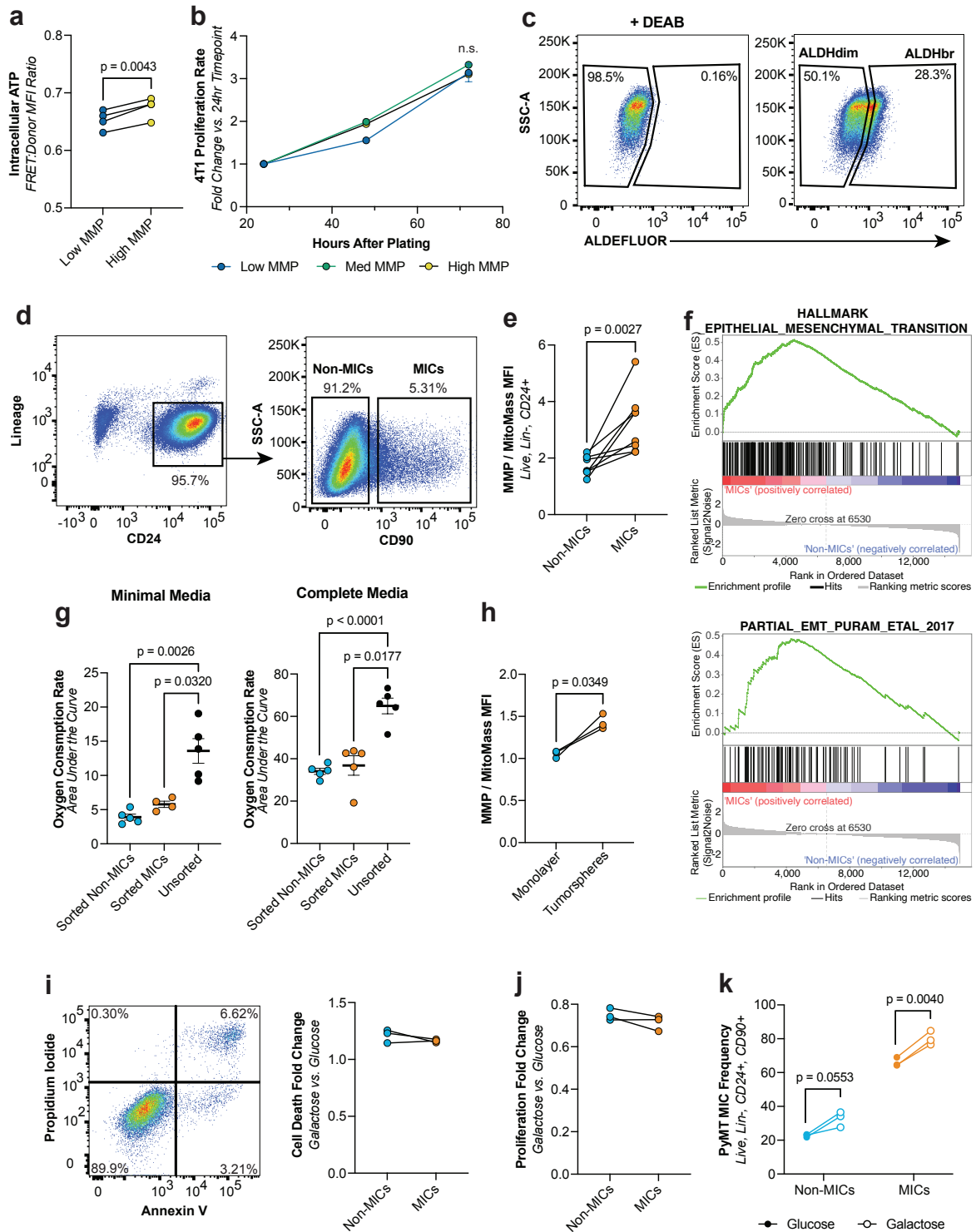


Fig. 8: Heightened mitochondrial activity is a key feature of MICs.

a) Lung metastases in recipient wildtype (wt) Balb/c after TVI of 4T1 cells sorted for low, med, and high MMP. Left top: Gating strategy for sorting cells. Left bottom: representative images of hematoxylin and eosin paraffin sections of lungs of recipient mice. Right: Quantification. (n=8, ordinary one-way ANOVA followed by Tukey's test). b) MMP MFI in ALDHdim vs. ALDHbright 4T1 cells. (n=5^a, paired t-test) c) MMP MFI in ex vivo PyMT non-MICs vs. MICs. (n=8^a, paired t-test) d) Upregulated gene sets when comparing ex vivo PyMT MICs vs non-MICs. Left: Gene set enrichment plot for the HALLMARK_OXIDATIVE_PHOSPHORYLATION signature from the Molecular Signature Database (MsigDB). Right: Top upregulated gene sets from the hallmark (top) and gene ontology (bottom) collections. Numbers beside bar plots indicate false discovery rate (FDR). (n=3^a) e) OCR over time in tumorsphere- vs. monolayer-grown PyMT cells (normalized to number of cells). Right: OCR area under the curve (AUC) for matched monolayer and tumorsphere-grown PyMT cells. (n=5^a, paired t-test) f) Extracellular acidification rate over time during the mito stress test in tumorsphere- vs. monolayer-grown PyMT cells (normalized to number of cells). Right: Glycolytic capacity AUC for matched monolayer- and tumorsphere-grown PyMT cells. (n≥3^a, paired t-test) g) PyMT MIC frequency after culture in either glucose or galactose containing media. (n=6^a, paired t-test) h) Number of lung metastases in recipient wt Balb/c mice after TVI with 4T1 cells cultured in either glucose- or galactose-containing media. (n=10 for glucose, n=9 for galactose, Mann-Whitney test). MFI = mean fluorescence intensity. Paired t-tests were two-tailed and by ratio. Values shown correspond to means +/- SEM. Source data are provided in the source data file. ^a signifies number of independent experiments or tumors.

Supplementary Figure 1



Supplementary Fig. 1: MICs have heightened mitochondrial activity

a) Intracellular ATP concentrations measured via FRET in high vs. low MMP 4T1 cells. ($n=4^a$, paired t-test) b) Proliferation rate of 4T1 cells sorted for low, med, and high MMP normalized to the first measured timepoint. ($n=3$, ordinary one-way ANOVA) c) Gating strategy to identify ALDH^{bright} (ALDHbr) vs. ALDH^{dim} (ALDHbr) 4T1 cells. DEAB control is used to determine the boundary between ALDHbr vs. dim. d) Gating strategy for PyMT MICs and non-MICs. PyMT MICs are identified as CD45-CD31-Ter119-(Lin-), CD24+, and CD90+. PyMT non-MICs are Lin-, CD24+, and CD90-. e) MMP MFI normalized to mitochondrial mass (MitoMass) MFI in ex vivo PyMT non-MICs vs. MICs. ($n=8^a$, paired t-test) f) Gene set enrichment plots for EMT and partial EMT in ex vivo PyMT MICs vs. non-MICs. ($n=3^a$) g) OCR area under the curve (AUC) for sorted vs. unsorted cells, left: in conditions where only glucose is provided as fuel, right: in conditions where complete media is provided ($n\geq 4^a$, paired t-test). h) MMP MFI normalized to MitoMass in monolayer vs. tumorspheres. ($n=3^a$, paired t-test) i) Cell death frequency measured by AnnexinV and propidium iodide staining in sorted PyMT non-MICs or MICs cultured for 36 hours in galactose- vs. glucose-containing cell culture media. Left: cells were considered viable when negative for Annexin V and propidium iodide. Right: quantification; expressed as a fold change over the glucose condition. ($n=3^a$, paired t-test) j) Proliferation measured by CellTrace Violet staining in sorted PyMT non-MICs or MICs cultured for 36 hours in galactose- vs. glucose-containing cell culture media. Expressed as a fold change over the glucose condition. ($n=3^a$, paired t-test) k) MIC frequency in sorted PyMT non-MICs or MICs after 36 hours of culturing in galactose- vs. glucose-containing cell culture media. ($n=3^a$, paired t-test). MFI = mean fluorescence intensity. Paired t-test were two-tailed and by ratio. Values shown correspond to means +/- SEM. Source data are provided in the source data file. ^a signifies number of independent experiments or tumors.

Metastasis initiating cells are dependent on enhanced fatty acid flux and usage

We then investigated if MICs have a preferential fuel source by performing a Seahorse-based fuel dependency test, which compares the change in OCR when first blocking the entry of one of the three main fuel sources into the mitochondria (pyruvate, glutamine, or long chain fatty acids (LCFAs)), then subsequently blocking the remaining two. We observed that in comparison to monolayer grown cells, tumorspheres do not differ in their dependency on either pyruvate or glutamine (**Supplementary Fig. 2a**), however, tumorspheres have a 60% increased dependency for LCFA oxidation (**Fig. 9a**). We then confirmed that this dependency is not due to a reduced capacity for LCFA oxidation in the monolayer cells because if we force the cells to oxidize LCFAs by first simultaneously blocking entry of pyruvate and glutamine into the mitochondria, we do not observe differences between the monolayer cells in comparison to the tumorspheres (**Supplementary Fig. 2b**).

We confirmed the dependency on LCFA oxidation by performing experimental metastasis assays via TVI with PyMT cells that had been pre-treated for 72 hours with etomoxir, an inhibitor of the rate limiting enzyme in FAO, CPT1. Despite not significantly altering proliferative potential (**Supplementary Fig. 2c**), etomoxir reduced both MIC frequency (**Fig. 9b**) and metastatic capacity (**Fig. 9c**), and these results were confirmed using miR-mediated knockdowns (KDs) of *Cpt1a* and *Cpt2* (**Fig. 9d**, **Supplementary Fig. 2d**). This was further validated by performing spontaneous metastasis assays where orthotopically implanted tumors that express miR-mediated KDs of either *Gfp* or *Cpt1a* were resected just before reaching 1000mm³. Since the tumors were growing at different rates, we chose to perform tumorectomies at a fixed size, rather than a fixed time to give slower growing tumors more time to metastasize (**Supplementary Fig. 2e**). We then analyzed the lungs 30 days after their respective tumor removal to examine the number of spontaneous metastatic nodules formed. We again observed a significant reduction of lung metastasis upon *Cpt1a* KD (**Supplementary Fig. 2f**). In order to confirm that this dependency was specific to lipids, TVI of cells that were pre-treated with UK5099, an inhibitor of the mitochondrial pyruvate carrier, did not change metastatic capacity (**Supplementary Fig. 2g**).

Using fluorescently tagged lipid probes *ex vivo*, we observed that MICs from both orthotopically implanted 4T1 tumors and spontaneous PyMT tumors have a 2-fold and over 30% increase in LCFA uptake (**Fig. 9e, f**) and a 3-fold and 30% increase of lipid stores, respectively (**Fig. 9g, h**). By sorting 4T1 cells that have high, med, and low levels of lipid stores, we confirmed that cells that have the highest levels of lipid stores also have the highest propensity to generate metastatic nodules (**Fig. 9i**), despite similar proliferation rates (**Supplementary Fig. 3a**). Likewise, in the early stage of metastasis formation (3 days after TVI), there was an over 4-fold enrichment of cells with elevated lipid stores observed by oil red o staining, compared to subsequent stages of metastasis formation (5 days after TVI and onwards; **Fig. 9j**, **Supplementary Fig. 3b**). In PyMT cells under starved conditions, lipid droplets are used up more rapidly in MICs than non-MICs (**Supplementary Fig. 3c**). This becomes more evident if lipid droplet generation is further blocked via DGAT1 & DGAT2 inhibition (using T863 & PF-06424439, respectively) in starved conditions compared to complete media conditions (**Supplementary Fig. 3d**). TVIs indicate

that blocking the generation of these lipid stores even under nutrient replete conditions prevents metastasis (**Fig. 9k**; without compromising proliferative potential **Supplementary Fig. 3f**). On the other hand, if breakdown of lipid stores is inhibited using the ATGL inhibitor, ATGListatin, in complete media conditions, there is an accumulation of lipid stores (**Supplementary Fig. 3e**), but metastatic activity is inhibited (**Fig. 9l**; without altering proliferation (**Supplementary Fig. 3f**). In summary, this indicates enhanced flux of lipids (uptake, storage, and oxidation) in MICs compared to non-MICs that enables the dynamic use of lipids which are crucial for metastasis generation.

Figure 9

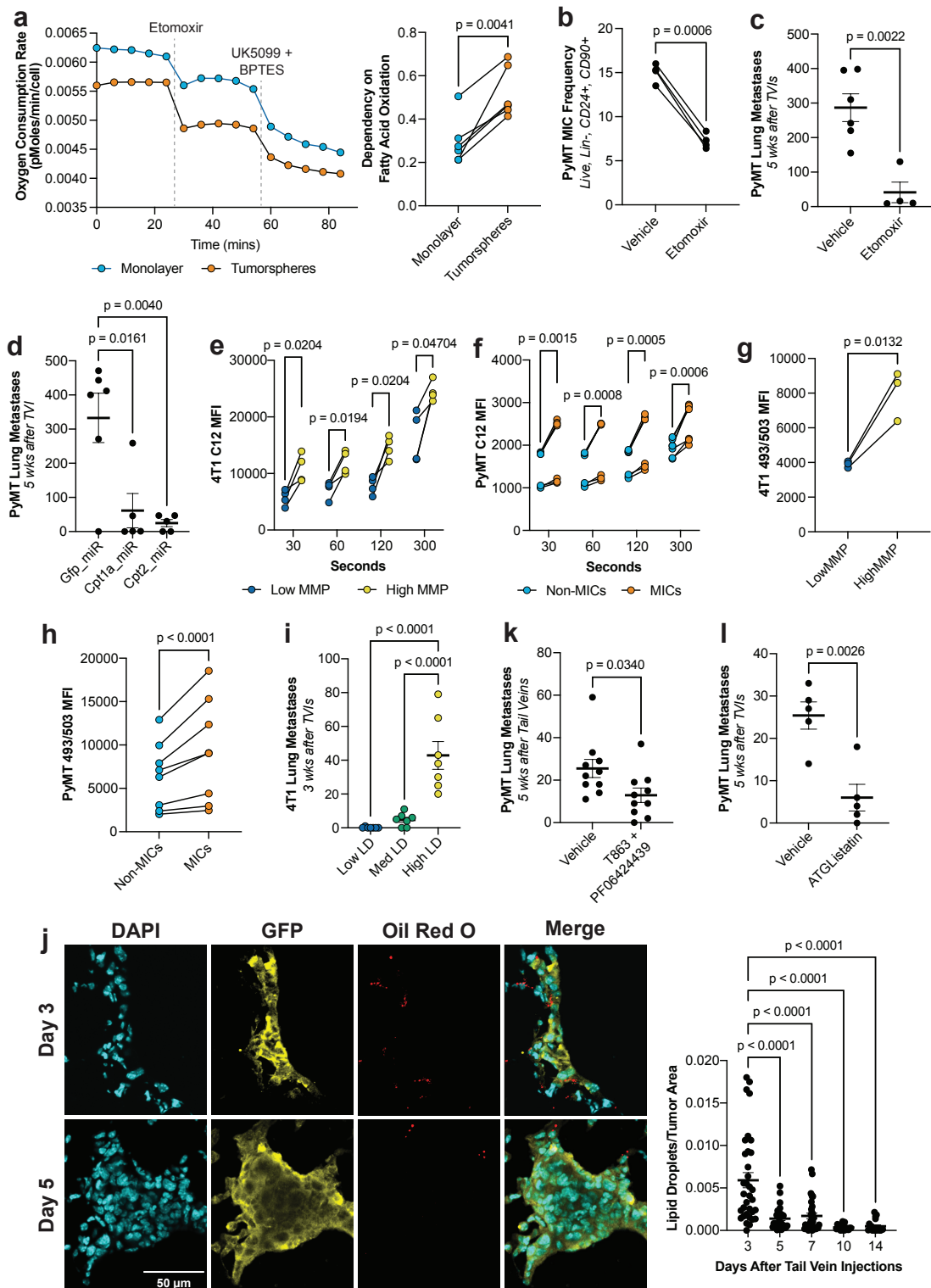
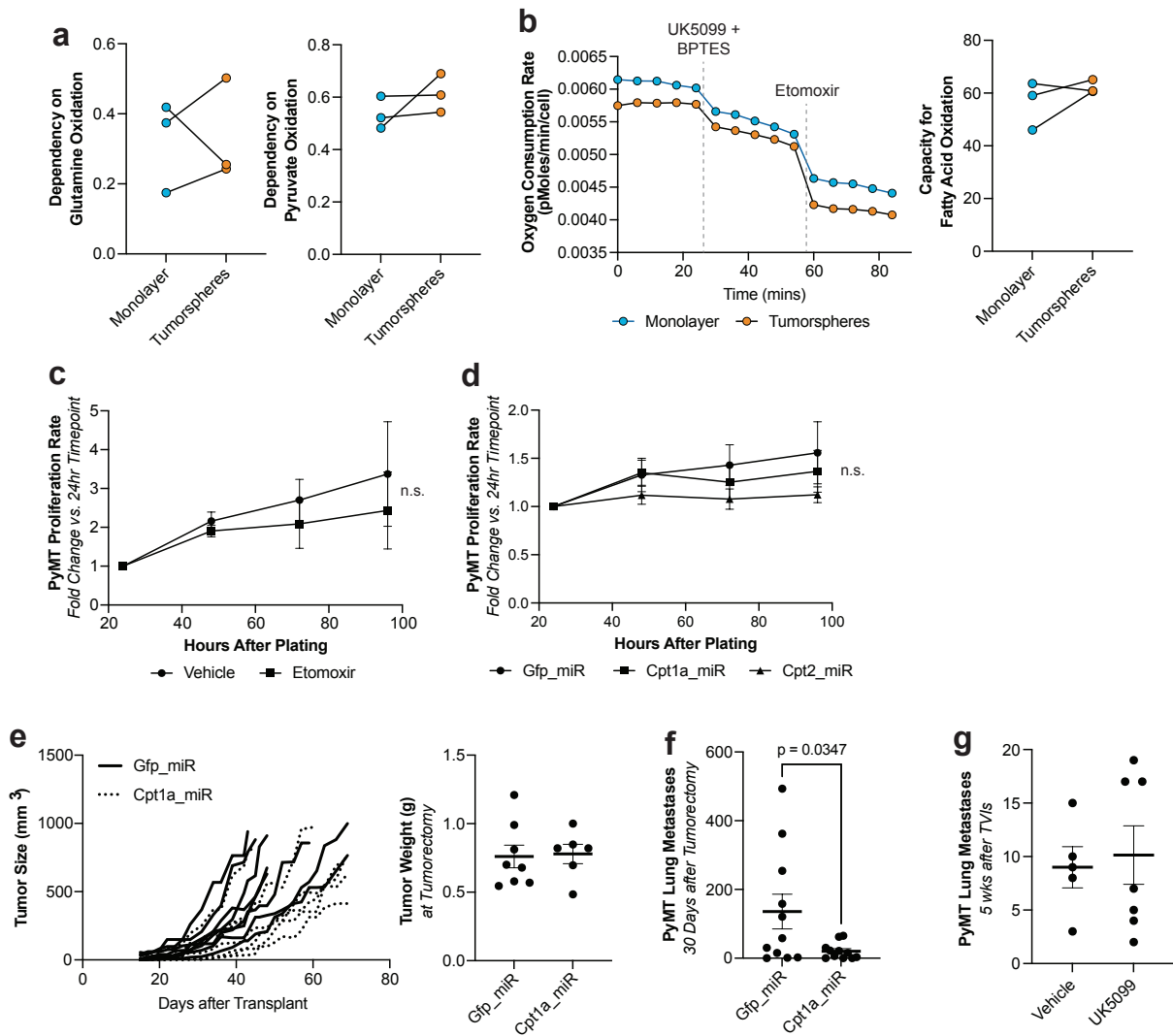


Fig. 9: MICs rely on fatty acid turnover and usage.

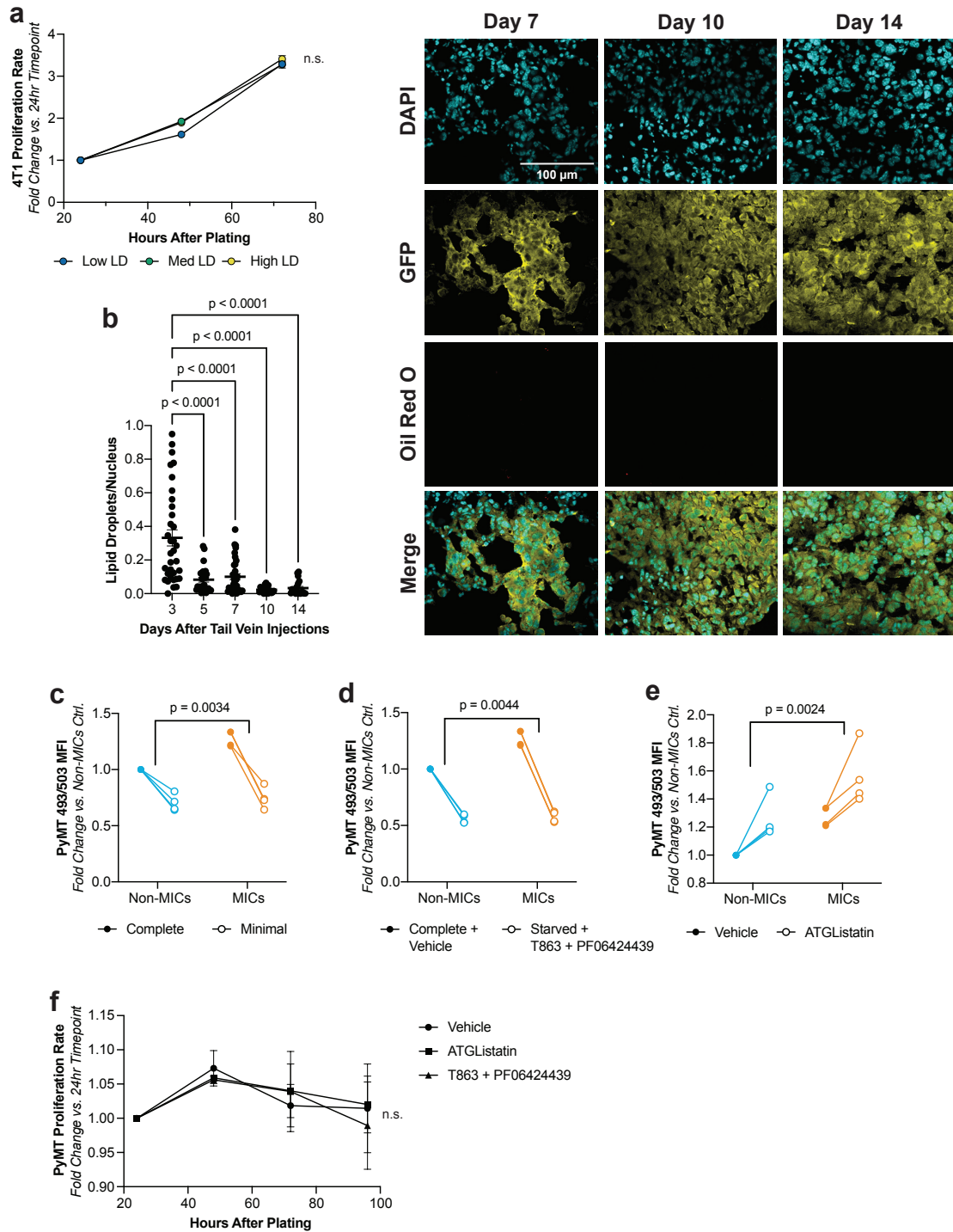
a) Left: normalized OCR over time in tumorsphere- vs. monolayer-grown cells. Right: dependence on LCFA oxidation calculated as described in the methods ($n \geq 3^a$, paired t-test) b) PyMT MIC frequency after treatment with etomoxir. ($n=4^a$, paired t-test) c) Number of lung metastases in recipient wildtype (wt) FVB/N mice after TVI of PyMT cells treated with etomoxir. ($n=5$, unpaired t-test) d) Number of lung metastases in recipient mice after TVI of PyMT cells containing miR-mediated KDs of Gfp, Cpt1a, and Cpt2. 84% KD efficiency for Cpt1a and Cpt2. ($n \geq 5$, unpaired t-test) e) LCFA uptake measured by MFI of 4T1 cells sorted for low and high MMP after BODIPY FL C12 staining for specified durations. ($n=4^a$, paired t-test) f) LCFA uptake measured by MFI of ex vivo PyMT non-MICs vs. MICs after BODIPY FL C12 staining for specified durations. ($n=7^a$, paired t-test) g) Lipid stores measured by MFI of 4T1 cells sorted for low and high MMP after BODIPY 493/503 staining. ($n=3^a$, paired t-test) h) Lipid stores measured by MFI of ex vivo PyMT non-MICs vs. MICs after BODIPY 493/503 staining. ($n=3^a$, paired t-test) i) Number of lung metastases in recipient wt Balb/c mice after TVI of 4T1 cells sorted for low, med, and high levels of lipid droplets. ($n=7$, ordinary one-way ANOVA followed by Tukey's test) j) Number of lipid droplets measured by oil red O, normalized to tumor area for the specified timepoints after TVI of GFP+ 4T1 cells into recipient DEREK mice. Left: representative images from each timepoint. Right: quantification ($n \geq 18$, one-way ANOVA followed by Dunnett's test). k) Number of lung macrometastases in recipient mice after TVI of PyMT cells treated with T863 and PF-06424439. ($n=10$, unpaired t-test) l) Number of lung macrometastases in recipient mice after TVI of PyMT cells treated with ATGListatin ($n=5$, unpaired t-test). MFI = mean fluorescence intensity. Paired t-test were two-tailed and by ratio. Unpaired t-test were parametric and two-tailed. Values shown correspond to means \pm SEM. Source data are provided in the source data file. ^a signifies number of independent experiments or tumors.



Supplementary Fig. 2: MICs specifically rely on fatty acid usage for metastasis and not for proliferation

a) Dependence on glutamine (left) and pyruvate (right) oxidation calculated as described in the methods. (n=3^a, paired t-test) b) Left: OCR over time during a mito fuel flex test in tumorsphere- vs. monolayer-grown cells (normalized to cell number). Right: capacity to undergo LCFA oxidation calculated as described in the methods. (n=3^a, paired t-test) c) Proliferation rates of PyMT cells after treatment with etomoxir. (n=3^a, unpaired t-test) d) Proliferation rates of PyMT cells containing KDs of Gfp, Cpt1a, and Cpt2. (n=6^a, unpaired t-test) e) Left: growth rates of tumors containing miR-mediated KDs of Gfp or Cpt1a. 72% KD efficiency for Cpt1a. Right: tumor weights at time of sacrifice. (n≥7, representative of two independent experiments, unpaired t-test) f) Resulting spontaneous macrometastases 30 days after removal of tumors containing miR-mediated KDs of Gfp or Cpt1a. (n=11, combination of two independent experiments, unpaired t-test) g) Lung metastases in recipient wildtype FVB/N mice after tail vein injection of PyMT cells treated with vehicle or UK5099. (n=5, n=7, respectively, unpaired t-test. MFI = mean fluorescence intensity. Paired t-test were two-tailed and by ratio. Unpaired t-test were parametric and two-tailed. Values shown correspond to means +/- SEM. Source data are provided in the source data file. ^a signifies number of independent experiments or tumors.

Supplementary Figure 3



Supplementary Fig. 3: MICs have enhanced lipid droplet dynamics

a) Proliferation rates of 4T1 cells sorted for low, med, and high BODIPY 493/503 MFI normalized to the first measured timepoint. (n=3, ordinary one-way ANOVA) b) Number of lipid droplets, measured by oil red O staining, normalized to number of detected nuclei, measured by DAPI staining at specified timepoints after TVI of GFP+ 4T1 cells into recipient DEREK mice. Right: representative images from each timepoint. (n≥18, ordinary one-way ANOVA followed by Dunnett's test) c) Change in lipid stores in PyMT MICs vs. non-MICs upon starvation for 48 hours. (n=4^a, paired t-test of differences between minimal and complete media conditions) d) Change in lipid stores in PyMT MICs vs. non-MICs upon starvation and inhibition of lipid droplet generation (using T863 and PF-06424439) for 48 hours. (n=4^a, paired t-test of differences between complete media with vehicle control and minimal media with inhibitor conditions) e) Change in lipid stores in PyMT MICs vs. non-MICs upon inhibition of lipolysis via treatment with ATGLinistatin for 48 hours. (n=4^a, paired t-test of differences between complete media with vehicle control and minimal media with inhibitor conditions) f) Proliferation rates of PyMT cells after pre-treatment with vehicle, ATGLinistatin, or T863 and PF-06424439. (n=3^a, unpaired t-test). Paired t-test were two-tailed and by ratio. Unpaired t-test were parametric and two-tailed. Values shown correspond to means +/- SEM. Source data are provided in the source data file. ^a signifies number of independent experiments or tumors.

Modulating acetyl-CoA generation and availability alters metastatic capacity

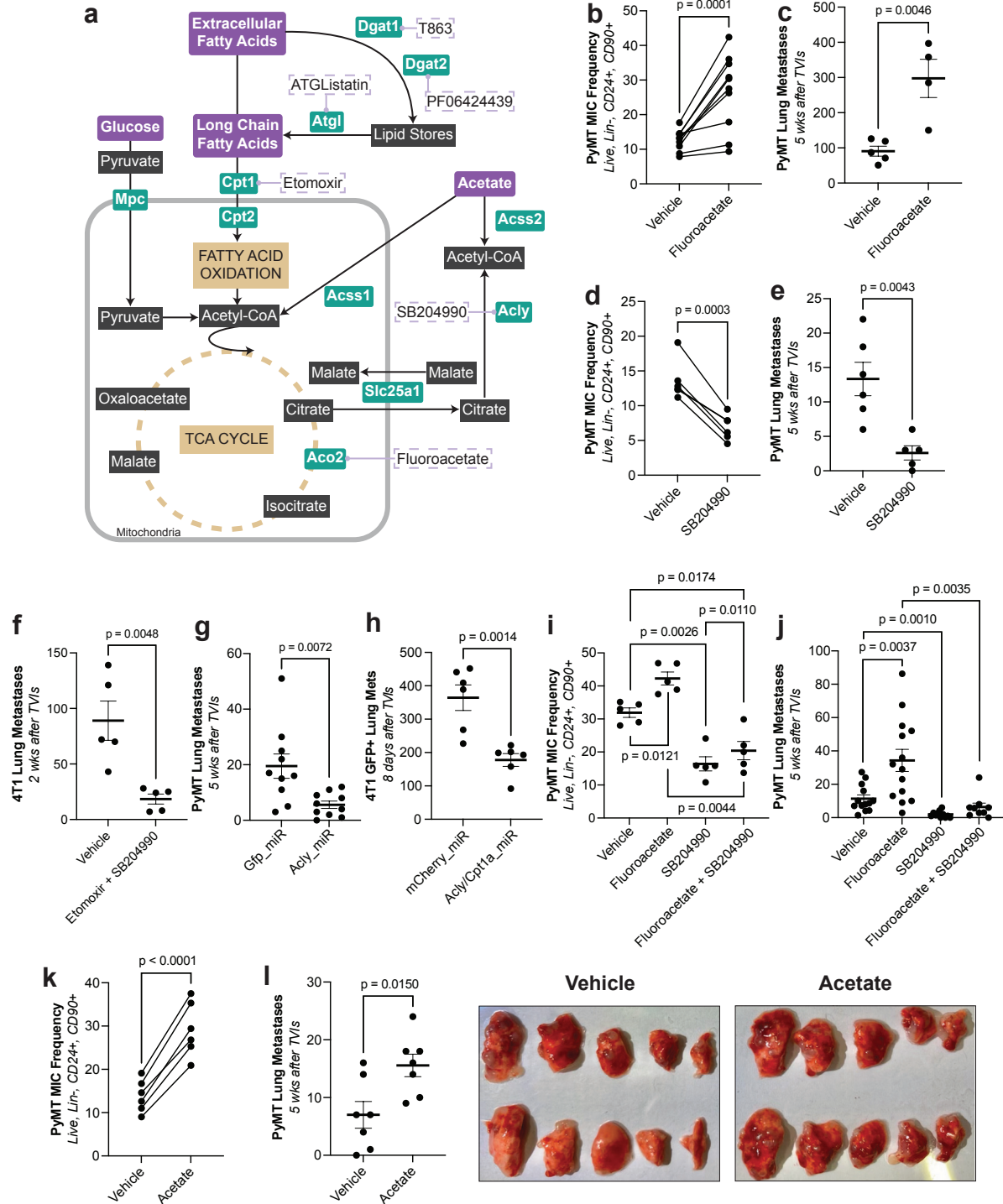
The data thus far showed that MICs preferentially utilize OXPHOS in contrast to glycolysis with enhanced dependency on FAO. Davis and collaborators had suggested that ATP generation may limit metastasis²²³. However, when PyMT and 4T1 cells were pre-treated with oligomycin to block mitochondrial ATP generation, metastasis formation was not reduced (**Supplementary Fig. 4a, b**). Further, when comparing oxygen consumption rates (OCR) as a proxy for ATP generation between tumorspheres and monolayer grown cells, we also observed no differences (**Supplementary Fig. 4c**). When inhibiting aconitase 2 (ACO2) which converts citrate to isocitrate in the mitochondrial TCA cycle (**Fig. 10a**) using fluoroacetate as pre-treatment, this increased both MIC frequency and metastatic capacity in both PyMT (**Fig. 10b, c**) and 4T1 cells (**Supplementary Fig. 4d**). Fluoroacetate causes accumulation of citrate²²⁴ (**Supplementary Fig. 4e**) which can be exported from mitochondria and converted to acetyl-CoA by ACLY. Using an inhibitor against ACLY (SB204990) as pre-treatment, this resulted in a significant reduction of MIC frequency (**Fig. 10d**) and metastasis in the PyMT model (**Fig. 10e**), and reduced metastasis when combined with etomoxir in the 4T1 model (**Fig. 10f**). These results were confirmed using miR-mediated KDs in both models (**Fig. 10g, h**). This

reduction in metastasis and MIC frequency by ACLY inhibition was rescued by the combined treatment with fluoroacetate (**Fig. 10i, j, Supplementary Fig. 4f**). Due to the reduction of metastasis, we observed by blocking ACLY, we then hypothesized that the generation of acetyl-CoA may be limiting for metastatic colonization. To test this, we increased the availability of acetyl-CoA by adding acetate, which gets converted into acetyl-CoA by ACSS1 and ACSS2, to the cell culture media. Acetylcarnitine, which has also been shown to support histone acetylation by serving as another acetyl-CoA precursor²²⁵, was confirmed to increase upon acetate treatment (**Supplementary Fig. 4g**). Cells that had been pre-treated with acetate prior to TVI, showed an increase of MIC frequency and metastasis, both in the PyMT (**Fig. 10k, l**) and the 4T1 models, although optimally at a concentration of 5 mM (**Supplementary Fig. 4h**). Further, TVI of cells with KDs of *Acss1* and *Acss2* resulted in reduced metastasis formation (**Supplementary Fig. 4i, j**). In all the cases described, we did not observe significant alterations in proliferation upon treatment or KD (**Supplementary Fig. 4k-n**). Overall, these data indicated that enhanced mitochondrial activity in MICs reflects an increased requirement for acetyl-CoA derived from citrate released from mitochondria into the cytoplasm.

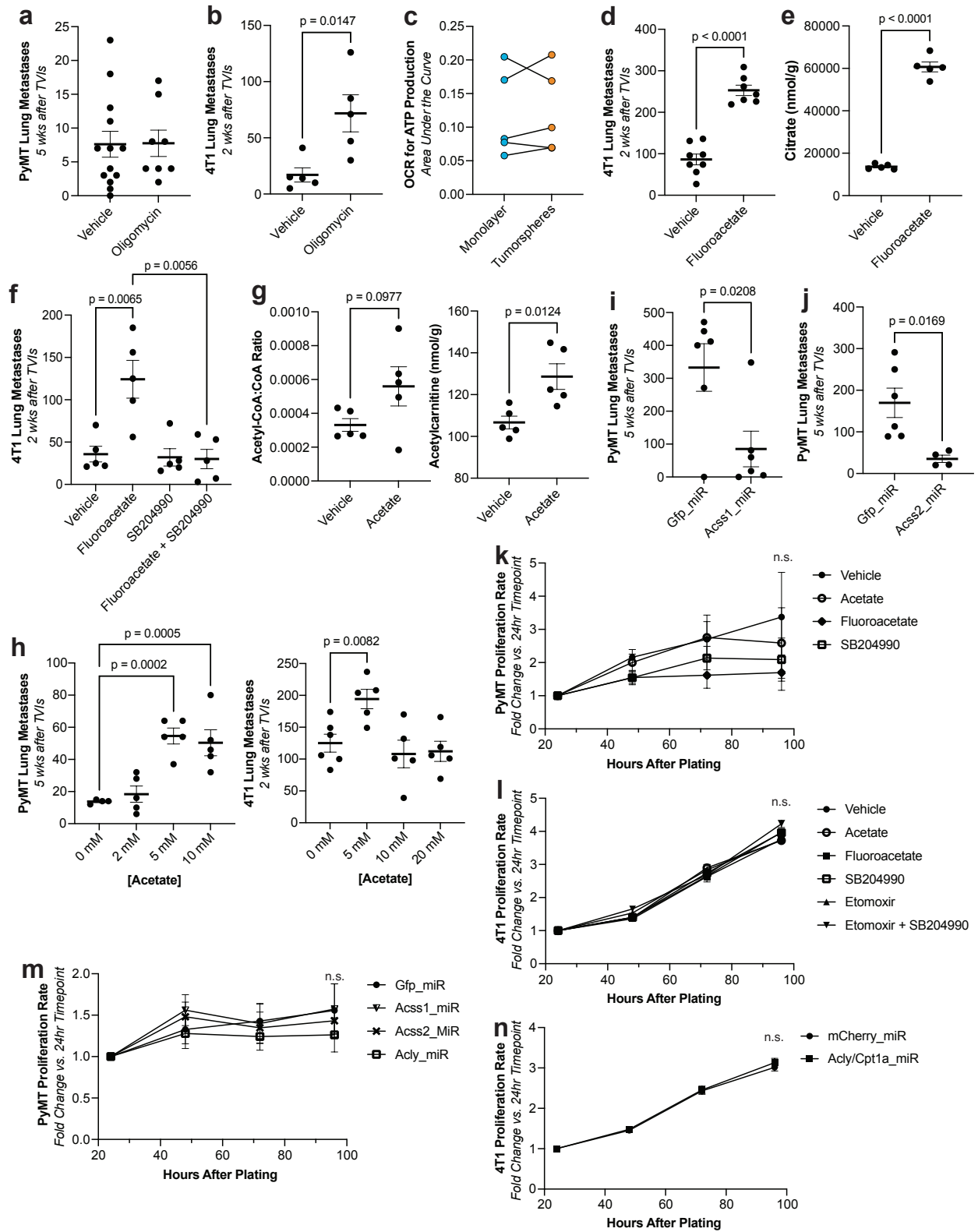
Fig. 10: MICs rely on pathways that generate acetyl-CoA.

*a) Diagram of the relevant metabolic pathways and their respective inhibitors. b) PyMT MIC frequency after treatment with fluoroacetate. (n=10^a, paired t-test) c) Lung metastases in recipient wildtype (wt) FVB/N mice after TVI of PyMT cells treated with vehicle or fluoroacetate. (n=5, n=4, respectively, unpaired t-test) d) PyMT MIC frequency after treatment with vehicle or SB204990. (n=6^a, paired t-test) e) Lung metastases in recipient wt FVB/N mice after TVI of PyMT cells treated with vehicle or SB204990. (n=6, n=5, respectively, unpaired t-test) f) Lung metastases in recipient wt Balb/c mice after TVI of 4T1 cells treated with vehicle or etomoxir and SB204990. (n=5, unpaired t-test) g) Lung metastases in recipient wt FVB/N mice after TVI of PyMT cells containing miR-mediated KDs of *Gfp* or *Acly*. 77% KD efficiency for *Acly*. (n=10, unpaired t-test) h) GFP+ lung metastases in recipient *Rag2*^{-/-}*γc*^{-/-} mice after TVI of GFP+ 4T1 cells containing miR-mediated KDs of *mCherry* or *Acly* and *Cpt1a*. 84% KD efficiency for *Acly* and 71% KD efficiency for *Cpt1a*. (n=6, unpaired t-test) i) PyMT MIC frequency after treatment with vehicle or fluoroacetate +/- SB204990. (n=5^a, paired t-test) j) Lung metastases in recipient wt FVB/N mice after TVI of PyMT cells treated with vehicle or fluoroacetate +/- SB204990. (n≥9, unpaired t-test) k) PyMT MIC frequency after treatment with acetate. (n=6^a, paired t-test) l) Lung metastases in recipient wt FVB/N mice after TVI of PyMT cells treated with vehicle or acetate. Left: quantification. Right: representative images of lung metastases of recipient mice. (n=7, unpaired t-test). Paired t-test were two-tailed and by ratio. Unpaired t-test were parametric and two-tailed. Values shown correspond to means +/- SEM. Source data are provided in the source data file. ^a signifies number of independent experiments or tumors.*

Figure 10



Supplementary Figure 4



Supplementary Fig. 4: Dependence on acetyl-CoA generation pathways are not due to ATP or proliferation

a) Lung metastases in recipient wildtype (wt) FVB/N mice after TVI of PyMT cells treated with oligomycin. (n=13, n=8, respectively, unpaired t-test) b) Lung metastases in recipient wt Balb/c mice after TVI of 4T1 cells treated with oligomycin. (n=5, unpaired t-test) c) Area under the OCR curve corresponding to ATP production for monolayer- vs. tumorsphere-grown cells during the mito stress test. (n=5^a, paired t-test) d) Lung metastases in recipient wt Balb/c mice after TVI of 4T1 cells treated with fluoroacetate. (n=8, n=7, respectively, unpaired t-test) e) Citrate concentration in 4T1 cells after treatment with fluoroacetate. (n=5, unpaired t-test) f) Lung metastases in recipient wt Balb/c mice after TVI of 4T1 cells treated with fluoroacetate +/- SB204990. (n=5, unpaired t-test) g) Acetyl-CoA to CoA ratio (left) and acetylcarnitine concentration (right) in 4T1 cells after acetate treatment. (n=5, unpaired t-test) h) Lung metastases in recipient wt Balb/c mice after TVI of PyMT (left) and 4T1 (right) cells treated with acetate. (n=8, unpaired t-test) i) Lung metastases in recipient wt FVB/N mice after TVI of PyMT cells containing miR-mediated KDs of Gfp or Acss1. 87% KD efficiency for Acss1. (n=6, unpaired t-test) j) Lung metastases in recipient wt FVB/N mice after TVI of PyMT cells containing miR-mediated KDs of Gfp or Acss2. 89% KD efficiency for Acss2. (n=6, n=4, respectively, unpaired t-test) k) Proliferation rate of PyMT cells after respective treatments normalized to the first timepoint. (n=3^a, unpaired t-test) l) Proliferation rate of 4T1 cells after respective treatments normalized to the first timepoint. (n=6, unpaired t-test) m) Proliferation rate of PyMT cells containing miR-mediated KDs of listed genes normalized to the first timepoint. (n=6^a, unpaired t-test) n) Proliferation rate of 4T1 cells containing miR-mediated KDs of mCherry or Aclly and Cpt1a normalized to the first timepoint. 84% KD efficiency for Aclly, 71% KD efficiency for Cpt1a. (n=6, unpaired t-test). Paired t-test were two-tailed and by ratio. Unpaired t-test were parametric and two-tailed. Values shown correspond to means +/- SEM. Source data are provided in the source data file. ^a signifies number of independent experiments or tumors.

MICs show enhanced requirement for acetyl-CoA supply to control histone acetylation

Since acetyl-CoA is a cofactor for histone acetylation, we sought to examine if the reliance of MICs on acetyl-CoA may be due to global alterations in epigenetic modifications between MICs and non-MICs. We observed a significant increase of the activating mark of promoters and enhancers, H3K27ac, in endogenous PyMT MICs vs. non-MICs (**Fig. 11a**). In the 4T1 model, we also observed that the cells that have the highest MMP and metastatic potential are also those that have the highest H3K27ac levels (**Fig. 11b**). Further, if we pre-treat cells with inhibitors that block writers and readers of H3K27ac (C646 for p300 and JQ1 for BET family members, respectively) and again perform TVI, we can significantly reduce the MIC frequency

and number of metastases formed (**Fig. 11c - e**) without significantly impacting proliferative potential (**Supplementary Fig. 5a**).

We therefore extended these measurements of H3K27ac to treatments that we had identified to reduce metastatic capacity and are involved in acetyl-CoA generation. In the PyMT model, we observed a significantly reduced level of H3K27ac upon *Acly* and *Cpt1a* inhibition either by pharmacological inhibitors (**Fig. 11f**) or miR-mediated KDs (**Supplementary Fig. 5b**). In contrast, acetate treatment, which increases metastatic capacity, increased H3K27ac (**Fig. 11f**). Similarly, in the 4T1 model, H3K27ac increased upon acetate treatment, reduced upon combined etomoxir and SB204990 treatment, and the combination of all three rescued the acetylation levels back to vehicle-treated controls (**Fig. 11g**). In addition, we can prevent the acetate-induced increase of MIC frequency in the PyMT model (**Fig. 11h, i, k**) and acetate-induced metastatic capacity in the 4T1 model with the addition of etomoxir, SB204990, or JQ1 (**Fig. 11j, l, Supplementary Fig. 5c, d**) without severely impacting proliferative potential (**Supplementary Fig. 5e**). These data suggest that in MICs, the supply of acetyl-CoA is rate-limiting in controlling epigenetic events which drive the metastatic cascade. Since there are many sources of acetyl-CoA in cells (lipid catabolism, citrate export from mitochondria to the cytoplasm, uptake of short chain fatty acids, recycling of acetyl groups after histone deacetylation, etc.) with often limited metabolic capacity, the contributions deriving from individual sources are likely additive and may partially compensate for each other. As we show now, increased mitochondrial activity aids metastasis, at least in part, by adding to the acetyl-CoA pool to allow for histone acetylation.

Figure 11

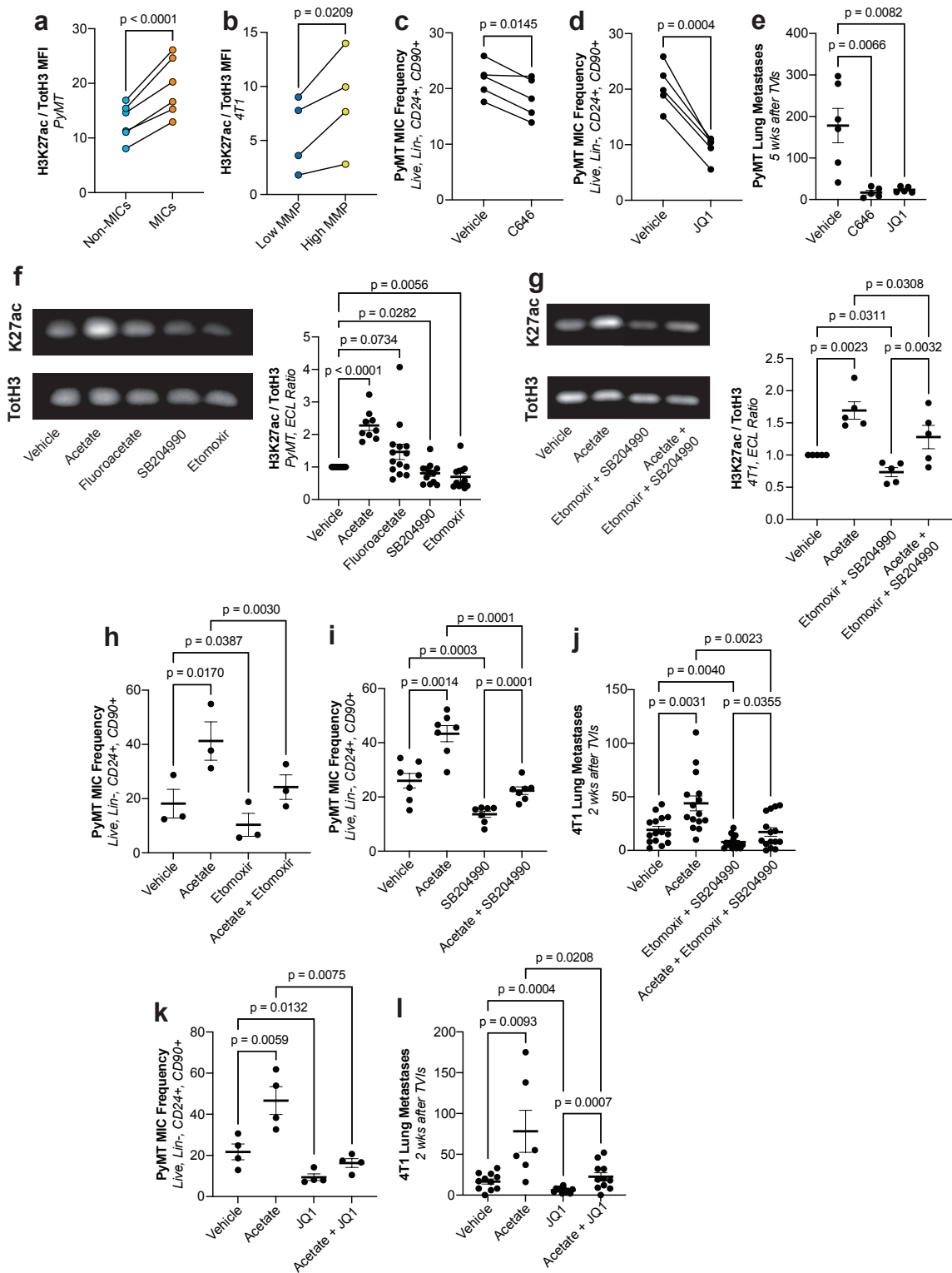


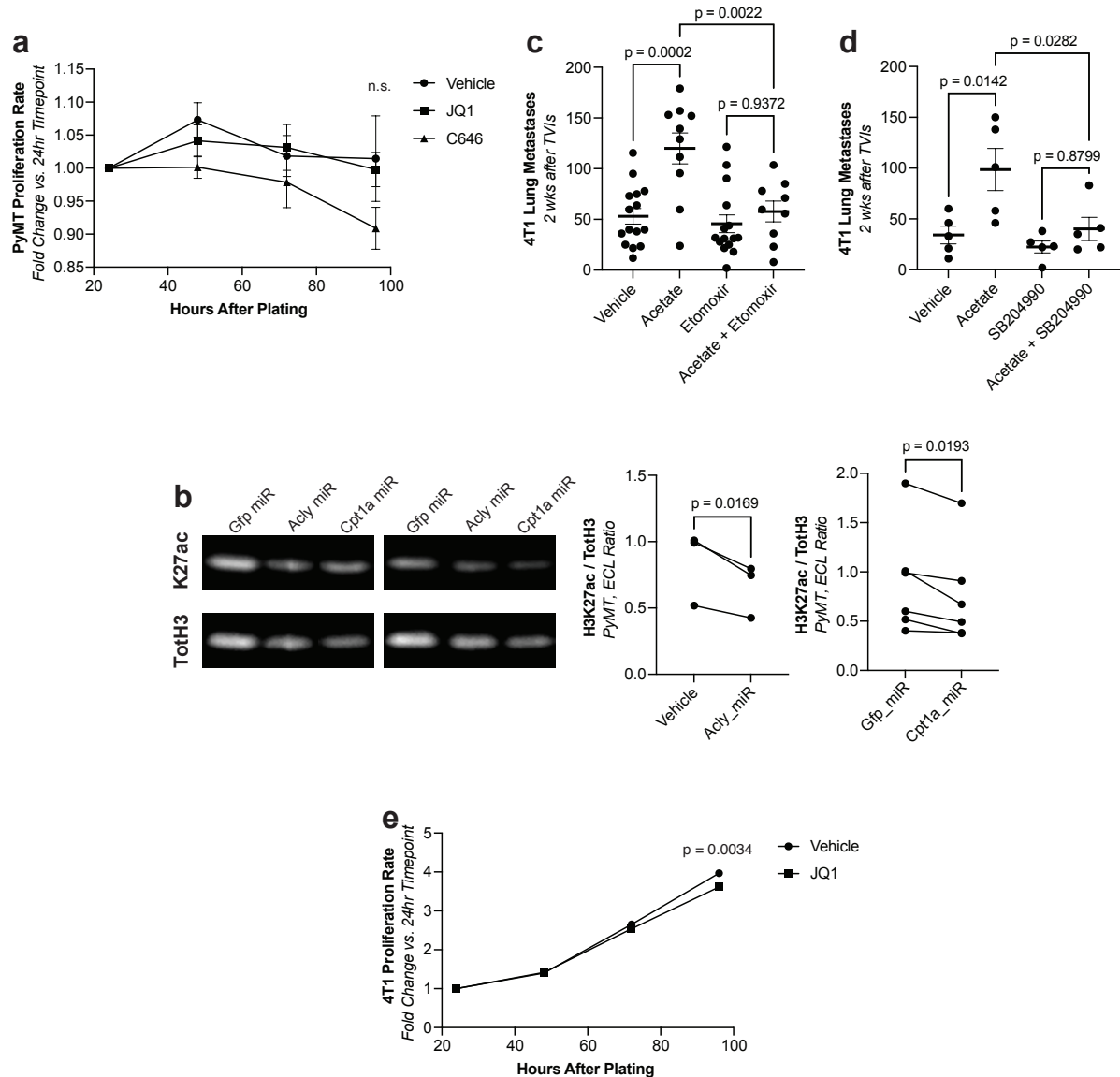
Fig. 11: Metabolism supports histone acetylation to facilitate metastatic capacity in MICs.

a) H3K27ac levels normalized to total histone 3 (TotH3) measured by flow cytometry in *ex vivo* PyMT non-MICs vs. MICs. ($n=6^a$, paired t-test) b) H3K27ac levels normalized to total histone 3 (TotH3) measured by flow cytometry in 4T1 cells sorted for high vs. low MMP. ($n=4^a$, paired t-test) c) MIC frequency in PyMT cells after treatment with vehicle or C646. ($n=5^a$, paired t-test) d) MIC frequency in PyMT cells after treatment with vehicle or JQ1. ($n=5^a$, paired t-test) e) Lung metastases in recipient wt FVB/N mice after TVI of PyMT cells treated with JQ1 or C646. ($n\geq 5$, unpaired t-test) f) Left: representative Western blot from PyMT cells treated with vehicle, acetate, fluoroacetate, SB204990, or etomoxir. Right: quantification of ratio of H3K27ac (K27ac) signal vs. total histone 3 (TotH3) signal, expressed as the fold change over vehicle treated cells. ($n\geq 9^a$, paired t-test) g) Left: representative Western blot from 4T1 cells treated with vehicle, acetate, etomoxir + SB204990, or acetate + etomoxir + SB204990. Right: quantification of ratio of H3K27ac (K27ac) signal vs. total histone 3 (TotH3) signal, expressed as the fold change over vehicle treated cells. ($n=5^a$, paired t-test) h) MIC frequency in PyMT cells after treatment with vehicle or acetate +/- etomoxir. ($n=3^a$, paired t-test) i) MIC frequency in PyMT cells after treatment with vehicle or acetate +/- SB204990. ($n=7^a$, paired t-test) j) Lung metastases in recipient wt Balb/c mice after TVI of 4T1 cells after treatment with vehicle, acetate, etomoxir + SB204990, or acetate + etomoxir + SB204990. ($n=15$, unpaired t-test) k) MIC frequency in PyMT cells after treatment with vehicle or acetate +/- JQ1. ($n=4^a$, paired t-test) l) Lung metastases in recipient wt Balb/c mice after TVI of 4T1 cells after treatment with vehicle or acetate +/- JQ1. ($n\geq 6$, paired t-test). Paired t-test were two-tailed and by ratio. Unpaired t-test were parametric and two-tailed. Values shown correspond to means +/- SEM. Source data are provided in the source data file. ^a signifies number of independent experiments or tumors.

Supplementary Fig. 5: Blocking acetyl-CoA generation and writing and reading of H3K27ac reduces metastasis without affecting proliferative capacity

a) Proliferation rates of PyMT cells after treatment with vehicle, JQ1, or C646 normalized to the first measured timepoint. ($n=3^a$, unpaired t-test) b) Left: Representative Western blots from PyMT cells containing miR-mediated KDs of Gfp, Acly, or Cpt1a. Right: Quantification of the ratio of H3K27ac (K27ac) signal vs. total histone 3 (TotH3) signal in PyMT cells containing miR-mediated KDs of Acly (left) or Cpt1a (right) vs. Gfp KD. ($n=3^a$, $n=6^a$, respectively, paired t-test). KD efficiencies are $\geq 70\%$ and $\geq 60\%$, respectively. c) Lung metastases in recipient wt Balb/c mice after TVI of 4T1 cells after treatment with vehicle or acetate +/- etomoxir. ($n\geq 9$, unpaired t-test) d) Lung metastases in recipient wt Balb/c mice after TVI of 4T1 cells after treatment with vehicle or acetate +/- SB204990. ($n=5$, unpaired t-test) e) Proliferation rates of 4T1 cells after treatment with vehicle or JQ1 normalized to the first measured timepoint. ($n\geq 6$, unpaired t-test). Paired t-test were two-tailed and by ratio. Unpaired t-test were parametric and two-tailed. Values shown correspond to means +/- SEM. Source data are provided in the source data file. ^a signifies number of independent experiments or tumors.

Supplementary Figure 5



Increased acetylation on H3K27 induces expression of genes for epithelial-to-mesenchymal transition

To determine how increased acetyl-CoA generation boosts metastasis formation, we performed RNA-sequencing on acetate- vs. vehicle-treated 4T1 cells. Gene-set enrichment analysis revealed that in acetate-treated cells the highest scoring Hallmark gene set is EMT (**Fig. 12a**), and several of the highest scoring Gene Ontology gene sets are related to extracellular matrix remodelling (**Supplementary Fig. 6a**). We also observed the upregulation of the Hallmark EMT gene set in high MMP cells compared to low MMP cells (**Supplementary Fig. 6b**). We validated the

acetate-induced phenotype by performing qPCR of known EMT markers such as collagens, matrix metalloproteases, and integrins. Not only did we see the expected increase of EMT markers in the acetate treatment, but when in combination with either etomoxir, SB204990, etomoxir + SB204990, or JQ1, the expression of these EMT markers returned to baseline levels (**Fig. 12b, Supplementary Fig. 6c**).

To confirm that these gene expression changes are due to increased H3K27ac acetylation, we performed an H3K27ac ChIP-Seq on 4T1 cells that had been treated with acetate, etomoxir, etomoxir + acetate, etomoxir + SB204990, and etomoxir + SB204990 + acetate. We observed increases in the acetylation peaks of several EMT genes of interest such as *Postn*, *Col1a1*, *Sparc*, and *Itga5* in the acetate-treated cells compared to vehicle-treated cells, and reductions in the same genes upon treatment with etomoxir or etomoxir + SB204990 (**Fig 12c, Supplementary Fig. 6d**). Additionally, the reduced peaks that were identified to be associated with EMT genes increased upon combination with acetate (**Fig. 12d; Supplementary Table 1**).

We therefore propose a model wherein MICs upregulate OXPHOS and FAO that generate citrate and acetyl-CoA for heightened H3K27ac. This then enables MICs to increase transcription of EMT-related genes and facilitates metastasis (**Fig. 12e**).

Figure 12

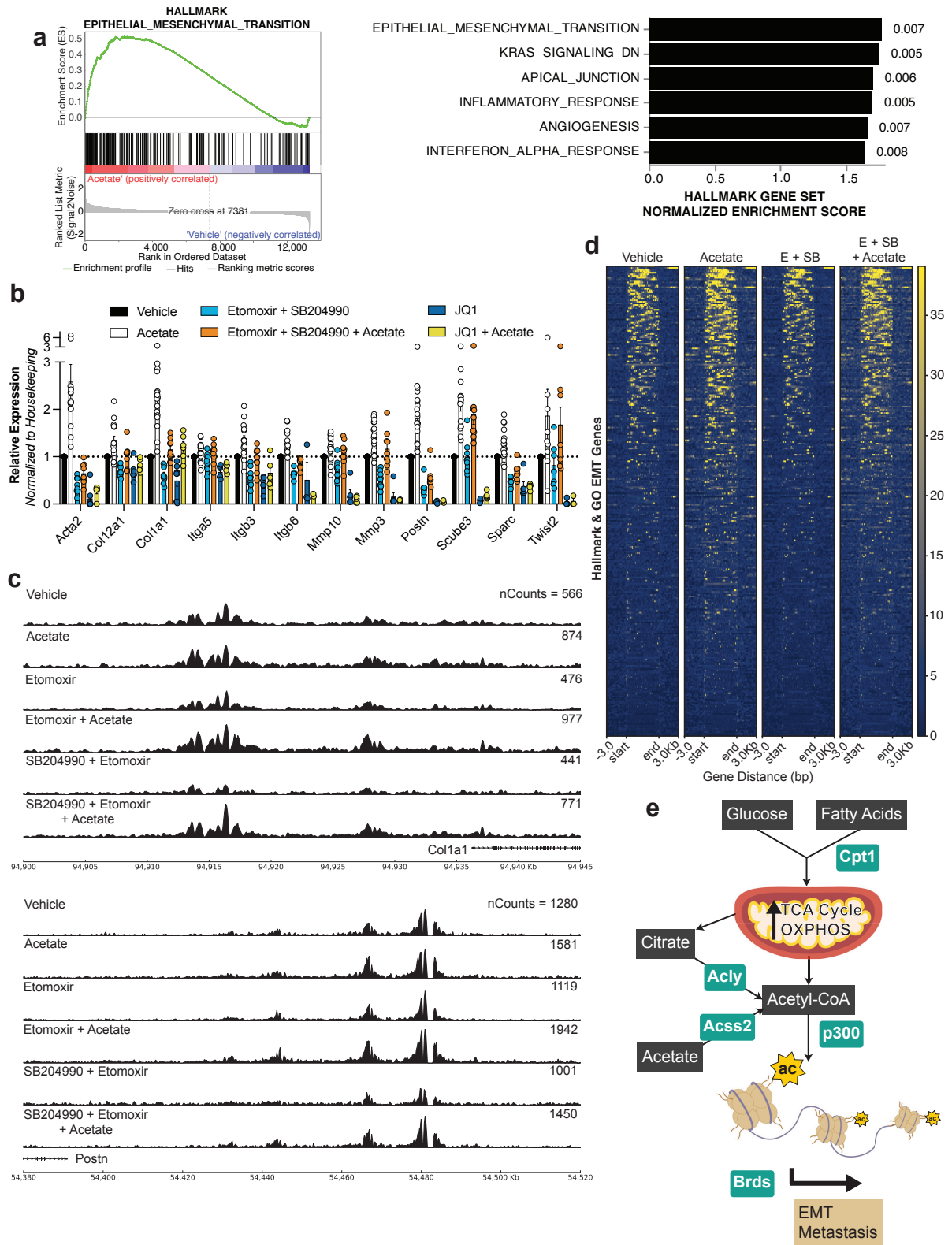


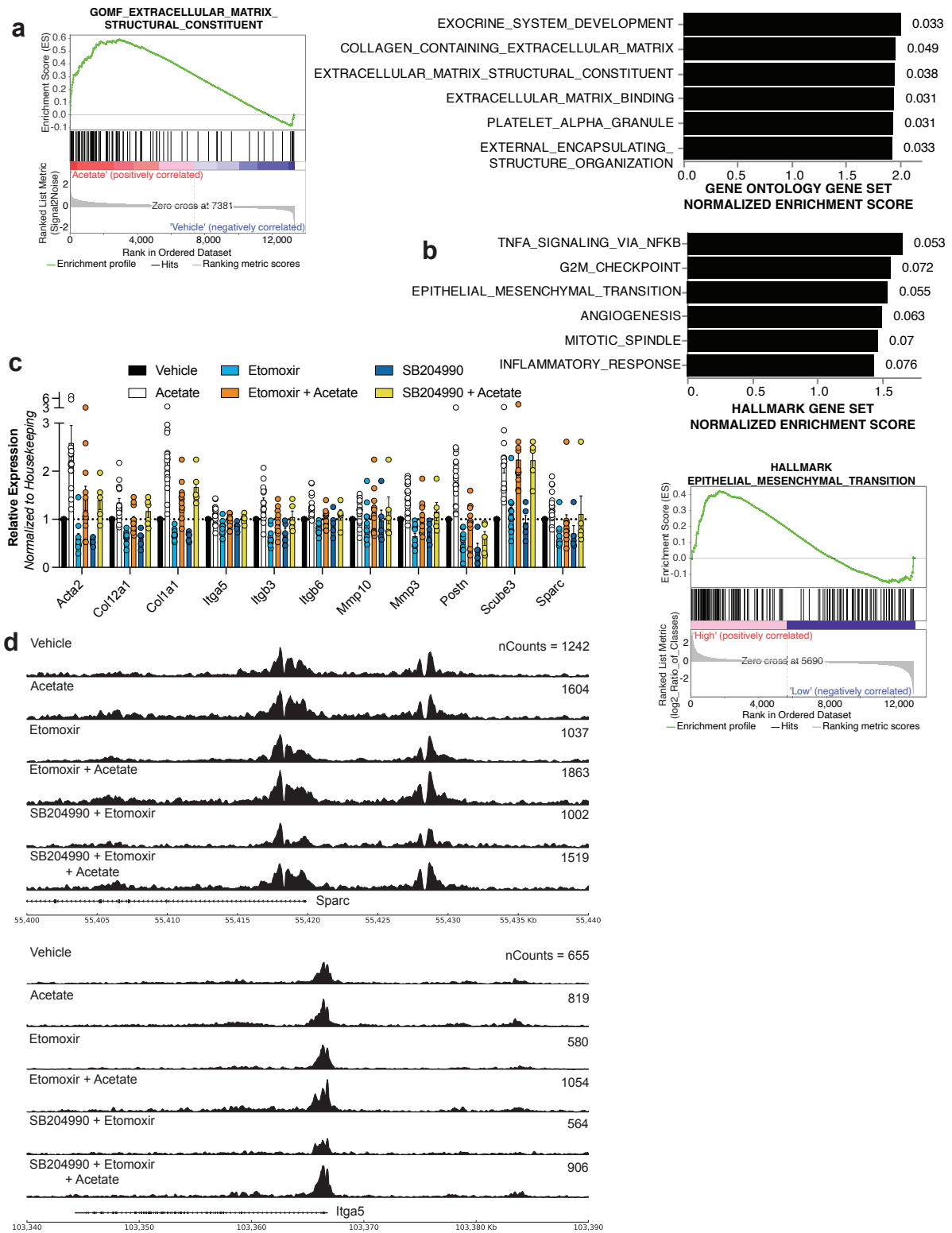
Fig. 12: Metabolism-induced histone acetylation enables expression of EMT-related genes.

a) Left: gene set enrichment plot for the HALLMARK_EPITHELIAL_MESENCHYMAL_TRANSITION signature in acetate- vs. vehicle-treated 4T1. Right: top upregulated gene sets from the Hallmark Collection in the molecular signatures database (mSigDB) in acetate- vs. vehicle-treated 4T1 cells. Numbers beside the bars are the false discovery rates. ($n=4^a$) b) Relative expression of EMT-related genes in 4T1 cells in response to the indicated treatments normalized to housekeeping genes and plotted as a fold change against vehicle-treated. ($n\geq 3^a$) c) H3K27ac ChIP-Seq tracks for Col1a1 (top) and Postn (bottom) from 4T1 cells in response to the indicated treatments. Numbers on the right-hand side of the tracks indicate the associated scaled counts per gene. d) Heatmap of identified H3K27ac chip-seq signals on the regions associated with the EMT genes found in union of the HALLMARK_EPITHELIAL_MESENCHYMAL_TRANSITION and GOBP_EPITHELIAL_TO_MESENCHYMAL_TRANSITION gene sets upon treatment of 4T1 cells with vehicle, acetate, etomoxir (E) + SB204990 (SB), and acetate + E + SB. e) Schematic of the working model proposed. Fuels such as glucose and fatty acids are preferentially utilized in the mitochondria of MICs to generate citrate and acetyl-CoA. Other pathways such as acetate to acetyl-CoA conversion contribute to this pool. Dependence on acetyl-CoA generating pathways is crucial to facilitate the acetylation of histones, particularly on H3K27, for the expression of EMT-related genes & subsequent metastatic capacity. Values shown correspond to means \pm SEM. Source data are provided in the source data file. ^a signifies number of independent experiments or tumors.

Supplementary Fig. 6: Additional data showing increased EMT gene expression mediated by acetyl-CoA generating pathways and histone acetylation

a) Left: gene set enrichment plot for the GOMF_EXTRACELLULAR_MATRIX_STRUCTURAL_COMPONENT signature in 5 mM acetate- vs. vehicle-treated 4T1. Right: top upregulated gene sets from the Gene Ontology Collection in the molecular signatures database (mSigDB) in acetate- vs. vehicle-treated 4T1 cells. Numbers beside the bars are the false discovery rates. ($n=4^a$) b) Top: top upregulated gene sets from the Hallmark Collection in mSigDB in 4T1 cells sorted for high vs. low MMP. Numbers beside the bars are the false discovery rates. Bottom: gene set enrichment plot for the HALLMARK_EPITHELIAL_MESENCHYMAL_TRANSITION in 4T1 cells sorted for high vs. low MMP. ($n=2^a$) c) Relative expression of EMT-related genes in 4T1 cells in response to the indicated treatments normalized to housekeeping genes and plotted as a fold change against vehicle-treated. ($n\geq 5^a$). Values shown correspond to means \pm SEM. d) H3K27ac ChIP-Seq tracks for Sparc (top) and Itga5 (bottom) from 4T1 cells in response to the indicated treatments. Numbers on the right-hand side of the tracks indicate the associated scaled counts per gene. Unpaired t-test were parametric and two-tailed. Values shown correspond to means \pm SEM. Source data are provided in the source data file. ^a signifies number of independent experiments or tumors.

Supplementary Figure 6



Human breast cancer cell lines exhibit a similar dependence on mitochondrial activity and acetyl-CoA for metastasis

To determine if we can observe similar phenotypes in human breast cancer, we first sorted human triple negative breast cancer (TNBC) cells, MDA-MB-231 and BT549, for those with high and low MMP. Just as we observed in the mouse models, the cells with high MMP also had higher levels of lipid uptake (**Fig. 13a, b**) and storage (**Fig. 13c**) in comparison to those with low MMP.

We were also able to reduce the ability of human TNBC cell lines to metastasize by knocking down enzymes that generate acetyl-CoA. We utilized miR-mediated KDs against *ACLY* and *ACSS2* in MDA-MB-231 and observed a significant reduction of metastasis (**Fig. 13d**) without severely compromising proliferative potential (**Supplementary Fig. 7a**). In HCC1806 cells, however, we observed no change in metastatic capacity upon KD of *ACLY* (**Supplementary Fig. 7b**). Considering we had observed a two-fold increase of *ACSS2* expression when knocking down *ACLY* in both HCC1806 and BT20 cells (**Supplementary Fig. 7c**), we surmised that *ACSS2* was acting to compensate for the loss of *ACLY*. *ACSS2* converts acetate to acetyl-CoA in the cytoplasm and nucleus and has been shown to be upregulated when *ACLY* is deficient to maintain intracellular levels of acetyl-CoA²²⁶. We therefore performed TVI with BT20 and HCC1806 cells containing miR-mediated KDs of both *ACLY* and *ACSS2* to avoid this compensation. In this case, we observed that metastasis numbers were reduced (**Fig. 13e, Supplementary Fig. 7d**), again, without affecting proliferation (**Supplementary Fig. 7e, f**). Finally, upon TVI of acetate-treated MDA-MB-231 and BT20 cells, we observed significantly increased numbers of metastatic nodules in the lungs (**Fig. 13f, Supplementary Fig. 7g**).

We then focused on analyzing previously published datasets by the Cancer Cell Line Encyclopedia (CCLE), which had characterized 42 combinations of histone marks in about 900 cell lines²²⁷ and measured the metastatic potential of over 500 cancer cell lines (MetMap)²²⁸. We focused on the MetMap breast cancer cohort where 21 barcoded TNBC cell lines were examined for their metastatic potential. Of these, 20 had corresponding chromatin profiling. Upon comparing these epigenetic patterns to their respective metastatic potential, we observed that only histone marks containing

H3K27ac were repeatedly significantly correlated with metastatic potential (**Fig. 13g, h, Supplementary Table 2**).

Next, we looked at breast cancer patient cohorts to determine if the OXPHOS signature identified in our PyMT MICs vs. non-MICs is predictive of distant relapse-free survival. We therefore stratified a cohort comprising of 50 individual microarray datasets based on their expression of just under 100 OXPHOS signature genes (**Supplementary Table 3**). Consistent with our hypothesis, patients that had higher expression of this signature were more likely to develop distant relapse (**Fig. 13i**). This becomes even more pronounced when performing the analysis only in patients with basal breast cancer as classified by Pam50 (**Supplementary Fig. 7g**). For patients who have not yet received systemic treatment, those who express higher levels of ACLY mRNA are also more likely to develop of distant relapse (**Supplementary Fig. 7h**). Moreover, in both the microarray cohort and the TCGA cohort, patients who have higher expression of CPT1A have a reduced probability of overall survival (**Supplementary Fig. 7i, j**). These data suggest a link between mitochondrial activity, lipid usage, acetyl-CoA generation, and disease progression in breast cancer that is not only evident in our experimental mouse settings, but also in patients.

Figure 13

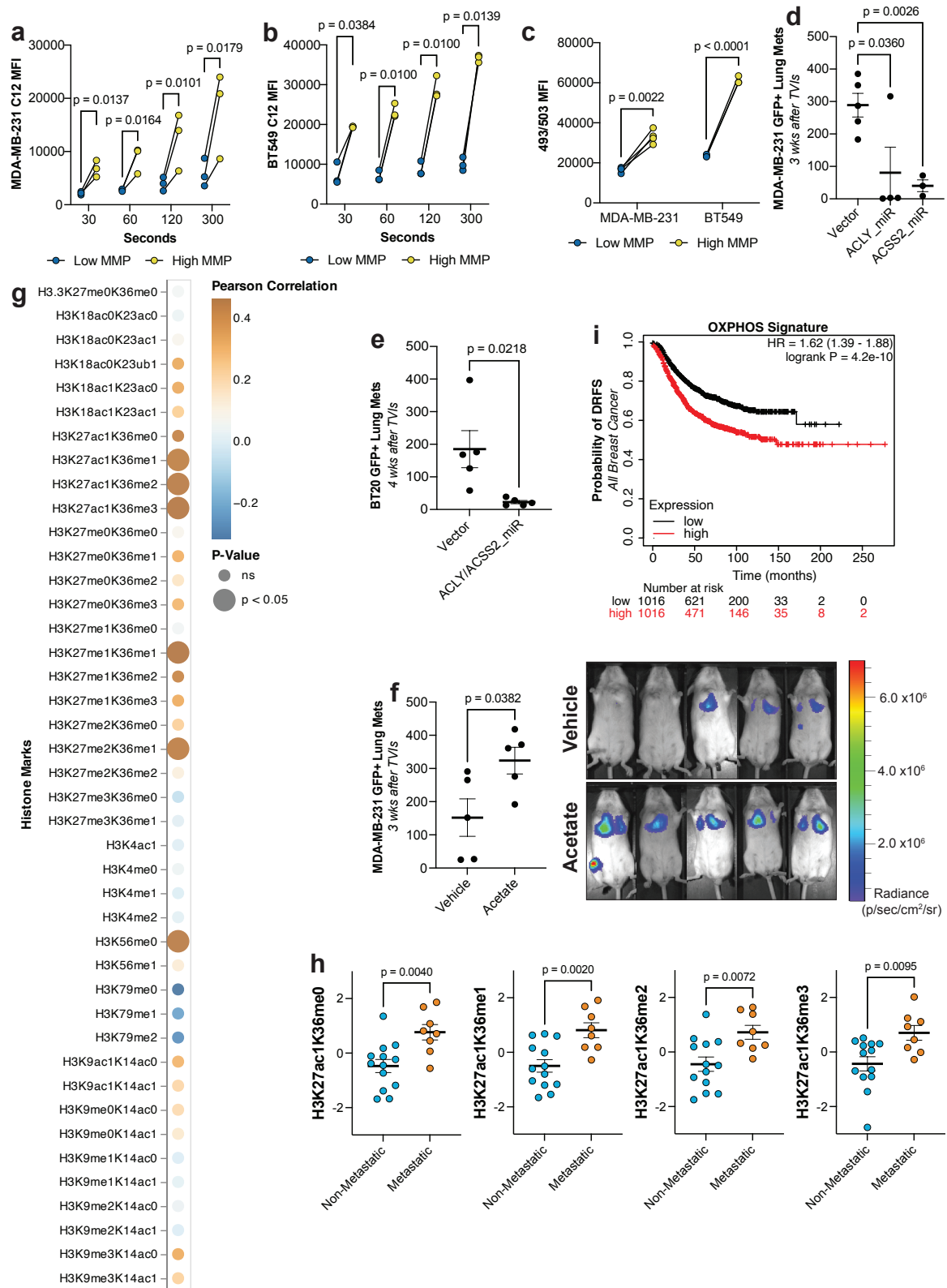
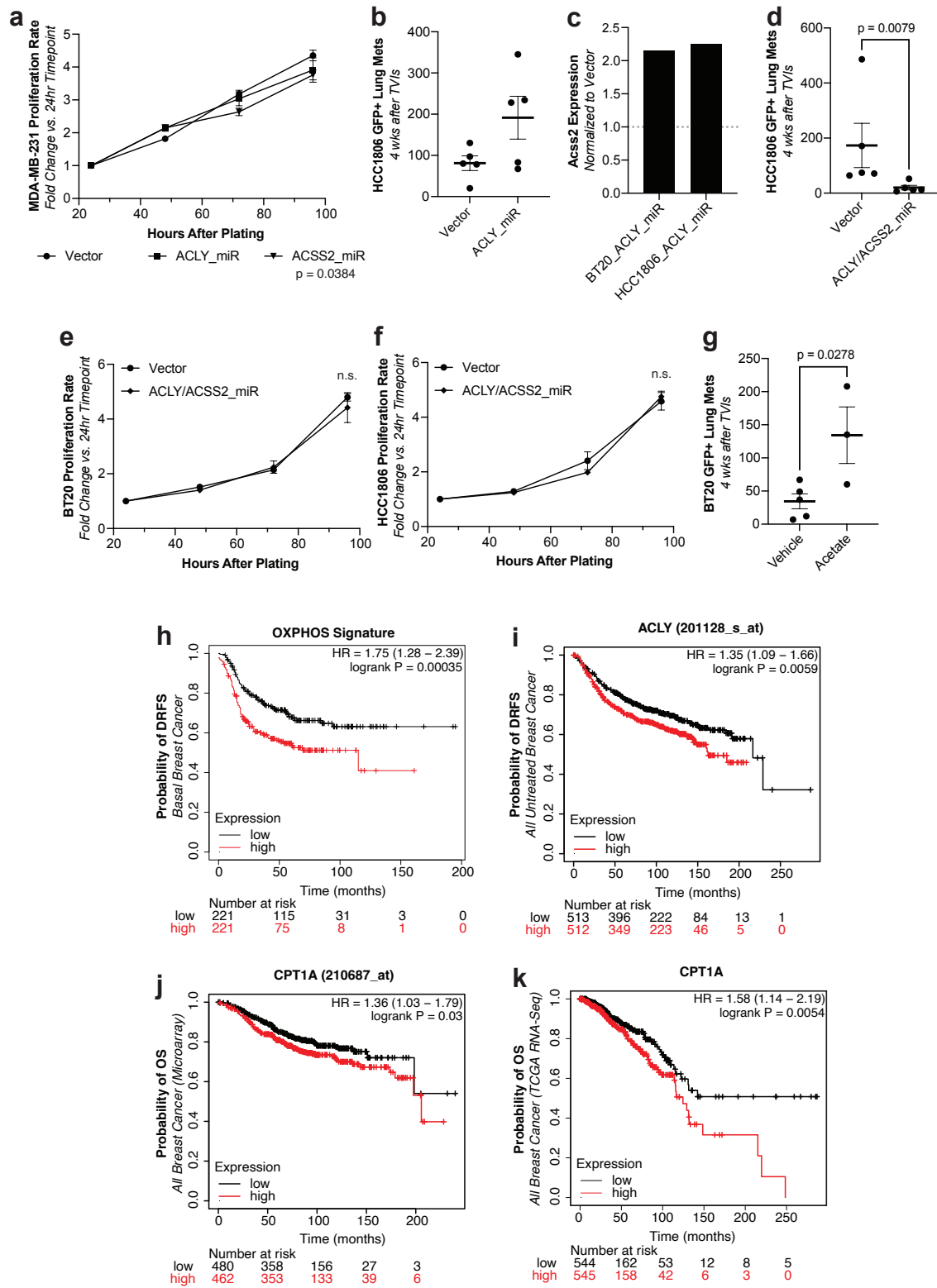


Fig. 13: Metabolic dependencies for mitochondrial activity and acetyl-CoA define metastatic activity in human breast cancer cell lines.

a) LCFA uptake measured by MFI of MDA-MB-231 cells sorted for low and high MMP after exposure to BODIPY FL C12 for specified durations. (n=3^a, paired t-test) b) LCFA uptake measured by MFI of BT549 cells sorted for low and high MMP after exposure to BODIPY FL C12 for specified durations. (n=3^a, paired t-test) c) Lipid stores measured by MFI of MDA-MB-231 and BT549 cells sorted for low and high MMP after staining with BODIPY 493/503. (n=4^a, n=3^a, respectively, paired t-test) d) Number of GFP+ metastases in recipient Rag2^{-/-}γc^{-/-} mice after TVI of MDA-MB-231 cells expressing a vector control or miR-mediated KDs of ACLY or ACSS2. 80% and 75% KD efficiency, respectively. (n=5, n=4, n=3, respectively, unpaired t-test) e) Number of GFP+ metastases in recipient Rag2^{-/-}γc^{-/-} mice after TVI of BT20 cells expressing a vector control or miR-mediated KDs of ACLY and ACSS2. 78% and 73% KD efficiency, respectively. (n=5, unpaired t-test) f) Number of GFP+ lung metastases in recipient Rag2^{-/-}γc^{-/-} mice after TVI of MDA-MB-231 cells treated with vehicle or acetate. Right: Bioluminescence images of mice at day 21 after TVI. (n=5, unpaired t-test) g) Heatmap of Pearson scores and two-tailed p-values calculated by correlating the metastatic potential of 21 TNBC cell lines derived from the MetMap study to their corresponding histone profile generated by the CCLE. h) Scaled quantification of selected histone marks from (g) between metastatic and non-metastatic TNBC cell lines. (n=8, n=13, respectively, unpaired t-test) i) Kaplan-Meier plots depicting distant relapse-free survival (DRFS) of breast cancer patients deriving from the microarray cohort of KM plotter that have been stratified by the mean expression of OXPHOS-related genes and segregated based on the median cut-off. MFI = mean fluorescence intensity. Paired t-test were two-tailed and by ratio. Unpaired t-test were parametric and two-tailed. Values shown correspond to means +/- SEM. Source data are provided in the source data file. ^a signifies number of independent experiments or tumors.

Supplementary Figure 7



Supplementary Fig. 7: Similar dependence on mitochondrial activity and acetyl-CoA generation in human cell lines and patient cohorts

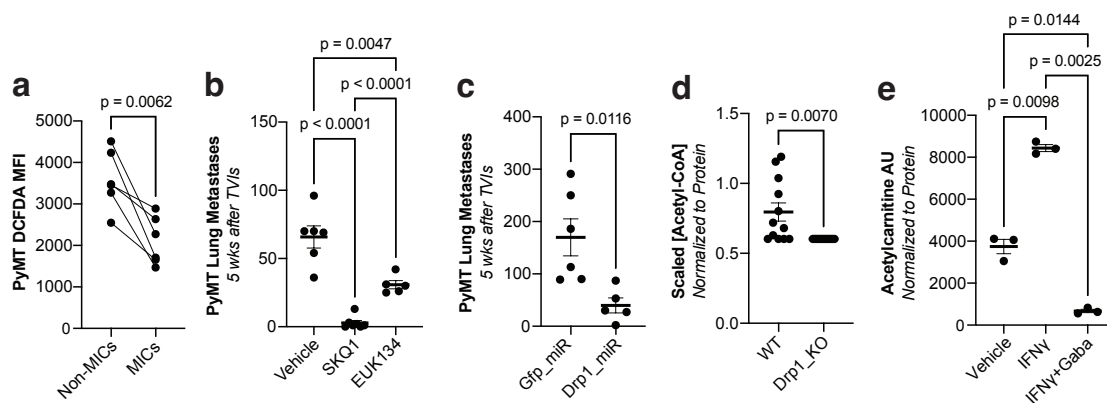
a) Proliferation of MDA-MB-231 cells expressing miR-mediated KDs of ACLY or ACSS2. 80% and 75% KD efficiencies, respectively. Shown as fold change of the first timepoint. (n=4, unpaired t-test) b) GFP+ metastases in recipient Rag2^{-/-}γc^{-/-} mice after TVI of HCC1806 cells expressing miR-mediated KD of ACLY. 83% KD efficiency (n=5, unpaired t-test) c) Relative expression of ACSS2 upon miR-mediated KD of ACLY in BT20 and HCC1806 cells normalized to vector-only controls. 81% and 83% KD efficiencies, respectively. d) GFP+ metastases in recipient Rag2^{-/-}γc^{-/-} mice after TVI of HCC1806 cells expressing miR-mediated KDs of ACLY and ACSS2. 76% and 73% KD efficiencies, respectively. (n=5, unpaired t-test) e) Proliferation of BT20 cells containing miR-mediated KDs of ACLY and ACSS2. 78% and 73% KD efficiencies, respectively. Shown as fold change of the first timepoint. (n=6, unpaired t-test) f) Proliferation of HCC1806 cells containing miR-mediated KDs of ACLY and ACSS2. 76% and 73% KD efficiencies, respectively. Shown as fold change of the first timepoint. (n=6, unpaired t-test) g) GFP+ metastases in recipient Rag2^{-/-}γc^{-/-} mice after TVI of BT20 cells treated with acetate (n≥3, unpaired t-test) h) Kaplan-Meier plots depicting distant relapse-free survival (DRFS) of PAM50-classified basal breast cancer patients derived from the microarray cohort of KM plotter, stratified based on mean expression of OXPHOS-related genes and segregated by median cut-off. i) Kaplan-Meier plots of DRFS of breast cancer patients that have not undergone systemic treatment derived from the microarray cohort of KM plotter. Patients were stratified by ACLY expression and segregated by median cut-off. j) Kaplan-Meier plots of overall survival (OS) of breast cancer derived from the microarray cohort of KM plotter. Patients were stratified by CPT1A expression, and the comparison is made between the upper and lower quartiles. k) Kaplan-Meier plots of OS of breast cancer patients derived from the TCGA dataset. Patients were stratified by CPT1A expression and segregated by median cut-off. Unpaired t-test were parametric and two-tailed. Values shown correspond to means +/- SEM. Source data are provided in the source data file.

Additional Results

Due to the observed heightened mitochondrial activity in MICs, we wanted to determine if this in turned caused increased ROS levels in MICS, as OXPHOS is the primary ROS contributor. We therefore stained PyMT cells using a fluorescent marker for ROS, 2',7'-dichlorofluorescein diacetate (DCFDA), and observed that MICs had reduced levels of ROS in comparison to non-MICs (**Supplementary Fig. 8a**), in agreement with another study²²⁹. As ROS has been shown to limit metastatic potential²³⁰, we wanted to determine whether limiting mitochondrial or cytoplasmic sources of ROS could increase metastasis. On the contrary, we observed significantly reduced numbers of metastases in response to pre-treatment with SKQ1, a mitochondrial ROS scavenger, and EUK134, a cytoplasmic ROS scavenger (**Supplementary Fig. 8b**). Notably, the reduction in metastasis was more pronounced in response to inhibition of mitochondrial as opposed to cytoplasmic ROS. Considering ROS is known to be a potent signaling molecule¹⁵⁷, these data suggest that a non-linear relationship between ROS levels and metastatic potential may exist.

Mitochondrial dynamics, which encompass mitochondrial fission and fusion events, are important in regulating mitochondrial health and activity as they enable removal of damaged subunits and regulate OXPHOS activity. Moreover, fission events are downstream targets of AMPK activation, which also activates FAO. In line with this, one study showed that DRP1, a GTPase responsible for carrying out fission events, is required for proper redistribution of exogenous fatty acids and subsequent FAO. Since we observed a dependence of MICs on FAO, we wanted to determine if blocking fission events would similarly reduce metastatic potential just as we observed with the *Cpt1a* and *Cpt2* KDs. Indeed, we observed that KD of *Drp1* significantly reduced metastasis in PyMT cells (**Supplementary Fig. 8c**). Further, upon reanalyzing data from a previous study that investigated the role of DRP1 in pancreatic tumor growth²³¹, we observed a significant reduction in intracellular acetyl-CoA concentrations (**Supplementary Fig. 8d**), suggesting that mitochondrial dynamics may also affect epigenetic marks and PTMs.

Our group recently reported that CD8 T-cell derived-IFN γ can increase MIC frequency and metastasis²³². IFN γ increases the expression of BCAT1, the first enzyme in the pathway that catabolizes branched chain amino acids (BCAA) by transamination to α KG, yielding glutamate and eventually acetyl-CoA. IFN γ treatment reduced intracellular levels of α KG, and pharmacologically inhibiting BCAT1 (using Gabapentin) rescues α KG levels back to baseline. In contrast, we observed an increase of acetylcarnitine (an acetyl-CoA sink) under IFN γ , which was reduced upon inhibition of BCAT1 (**Supplementary Fig. 8e**). Although we had shown that IFN γ -mediated increase in metastasis can be blunted by administration of α KG and/or BCAT1 inhibition, heightened availability of acetylcarnitine, and thus acetyl-CoA may be an additional mechanism by which IFN γ exerts its pro-metastatic effects.



Supplementary Fig. 8:

- a) Number of lung metastases after TVI of PyMT cells that were pre-treated with 300 nM SKQ1 (mitochondrial ROS scavenger) or 10 μ M EUK134 (cytoplasmic ROS scavenger; $n=5$, unpaired parametric t -test). b) ROS measurements via DCFDA staining of PyMT non-MICs vs. MICs ($n=5$, ratio paired t -test). c) Number of lung metastases after TVI of PyMT cells expressing miR-mediated KDs of Gfp or Drp1. 98% KD efficiency for Drp1 (minimum $n=5$, unpaired parametric t -test). d) Normalized acetyl-CoA concentrations in mouse pancreatic cancer cells harboring mutations in KRAS and TP53, plotted from the supplementary data in Nagdas et al. (2019)²³¹ ($n=12$, unpaired parametric t -test). e) Normalized acetylcarnitine concentrations in PyMT cells treated with vehicle, 10 U/ml of IFN γ , or IFN γ with 20 mM Gabapentin (Gaba; $n=3$, ratio paired t -test). Values shown correspond to means \pm SEM.

Discussion

Dissecting the mechanisms that endow MICs with the ability to metastasize is essential to preventing cancer progression and potentially improving available therapies. In this study, we identified a metabolic program unique to MICs which contributes to their metastatic phenotype. We found that endogenous MICs in breast cancer depend on high mitochondrial activity in part fueled by FAO and export of citrate from mitochondria to generate acetyl-CoA. Acetyl-CoA is required for histone acetylation which is globally elevated in MICs and drives expression of EMT-related genes. Blocking either metabolic pathways or epigenetic modifiers that interrupt this process reduces the metastatic capacity of MICs, while supplementing with an exogenous source of acetyl-CoA enhances metastatic capacity.

High mitochondrial activity is constituent to the MIC phenotype. We show for the first time that by sorting cells for just one parameter, high MMP, we can identify the cells that are solely responsible for generating metastatic lesions. Further by forcing cells to undergo OXPHOS, we can convert non-MICs to MICs and increase metastasis. Our results extend previous work that demonstrates that cells devoid of mitochondria need to reacquire them from their host tissue for tumor initiation and metastasis^{233,234}. It has been postulated by other groups that mitochondrial metabolism is important for metastasis due to the heightened ATP requirement^{80,223}, but we show here that pre-treatment of cells with oligomycin, which blocks mitochondrial ATP generation, does not reduce the ability of MICs to metastasize. Instead, we observe that the high mitochondrial activity is commensurate with increased H3K27ac and increased expression of EMT-related genes.

We also show that this high mitochondrial activity is fueled at least in part by heightened FAO in MICs. Considering that we also observed high levels of H3K27ac in MICs, we hypothesized that the increased FAO could contribute to this heightened histone acetylation in MICs. Glucose has been canonically shown to be the primary nutrient that contributes to histone acetylation²³⁵, however, it has also been shown that medium-chain fatty acids are able to contribute up to 90% of the carbon for histone acetylation in a mouse hepatocyte cell line²³⁶. We now show that blocking the entry of LCFAs into the mitochondria by genetic or pharmacological means can

not only reduce histone acetylation on H3K27, but also MIC frequency, endogenous metastatic potential, and the expression of EMT-related genes in breast cancer cells. This is the first report to our knowledge that shows that blocking FAO can prevent endogenous metastasis; earlier reports had only shown that FAO is required for EMT induction upon overexpression of EMT-inducing transcription factors²³⁷.

It has been shown recently that for EMT to be activated, only few histone marks are required to be altered, and these epigenetic changes occur quickly –within the first 6 hours of EMT induction⁸². The fact that we observe global differences in histone acetylation that are in the order of percentage change rather than in the order of several fold changes, is therefore, expected. In addition, cells exhibiting a partial EMT phenotype, where they oscillate between mesenchymal and epithelial features, are most efficient at metastasizing due to their plasticity⁵¹, increased propensity to migrate and seed in clusters⁴⁴, and their ability to re-epithelialize upon colonization of the target tissue⁴⁹. Since our RNA-sequencing revealed partial EMT features in the endogenous MICs, it is likely that metabolism serves as a mechanism for MICs to precisely modulate and fine tune the extent of both epithelial and mesenchymal characteristics needed during the different steps of metastatic dissemination. Other TCA cycle metabolites have been shown to regulate histone methylation of EMT genes, such as succinate¹⁶¹ and fumarate¹⁶². However, methylation is a relatively stable epigenetic modification²³⁸. Since acetylation turns over in the timescale of seconds to minutes, highly plastic MICs may exploit acetyl-CoA generating pathways to enable this rapid phenotypic switching.

We further show that sorting for cells with high lipid storage is sufficient to identify MICs, and this high level of lipid stores is enriched in early micrometastatic lesions. We also observed that MICs have a heightened flux of lipids through these stores and pharmacologically disrupting this flux inhibits metastasis. This suggests that lipid stores may act as buffers to maintain FAO when lipid uptake is insufficient in order to ensure a continuous supply of acetyl-CoA for EMT-like phenotypic switching. In addition, lipid droplets have been shown to limit reactive oxygen species by sequestering polyunsaturated fatty acids that are vulnerable to chain peroxidation reactions²³⁹. Considering the existing evidence that detachment from substrate causes increased ROS due to reduced antioxidant generation^{20,21}, circulating tumor

cells could rely on lipid droplets to prevent peroxidation reactions by sequestering “excess” lipids and to battle heightened ROS through subsequent lipolysis and FAO for antioxidant (NADPH) generation.

We’ve now described several metabolic differences between MICs and non-MICs. What remains unknown is how these phenotypes arise and how they are maintained. Using an intracellular glucose biosensor, one study showed that intratumor metabolic heterogeneity can be maintained at least over one cell division²¹². It has also been shown that claudin-low, basal, and luminal breast cancer subtypes maintain the metabolic phenotype of their respective cells-of-origin (normal basal, luminal progenitor, and mature luminal mammary epithelial cells, respectively)²⁴⁰. These examples suggest that metabolic state is not only heritable but is also intrinsically regulated.

In this study, we show for the first time that acetate can induce EMT features, MIC frequency, and metastatic potential in breast cancer cells. Additionally, we demonstrate that the metastasis-promoting function of acetate can be blunted not just by blocking the direct enzymes that generate acetyl-CoA from acetate, ACSS1 and ACSS2²⁴¹, but also by inhibiting FAO, ACLY, or readers of H3K27ac. Acetate is the most common short chain fatty acid produced by the gut microbiome and about 10% of human energy is estimated to stem from acetate metabolism²⁴². While its concentration in the blood is between 50 to 200 μ M, acetate concentration is known to increase 2 or 3-fold in response to dietary changes such as alcohol consumption (since alcohol is detoxified to acetate through alcohol dehydrogenases)²⁴³ and high fat diet (HFD; through HFD-induced overrepresentation of certain gut microbiota)²⁴⁴, respectively. As it has been reported that both alcohol consumption²⁴⁵ and HFD²⁴⁶ are associated with increased metastatic potential in breast cancer, it appears possible that acetate-induced histone alterations, at least in part, play a mechanistic role in these settings, and may therefore be a suitable therapeutic target for certain patients.

Finally, our work demonstrates that precise regulation of histone acetylation is crucial for metastasis. Others have shown how histone acetylation is also important in other cancer promoting phenotypes such as in DNA damage repair²⁴⁷ and resistance to

conventional chemotherapy²⁴⁸, indicating that perturbing histone acetylation can be an effective and multimodal treatment strategy. Pan-histone deacetylase (HDAC) inhibitors have been used to increase histone acetylation, however, while these can cause cancer cell death in cells with very high histone acetylation levels, this may also cause an undesired conversion of non-MICs to MICs. We have also shown that due to the plurality of mechanisms for acetyl-CoA generation and the inherent plasticity of MICs, blocking one pathway may not always be sufficient due to compensatory mechanisms such as the upregulation of ACSS2 in the absence of ACLY^{226,249}. It may therefore be essential to target multiple acetyl-CoA generating pathways and additionally target downstream epigenetic modifiers coupled to closely monitoring response to treatment for full and long-lasting efficacy.

Conflict of Interest

The authors declare no competing interests.

Acknowledgements

C.M.Y., L.B., and A.M.A., were supported in part by grants from the SNF and the Swiss League against Cancer. We thank R.A. Lambuta, and N. Katanayeva for providing guidance on the ChIP preparation, B. Mangeat for help with the RNA-seq and ChIP-Seq, M. Norkin for analyzing the sequencing data, S. Rettie for computational support, and all the EPFL core facilities including the GECF, SIB, HCF, CPG, FCCF, and BIOP, Agora core facilities, including the AIVC, MPF, CIF, and FCF, and the UNIL MEP for their tremendous help during various parts of the project.

BRIEF SUMMARY OF RESULTS

Metastasis is a multi-step process that requires precise orchestration of several cell functions and phenotypes that can often be short-lived and opposing^{4,6,216,250}. Thus, only very few cells can successfully metastasize to distant organs. However, despite the “rarity” of this process, the consequences are dire since most cancer deaths are attributed to the presence of metastatic disease. It is therefore of utmost importance to determine the vulnerabilities of MICs to better develop strategies to prevent and treat metastatic cancers.

Addressing Aim 1: Identifying metabolic dependencies of MICs

In this study, we examined how MICs exploit metabolic adaptations for metastasis. We observed that endogenous MICs have heightened mitochondrial activity both on the transcriptional and functional level, and forcing non-MICs to use OXPHOS converts them to MICs. We additionally observed that cells sorted for the highest MMP had the highest metastatic potential. We also observed that MICs are more dependent than non-MICs on the use of LCFAs compared to glucose and glutamine. These were confirmed as we were able to reduce metastatic capacity by blocking lipid droplet dynamics and LCFA oxidation via pharmacological and genetic means. Additionally, cells that have the highest lipid stores have the highest metastatic capacity, and high levels of lipid stores were maintained only during the early stages of metastatic outgrowth.

Since we had determined that mitochondrial ATP synthesis was not limiting for metastasis, we used pharmacological and genetic means to investigate how the TCA cycle may contribute to MIC function. We determined that the enzymes involved in the generation of mitochondrial citrate and its subsequent export and generation into cytosolic acetyl-CoA are necessary for metastasis. Further, by boosting levels of acetyl-CoA by exogenous addition of acetate, we were able to increase metastatic potential.

Addressing Aim 2: How MIC metabolism contributes to MIC function

We observed that MICs endogenously have a higher level of H3K27ac. Further, we observed that the metabolic inhibitors that reduced metastatic capacity reduced H3K27ac. In contrast, metabolic substrates and inhibitors that increased metastatic capacity also increased H3K27ac. Further, blocking the recognition of H3K27ac marks by pharmacological means reduces metastatic capacity. RNA-sequencing and subsequent validation by qPCR confirmed that these treatments alter MIC function by modulating the expression of EMT genes. Finally, we performed ChIP-seq to show that there indeed is an alteration of H3K27ac on the regulatory regions of EMT genes.

Addressing Aim 3: Confirmation in human models

We were also able to increase metastatic capacity in human cell line models by addition of an exogenous acetyl-CoA source and limit metastatic capacity by inhibiting enzymes that generate acetyl-CoA. Further, by correlating the metastatic potential of 20 TNBC lines to their global histone profile, we observed that only H3K27ac was repeatedly significantly and positively correlated with metastatic potential. Finally, by examining patient cohorts and stratifying them based on the expression of our MIC-derived OXPPOS gene signature and acetyl-CoA generating enzymes, we confirmed that their higher expression is predictive of poor prognosis.

DISCUSSION & OUTLOOK

Mitochondria have long been known to be required for tumorigenic²⁵¹ and metastatic capacity^{233,234}. We and others have observed that metastatic cells exhibit higher levels of mitochondrial activity evidenced by their dependence on FAO^{98,252,253}, TCA cycle flux²⁵⁴, and OXPHOS^{80,207,223}. However, it has only been recently that the mechanisms by which mitochondria fuel cancer progression are delving outside of energy production. We found that the abovementioned metabolic pathways are important for generating metabolic intermediates that regulate the expression of metastasis-related genes in TNBC. This mechanism has also been independently validated recently by another group that was primarily using human cell lines²³⁷ as opposed to the autochthonous GEMM or mouse cell line that we utilized, where they showed that blocking FAO blunted metastasis upon expression of two EMT and stem TFs (SOX9 and SNAI2)²³⁷. While both our studies suggest that metabolism regulates TNBC metastasis on the histone level, others have shown that PTM (acetylation) of non-histone proteins can be another mechanism by which metabolism boosts metastasis^{255,256}. It could be argued that the differences in the experimental procedures can account for this discrepancy, but it is also possible that both mechanisms work on staggered timescales, collectively contributing to the overall MIC phenotype, and serving as a way to fine-tune the expression of the required partially opposing phenotypes during metastasis.

After all, the acquisition of the MIC phenotype is a balancing act. Cells must adapt the right proportions of epithelial and mesenchymal characteristics to metastasize^{39,44,49-51}. This is similar to the observations that some signaling pathways such as those via RAS²⁵⁷ and WNT²⁵⁸ must be “just-right” to exert their protumoral roles. Metabolic alterations must also be carefully adjusted to achieve the right concentration of metabolites for optimal metastatic capacity. As an example, we observed that cells only respond optimally to intermediate levels of exogenous acetyl-CoA supplementation likely because histone hyperacetylation has been shown to induce cell death²⁵⁹. Further, although excessive ROS is also known to induce cell death, intermediate levels of ROS are known to activate protumor signaling pathways such as PI3K^{158,260} and NFκB²⁶¹. It is therefore unsurprising that we and others have observed that not only is mitochondrial ROS important for

metastasis²⁶², but antioxidant administration can also blunt metastatic potential^{263–265}, despite ROS levels being endogenously lower in MICs²²⁹. Moreover, the existence of what is termed a “non-canonical TCA cycle” has been demonstrated in embryonic stem cells and adult stem cells, where citrate produced in the mitochondrial TCA cycle is exported out to regenerate oxaloacetate and is imported back into the mitochondria as malate²⁶⁶ (**Fig. 14**). In a way, we observed something similar in MICs, where inducing citrate export by blocking ACO2 increases MIC activity and preventing the regeneration of oxaloacetate (and acetyl-CoA production) by blocking ACLY reduces MIC activity. Blocking both enzymes in combination reverts the metastatic activity back to baseline, suggesting that MICs could be utilizing this non-canonical TCA cycle. The authors suggested that an advantage of using the non-canonical TCA cycle could be to reduce the amount of NADH produced which may hinder proliferation²⁶⁷, but this is yet to be confirmed. As the canonical TCA cycle is known to be essential for generation of histone modifications²⁶⁸, the usage of the non-canonical TCA cycle may be to preferentially generate acetyl-CoA over succinate and fumarate as the latter two inhibit demethylases thereby increasing histone methylation and possibly counteracting histone acetylation. Further, it could also limit the amount of NADH and FADH₂ which can limit OXPHOS and consequently ROS production. These suggest that even though MICs rely on the mitochondria for various cellular functions and phenotypes, MICs must employ multiple mechanisms to regulate their metabolism and titre the levels of metabolic intermediates to boost their metastatic potential.

Healthy mitochondria are maintained by the coordination of their fission and fusion dynamics that enables clearing of damaged subunits and modulation of OXPHOS activity²⁶⁹. MICs were recently shown to depend on mitochondrial fission events, as pharmacological and genetic inhibition of DRP1, the protein responsible for mitochondrial fission, significantly reduced metastasis in the brain. Interestingly, they determined that blocking fission events affected the ability of MICs to utilize their heightened uptake and storage of lipids via FAO²⁷⁰. As we had also observed that *Drp1* KD reduced metastatic capacity in the lungs and we had also observed increased FAO dependency in MICs, it is not unreasonable to postulate that mitochondrial dynamics may also influence gene expression through limiting acetyl-CoA production. To support this, another group observed that acetyl-CoA

concentrations were significantly reduced in pancreatic cancer cells that contained *Drp1* knockouts²³¹. Interestingly, it has also been shown that BRD4, a member of the BET family of acetylation readers, controls the transcription of *Mff*, another protein integral to carrying out mitochondrial fission events. Blocking BRD4 prevents mitochondrial fission and slows tumor growth in prostate cancer cells; further, high MFF expression was detected in hormone-refractory metastatic tumors²⁷¹. These suggests that there may be a feed forward loop that exists to maintain mitochondrial flexibility and plasticity in MICs. MICs may therefore balance their mitochondrial fission and fusion dynamics to firstly ensure sufficient FAO, TCA cycle, and OXPHOS activity for the generation of energy and certain metabolic intermediates, the latter of which being important to maintain their MIC phenotype, but at the same time limit ROS to “just-right” levels to maximize protumoral signaling without inducing cell death.

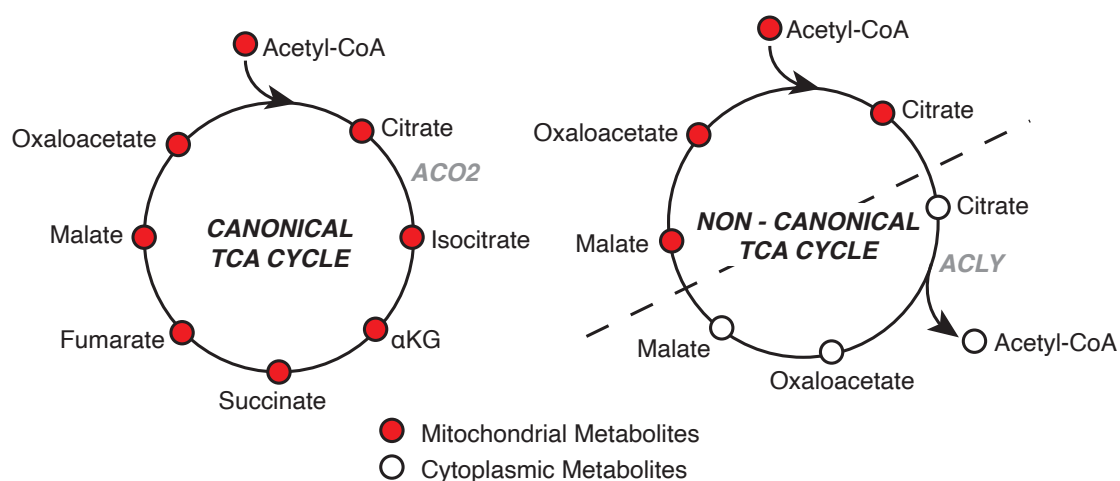


Fig. 14: Canonical vs. non-canonical TCA cycle adapted from Arnold et al. (2022)²⁶⁶.

As mentioned in the introduction, MICs can also be induced by the microenvironment. Our lab has recently shown that the interaction between CD8 T-cells with TNBC cells can unexpectedly result in increased metastasis through IFN γ -induced metabolic alterations. IFN γ increases the expression of BCAT1, which reduces the levels of α KG and subsequently enables the conversion of non-MICs to MICs²³². In colon cancer cells, α KG has been shown to reduce stemness and tumor growth by increasing the activity of α KG-dependent demethylases, thereby reducing DNA methylation on intestinal differentiation genes and reducing the activating

H3K4me3 mark on stem-promoting WNT-target genes²⁷². Although this could also be a mechanism by which IFN γ induces the MIC phenotype, BCAA catabolism via BCAT1 is known to generate acetyl-CoA. In line with this, we had also observed a 10-fold increase of acetylcarnitine upon IFN γ treatment. Acetylcarnitine is a sink for acetyl-CoA, where excess acetyl-CoA is reversibly converted via the enzyme CRAT to enable reduction of the acetyl-CoA:CoA ratio (since a high acetyl-CoA:CoA ratio will inhibit TCA cycle flux) and interorganlle shuttling of acetyl-CoA²⁷³ (since acetyl-CoA itself cannot pass through membranes). Because acetylcarnitine has also been shown to be an important source for histone acetylation^{225,274} it could be that histone acetylation serves as an additional mechanism by which IFN γ induces metastasis. In line with this, it is known that STAT1 phosphorylation which occurs downstream of IFN γ , activates the HAT, p300²⁷⁵. Further, blocking BET-bromodomains via JQ1 inhibits the downstream effects of IFN γ ²⁷⁶. These indicate that blocking these downstream protumor metabolic or epigenetic pathways may be a way to boost current immunotherapies for solid tumors, where response rates are not nearly universal, such as in TNBC, non-small cell lung cancer, and melanoma^{232,277}.

We identified that H3K27ac is specifically altered in response to metabolic perturbations and is correlated with metastatic potential. Although this mark is frequently associated with increased transcriptional output, it is still debated whether simple deposition of H3K27ac is sufficient at inducing gene expression. In mouse embryonic stem cells that have been genetically engineered to be unable to harbor H3K27ac marks, they were still able to express the necessary genes for differentiation into epiblast-like cells, suggesting that at least for this specific context, H3K27ac is dispensible¹²⁵. In contrast, it has been shown that deposition of H3K27ac is sufficient at increasing chromatin accessibility and eliciting an over 3-fold induction of gene expression. Further, preventing the acquisition of H3K27ac blocks the ability of H3K4me3 from initiating transcription. However, these effects can be limited depending on the genetic context; in the presence of certain DNA motifs, transcriptional activation in the presence of H3K27ac is blunted²⁷⁸. This suggests that there is likely a specific cohort of genes that is more susceptible to activation upon H3K27ac and thus by metabolic perturbation.

Although MICs have been detected in a variety of cancer types, their identity is often difficult to define as common markers are rare. Expression of the EMT program is known to be required for MIC function, however, the extent of EMT and which combination of genes and TFs are required is often dependent on the cancer type. Considering that plasticity is arguably the central feature to MICs, it may be that what ultimately dictates the MIC phenotype is their epigenetic flexibility; in other words, it may depend on how responsive their chromatin is to environmental stimuli. Mechanistically, open chromatin regions permit cells to take on protumoral and pro-MIC phenotypes. This is best exemplified by studies done with TGF β signaling. It has been shown that TGF β can induce either a protumor or antitumor effect depending on whether tumor cells harbor pre-existing accessible or closed chromatin regions on promoters of key SMAD3 binding sites (a downstream effector of TGF β signaling), respectively²⁷⁹. Moreover, non-MICs that have poised chromatin marks on certain loci, characterized by the presence of both the activating H3K4me3 and inactivating H3K27me3 marks, are able to dedifferentiate into MICs upon TGF β stimulation⁸⁴.

Evidence of permissive chromatin being an identifying feature of highly aggressive cancer cells can be found in therapy resistant TNBC. The cells that harbored poised chromatin were more likely to resist chemotherapy as H3K27me3 can be quickly lost and thus activate the expression of certain gene programs²⁸⁰. Similarly, drug resistant subpopulations were identifiable in the bulk population by loss of H3K27me3²¹¹. More related to metastasis, one study showed that a generally more open chromatin conformation can be necessary and sufficient for metastasis in small cell lung cancer⁸¹. In addition, distant metastases in pancreas cancer were observed to have elevated chromatin accessibility, evidenced by increased histone acetylation and reduced DNA and histone methylation in comparison to locoregional metastases²⁸¹. Locoregional metastases do not have to undergo the metastatic cascade, but rather just invade into the neighboring tissue. We had also observed that upon examining the global histone profile of metastatic vs. non-metastatic TNBC lines, specifically H3K27ac was significantly correlated with metastatic potential. These lines of evidence suggest that adoption of an open chromatin may be a prerequisite for the MIC phenotype. Increased histone acetylation instead of or in conjunction with loss of repressive histone and DNA methylation marks may also be

preferentially leveraged to adapt to the challenges of metastasis. The advantage of histone acetylation is that the turnover is quick²³⁸, and so transient changes in gene expression can be more easily achievable. Further, histones are a reservoir for acetyl-CoA, as deacetylation of histones yields nuclear acetate, which can then be converted back into acetyl-CoA via ACSS2. Conversely, histones are a sink for SAM, as demethylation yields formaldehyde, which cannot be converted back into SAM. Histones, therefore, hold about 4 billion acetyl-CoA molecules across the human genome²⁸² which can be readily mobilized during times of cellular stress to reinvigorate mitochondrial metabolism²⁸³ or to redistribute histone acetylation marks to activate stress-alleviating gene programs and even promotion of tumorigenesis²⁸⁴. Single cell studies of chromatin profiling in primary tumors vs. micro- and macrometastatic lesions should be performed to validate these hypotheses, but considering these epigenetic patterns hold across at least three different cancer types, this may be a feature that unifies all MICs regardless of tissue-of-origin.

Current state of related metabolic and epigenetic therapies

The mechanisms by which fatty acid metabolism contributes to the pathogenesis and progression of cancer is multi-faceted and multi-mechanistic. As we in this paper and others have shown, FAO contributes to epigenetic marks and PTMs that induce the expression of protumor gene programs and thus, metastasis^{237,256}. FAO is also an important source of ATP in times of metabolic stress^{20,285}, as oxidation of palmitate, for example, generates three times more ATP than one molecule of glucose. Cancer cells are also known to depend on lipid synthesis for growth and proliferation²⁸⁶ and lipid remodeling for tumor initiation²⁸⁷ and drug resistance^{288,289}. Cholesterol biosynthesis is similarly important for cancer progression as sterols act as potent signaling molecules (particularly in the form of hormones), substrates for PTMs, and modulators of membrane fluidity integral to transmembrane signaling²⁹⁰. We additionally suggest here that exogenous lipid uptake and subsequent lipid droplet dynamics supports metastasis by serving as a reservoir for FAO to fuel histone acetylation, but lipid droplets may also contribute to metastasis via their roles as inflammatory signaling hubs. Arachidonic acid derived from the lipid droplet phospholipid membrane is metabolized into various eicosanoids like prostaglandins and leukotrienes¹⁵⁹ which have been shown to increase metastasis promoting cell-

intrinsic features such as proliferation, invasion, and survival, and cell-extrinsic features such as angiogenesis, inflammation, and immune escape²⁹¹. These indicate that there are plenty of avenues to target fatty acid metabolism, and that these present a multifactorial way of blocking MICs.

Central to fatty acid metabolism is acetyl-CoA. Acetyl-CoA sits at the nexus of virtually all cellular processes (**Fig. 15**), from energy-generating catabolic reactions (FAO, TCA cycle), anabolic reactions (*de novo* lipid synthesis, sterol synthesis), signaling (PTMs), gene expression (histone modifications), and response to cellular stress (histones being an acetyl-CoA reservoir, DNA damage repair²⁴⁷). It is therefore not surprising that there are several therapies in development that target enzymes involved in acetyl-CoA metabolism.

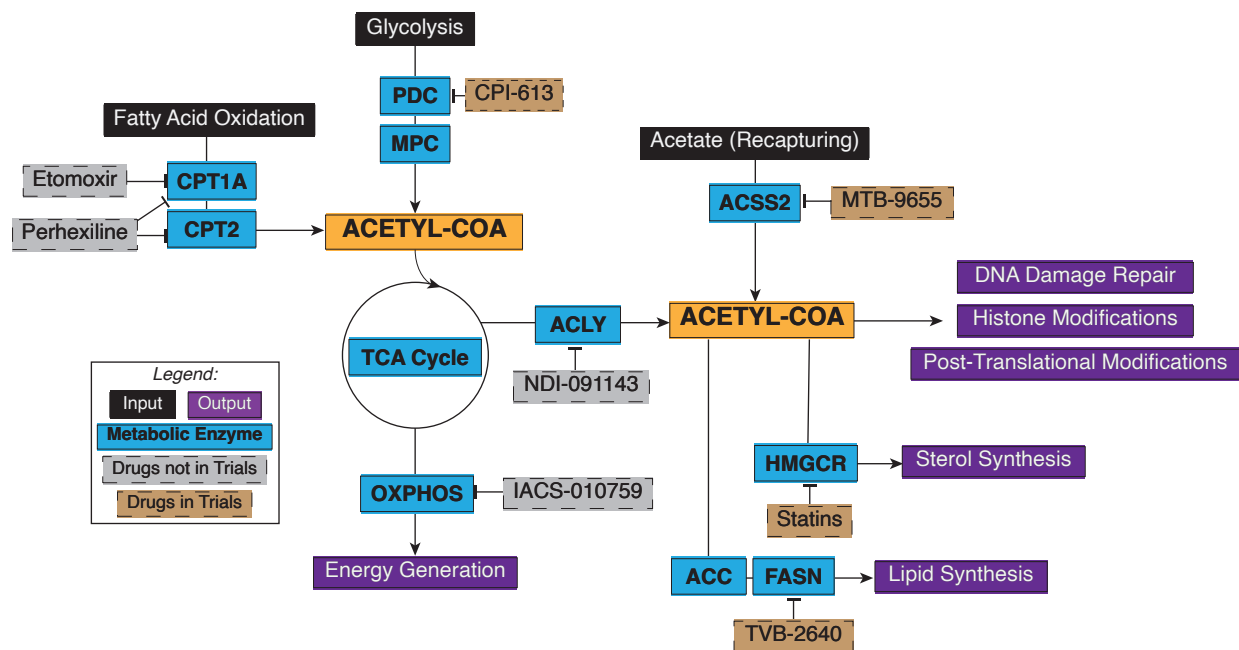


Fig. 15: Acetyl-CoA at the nexus of vital cellular processes.

Acetyl-CoA is mainly generated through glucose and fatty acid catabolism. Acetyl-CoA then enters the TCA cycle for energy generation or gets converted into citrate to then be exported out into the cytoplasm or nucleus. Cytoplasmic acetyl-CoA can then be used for lipid and sterol synthesis or PTMs. Nuclear acetyl-CoA can be used for histone modifications and assisting in DNA damage repair mechanisms. Acetyl-CoA can also be generated through extracellularly derived acetate or acetate released from histone deacetylation reactions (acetate recapturing) for re-entry into the TCA cycle, PTMs, or redistribution of histone modifications.

Unfortunately, some of these therapies have not yet been particularly successful in the clinic. Firstly, some targets are still “undruggable” as the current available inhibitors for FAO, for example, exhibit off-target effects²⁹² and dose-limiting toxicities²⁹³. One of the drugs inhibiting CPT1 and CPT2, perhexiline, had once been distributed globally for the treatment of angina (insufficient blood flow); however, its use was reduced due to reports of severe liver and neurotoxicity. On the other hand, many inhibitors of ACLY have been developed, but most compounds have weak activity with IC50s in the μM ranges²⁹⁴. There has been a recent development of an allosteric ACLY inhibitor that functions in the low nM range²⁹⁵, however, pre-clinical studies still have to be conducted. Secondly, metabolic inhibitors are always a bit tricky, as these metabolic pathways tend to also be active and important in normal cells. A phase I trial assessing the safety profile of a mitochondrial complex I inhibitor, IACS-010759, was discontinued due to dose-limiting toxicities, particularly neurotoxicity and lactic acidosis that prevented any substantial therapeutic benefit²⁹⁶. Complex I inhibition will force all cells (both tumor and normal) to use anaerobic glycolysis to generate energy, therefore elevated blood lactate levels resulting in lactic acidosis is expected; however, it can be fatal, as was observed in diabetic patients that were once treated with phenformin (an even more potent complex I inhibitor)²⁹⁷. Similarly, neurons are critically dependent on mitochondria as they are integral to synaptic development and neurotransmission²⁹⁸, therefore the observation of neurotoxicity was also expected to some extent. To avoid these adverse effects, a less potent version of phenformin, metformin, was gaining interest, however, there was a lack of clinical efficacy in phase III trials²⁹⁹. This is likely explained by the observation in preclinical studies that metformin can activate AMPK, which can then exert protumoral roles such as maintaining cellular homeostasis in response to stress¹⁷² and even driving metastasis¹⁷³.

With that being said, all is not yet lost. There are still some small molecules that are making their way into clinical trials that are promising. Although there has not yet been any major breakthroughs with targeting FAO, the group responsible for identifying MICs in oral squamous cell carcinoma is developing a drug to target CD36, the transporter responsible for fatty acid uptake and metastasis^{98,300}. There is also ongoing recruitment of patients with advanced solid tumors to a phase I trial to test an inhibitor for ACSS2, which converts exogenous or histone-derived acetate

into acetyl-CoA³⁰¹. TVB-2640, which inhibits the lipid synthesis enzyme, FASN, has passed phase I trials with promising results for several cancer types including breast cancer patients³⁰², thus, recruitment for phase II trials are now ongoing (NCT03179904 for HER2+ metastatic breast cancer). The drug that is furthest along is CPI-613, which inhibits PDH and OGDH, the former being responsible for funneling glucose into the mitochondria for subsequent OXPHOS and the latter being an enzyme in the TCA cycle. Phase I trials were promising as patients with metastatic pancreatic cancer experienced increased remissions and response rates when treated with CPI-613 in combination with standard-of-care chemotherapies³⁰³. Phase III trials have now been completed, but unfortunately failed to show improved outcomes³⁰⁴. A pre-clinical study in head and neck cancer showed that use of CPI-613 causes upregulation of glutaminolysis as a compensatory mechanism³⁰⁵. Considering pancreatic cancers are notoriously glutamine addicted¹⁷⁰, this may be one of the reasons why the phase III trials were unsuccessful. Further studies need to evaluate whether additional combination therapies that can prevent compensation may be more beneficial or if CPI-613 would be better suited to other cancer types.

Another proposed way to increase the efficacy of both experimental and standard-of-care therapies is diet modulation, as is it a low cost and low risk way to improve outcomes. Both aspects of a Western diet (high fat^{191,306} and high fructose^{307,308}) have been linked to increased cancer risk and progression. HFDs increase inflammatory signals that generate a permissive environment for MIC dissemination and seeding²⁴⁶ and cause PTMs (in part via acetylation) that increase pro-MIC cell-intrinsic signaling^{256,309}. High fructose diets have been reported to support cell proliferation by increasing inputs for lipid synthesis³⁰⁷ and increase metastatic capacity by activating EMT TFs³⁰⁸. In contrast, limiting certain fuel sources have been shown to be successful in delaying breast cancer progression, improving quality of life, and boosting efficacy of chemotherapies³¹⁰. In the most “extreme” case, pre-clinical models show that caloric restriction (CR) reduced tumor growth and metastasis in a dose-dependent manner, likely due to reduced circulating IGF1 levels (which can activate protumor PI3K signaling) and causing an antitumor immunological signature in the tumor microenvironment³¹¹. Similarly, fasting-mimicking diets (FMDs) which cycle between caloric intake and long stretches of fasting have been shown to cause delays in tumor progression, reduced MIC and

metastasis, and synergy with hormone or chemotherapy in pre-clinical models^{312–314}. In both cases, there have only been small scale clinical trials, however, the results are promising, having observed improvements in disease-free survival³¹⁵ and response to chemotherapy³¹⁶. On the other hand, low-fat diets (LFDs), which restrict fat intake to less than 30% of total calories, are now being recommended in standard clinical practice. Large scale trials have shown that prescription of an LFD increased overall survival in patients that were subsequently diagnosed with breast or even other cancers while on the diet³¹⁷. Further, LFDs reduce the risk of breast cancer relapse (including local, regional, and distant) most notably in patients harboring tumors that were ER negative³¹⁸. Despite the seeming success of these interventions, precision therapy still needs to be taken into consideration as certain subgroups of patients will respond more or less to the different dietary interventions. As an example, CR is likely to be ineffective in patients that harbor mutations that constitutively activate the PI3K pathway, as IGF1 levels (which are reduced upon CR) signal through the same pathway³¹⁹. Further, these diets are unlikely to work alone, but instead can boost effects of pharmacological or immunological therapies³²⁰. Therefore, studies identifying synergistic treatment-diet pairings in the optimal patient subgroup(s) will be crucial for the success of these interventions.

Downstream of metabolic interventions, it may also be possible to target epigenetic dependencies of MICs. Although there are currently no HAT inhibitors that are being tested in clinical trials due to off-target effects³²¹, there are now several HDAC inhibitors that have been approved for the treatment of hematological malignancies. But for solid cancers including breast cancer, they are still under evaluation in Phase II and Phase III trials. The limitation of these HDAC inhibitors is that they have been shown to promote MICs in some preclinical studies^{322–324}. Moreover, early clinical data show that HDAC inhibitors are not particularly effective at blocking tumor progression as single agents^{325,326}; however, there seems to be promise when used in combination with other therapies³²⁷. Most notably for breast cancer is that one HDAC inhibitor, tucidinostat, in combination with an antiestrogen therapy, exemestane, improved progression-free survival in advanced luminal breast cancers³²⁸. No trials have yet reached phase III trials for the treatment of TNBC with HDAC inhibitors due to low accrual or poor outcomes. Inhibitors of the BET family of bromodomain-containing proteins are also now being evaluated in clinical trials,

however, similarly to HDACs, their use as single agents seems to be limited, and moreover, they tend to induce dose-limiting toxicities³²⁹. For now, no trials have yet reached phase III in breast cancer, but pre-clinical studies continue to be promising, where studies show that blocking BETs reduces tumor initiation, inhibits metastasis, and synergizes with targeted therapies in TNBC^{330,331}. Similar to the metabolic inhibitors, epigenetic enzymes are also crucial for the functioning of normal cells, so finding ways to drug the cancer-specific vulnerabilities or at least find a therapeutic window is not so trivial. Efforts should be placed into finding subpopulations that are more likely to respond to the treatment and identify pharmacodynamic biomarkers to determine whether a proper dosage is reached, to maximize tumor treatment but minimize adverse effects³³².

It is also important to realize that currently, the way that drugs are evaluated in clinical trials is not ideally set-up for identifying therapies that will prevent or reduce metastatic burden³³³. When a promising therapy is first introduced into a trial, the patients that are recruited are already at a very advanced stage, likely with multiple sizeable metastatic lesions. Hence, only one parameter, tumor growth, is typically being measured as a response outcome. However, as discussed, MICs and non-MICs (the latter of which makes up the bulk of the tumor) are phenotypically different, and therapies that might block non-MICs may not necessarily block or may even increase the frequency of MICs²³², and vice versa. Additionally, the endpoints that are considered to determine antitumor efficacy only measure time-to-event, such as overall survival, disease-free survival, or relapse/progression-free survival. They often fail to detail, for example, whether the progression was due to an increase in tumor size or appearance of new distant metastatic lesions. One demonstration of this is in castration-resistant prostate cancer –despite Denosumab being determined in Phase III trials to be superior than standard-of-care in increasing metastases-free survival³³⁴, it was not approved by the United States Food and Drug Administration or the European Medicines Agency because it did not prolong overall survival³³⁵. This shows that until metastasis-related endpoints are considered as an important part of the standard outcome measures, it will continue to be difficult to identify anti-metastatic agents and assess how candidate therapies truly influence disease progression.

CONCLUSION

Metastasis is a systemic disease, where MICs require the orchestration of multiple cellular processes and even multiple players in the micro- and macroenvironment to efficiently metastasize. We show here that MICs co-opt both metabolism and epigenetics to rewire their phenotype, and that compensatory mechanisms can occur to circumvent single points of inhibition. Thus, to appropriately treat a systemic disease, it must require a systemic solution, where multiple therapies must synergize and cooperate to fully block and eradicate MICs. It will therefore be of value to the patients-in-need to further the efforts in identifying ideal interdisciplinary combination therapies that can significantly reduce the deadliest feature of cancer, metastasis.

SUPPLEMENTARY DATA

Supplementary Table 1:

Loci of identified H3K27ac signals associated with EMT genes. EMT genes were determined by taking the union of genes present in the HALLMARK_EPITHELIAL_MESENCHYMAL_TRANSITION and GOBP_EPITHELIAL_TO_MESENCHYMAL_TRANSITION gene sets.

Chromosome	Start	End
chr18	3479964	3767672
chr6	3942743	3978419
chr6	4416574	4508666
chr16	4633224	4660913
chr4	6364573	6391559
chr15	6381003	6413817
chr11	7235957	7240426
chr9	7441808	7466724
chr12	8448575	8504781
chr3	8666689	8668332
chr12	8769615	8814869
chr18	8803600	9201197
chr12	8937546	8946380
chr2	9736550	9892030
chr18	10086555	10293202
chr16	10280606	10320635
chr19	10504289	10529227
chr8	11240595	11426267
chr8	11430549	11456111
chr4	11703551	11704773
chr18	12453447	12510826
chr7	13003999	13004844
chr15	13049470	13369093
chr2	13569861	13596582
chr17	14606816	14755800
chr16	14755697	14796880
chr13	16005839	16027133
chr18	16806772	16808451
chr12	16914768	16986039
chr11	17189543	17200276
chr6	17943704	18002849
chr10	18948828	19055082
chr11	19827309	20028592
chr16	20732844	20765846

chrX	20859362	20879936
chr6	22215564	22315738
chr8	23411524	23523969
chr14	24135382	24179947
chr7	24442086	24483623
chr10	24578957	24639390
chr17	24597799	24621456
chr12	25090074	25114472
chr15	25364700	25414879
chr8	25573487	25576020
chr7	25679959	25700978
chr2	26464278	26526987
chr8	26971130	26983026
chr14	27039056	27071973
chr10	27116465	27251090
chr14	27297086	27431463
chr2	27959648	28020229
chr9	28992621	29000490
chr7	29160276	29180562
chr6	29343281	29370212
chr11	29688109	29747258
chr5	30011423	30042074
chr19	30559030	30559304
chr6	30737739	30805610
chr10	30762532	30920977
chr13	31801228	31877081
chr2	32640996	32695759
chr19	32754913	32832054
chr16	33842796	33929440
chr12	33954900	34227177
chr1	33980336	34085773
chr19	34243070	34264283
chr19	34280879	34371537
chr15	34306275	34332125
chr14	34499185	34505800
chr17	34585427	34613136
chr6	34764306	34773150
chr16	34811985	34894055
chr11	35061818	35157559
chr2	35644621	35742659
chr10	36964837	37055909
chr3	37331831	37332118

chr3	37639459	37680693
chr2	37701277	37798429
chr16	37727067	37816025
chr5	37824332	37824832
chr16	38085421	38252042
chr13	40937577	40976914
chr13	42233481	42297855
chr4	43517847	43540844
chr4	43957395	43960474
chr9	44048266	44049975
chr16	44171244	44213571
chr9	44475404	44516997
chr9	44685334	44737326
chr1	45051802	45247120
chr1	45365363	45581738
chr14	45467315	45507748
chr16	45757448	45853595
chr7	45912985	45928504
chr17	46003363	46038447
chr19	46067102	46089014
chr17	46642515	46661737
chr4	47317486	47410299
chr9	47403371	47747920
chr11	47423406	48098757
chr6	47555388	47673703
chr11	52095060	52131255
chr18	52559240	52565510
chr13	53442285	53498002
chr5	53583173	53672459
chr19	53902593	53904474
chr8	53968154	54275960
chr11	54057777	54066294
chr15	54091851	54335984
chr3	54357746	54522836
chr14	54423018	54451080
chr11	55393817	55439854
chr19	55532264	55790633
chr15	55847288	55847587
chr17	56126967	56128409
chr10	56375797	56391296
chr16	56428968	56502069
chr13	56614901	56667196

chr15	56707298	56851263
chr17	57242882	57276999
chr13	57413876	57907937
chr3	57485486	57581460
chr12	57542954	57549129
chr3	57845884	57848363
chr18	58144941	58145188
chr9	58282732	58318560
chr2	58454169	58571567
chr13	60178430	60179081
chr18	60829995	60879931
chr18	61046120	61072847
chr11	63113461	63137329
chr4	63372297	63380781
chr9	63636975	63807766
chr16	63807839	63945272
chr4	63957590	64059950
chr11	65205340	65205669
chr9	66012025	66070155
chr3	66113133	66225164
chr9	66980749	67066563
chr6	67028144	67044052
chr17	67686392	67688651
chr18	68174333	68263752
chr8	70373661	70402810
chr14	70473726	70493582
chr8	70491137	70494101
chr8	71610141	71642147
chr1	71665497	71770437
chr8	72126333	72126809
chr6	72531669	72569489
chr15	73337639	73415740
chr2	73443943	73455668
chrX	73464075	73492830
chr18	73622731	73680371
chr5	73647054	73647772
chrX	73670428	73694885
chr12	73898418	73952347
chrX	74202528	74252266
chr13	74293964	74331843
chr18	75337891	75442863
chr11	76017732	76101280

chr18	76240600	76350426
chr10	77292977	77330335
chr1	77369501	77518207
chr8	77736480	77827137
chr14	79301228	79301473
chr1	79504919	79548994
chr15	79532689	79548906
chr9	79717176	79721248
chr10	79776346	79782307
chr1	79818542	79960763
chr18	80607954	80664561
chr10	80925347	80972931
chr8	82295702	82522846
chr6	83036856	83046162
chr2	83712511	83749446
chr15	85290840	85291130
chr10	86233482	86346586
chr6	87670672	87677262
chr9	88316700	88375140
chr13	88798586	89178642
chr11	89232184	89303552
chr3	89266305	89289371
chr13	89738702	89889653
chr16	89774087	89992401
chr5	90675757	90770528
chr5	90799979	90800190
chr1	90832655	90867976
chr5	91107238	91207741
chr6	91178137	91281010
chr2	91930754	91931338
chr9	92536795	92585003
chr1	92794385	92829930
chr8	92810274	92850735
chr11	94911250	94949137
chr4	95048299	95061968
chr6	95117526	95215891
chr9	95665800	95693037
chr3	95705876	95749327
chr11	97003543	97022910
chr10	97307286	97448912
chr10	97535050	97538408
chr3	97975609	98070069

chr7	98812810	98870486
chr11	99016968	99057583
chr7	99339574	99374357
chr8	101710652	102865635
chr2	102831212	102988561
chr10	103028404	103028926
chr15	103343145	103385115
chr5	104390066	104468690
chr11	104609626	104659171
chrX	105120455	105120929
chr14	105885753	106001639
chr11	106776226	106795810
chr5	107171209	107297204
chr9	108202645	108265958
chr10	108291141	108393509
chr4	108399968	108400405
chr11	108885020	108888410
chr9	108942895	108993608
chr12	109625850	109627480
chr2	109692603	109729844
chr10	111987919	112003089
chr11	112747289	112792126
chr9	113723176	113830989
chr2	113763720	113789625
chr3	113951579	114416034
chr13	114863451	114964338
chr13	115756727	116444171
chr3	116075639	116124804
chr9	116084515	116180360
chr2	117080133	117183971
chr6	117167126	117270744
chr9	118471381	118471965
chr1	118488706	118569626
chr4	119231601	119243431
chr1	119606580	119650582
chr10	120482866	120571948
chr11	120540733	120552227
chr9	120944477	120970341
chr8	121111131	121127700
chr2	121428137	121444668
chr11	121480445	121556248
chr6	122531453	122535172

chr6	124762661	124771117
chr2	125524364	125559557
chr4	126281167	126305610
chr10	127538871	127560791
chr8	128557340	128732117
chr2	129341491	129372021
chr4	130041972	130078342
chr4	130078919	130115074
chr7	130169744	130266243
chr7	130918570	130990203
chr3	131139082	131139894
chr2	133663367	133942536
chr7	134217877	134349309
chr1	134405320	134425526
chr6	134446830	134524737
chr1	134455048	134458631
chr5	134703598	134703888
chr4	135920443	135938151
chr6	136876172	136896182
chr5	136983412	137002916
chr2	137005052	137136380
chr5	137050047	137108615
chr5	137595146	137619323
chr5	138160557	138175861
chr4	143258114	143311303
chr2	144316955	144332554
chr3	145614345	145645451
chr6	147256320	147302120
chr4	147912722	147932603
chr2	148122497	148200139
chr4	148138227	148138433
chr4	148506367	148561843
chr1	153114286	153193967
chr1	153195306	153334986
chrX	155177355	155229698
chr1	155778417	155796103
chr2	156748033	156766093
chr2	158150030	158171287
chr2	158767417	158801060
chr1	163284111	163343394
chr2	164416276	164446147
chr2	167532413	167535369

chr1	169721405	169837828
chr1	172020035	172028016
chr1	172098157	172106818
chr2	172892528	172962408
chr2	173220240	173285869
chr1	186712318	186725769

*Supplementary Table 2:
Pearson scores and p-values when correlating the metastatic potential and histone profiles of 20 TNBC lines from the MetMap project.*

Histone Marks	P-Value	Pearson Correlation
H3K4me0	0.8448	0.0455
H3K4me1	0.9921	-0.0023
H3K4me2	0.9452	0.016
H3K4ac1	0.9837	0.0048
H3K9me0K14ac0	0.4121	0.1889
H3K9me1K14ac0	0.9797	-0.0059
H3K9me2K14ac0	0.8837	0.034
H3K9me3K14ac0	0.1731	0.3088
H3K9ac1K14ac0	0.2015	0.2905
H3K9me0K14ac1	0.5277	0.146
H3K9me1K14ac1	0.9272	0.0212
H3K9me2K14ac1	0.9791	-0.0061
H3K9me3K14ac1	0.3429	0.2178
H3K9ac1K14ac1	0.3814	0.2014
H3K18ac0K23ac0	0.8652	0.0394
H3K18ac1K23ac0	0.1636	0.3155
H3K18ac0K23ac1	0.7065	0.0874
H3K18ac1K23ac1	0.3209	0.2277
H3K18ac0K23ub1	0.1603	0.3178
H3K27me0K36me0	0.704	0.0881
H3K27me0K36me1	0.1818	0.303
H3K27me0K36me2	0.4944	0.1578
H3K27me0K36me3	0.21	0.2853
H3K27me1K36me0	0.8268	0.0508
H3K27me1K36me1	0.0343	0.4636
H3K27me1K36me2	0.0607	0.4159
H3K27me1K36me3	0.1721	0.3095
H3K27me2K36me0	0.3307	0.2232
H3K27me2K36me1	0.0452	0.4413
H3K27me2K36me2	0.6122	0.1174
H3K27me3K36me0	0.8155	-0.0542
H3K27me3K36me1	0.9607	0.0115
H3K27ac1K36me0	0.0547	0.4251
H3K27ac1K36me1	0.049	0.4346
H3K27ac1K36me2	0.0411	0.4491
H3K27ac1K36me3	0.0362	0.4594
H3.3K27me0K36me0	0.8008	0.0586
H3K56me0	0.0412	0.4489

H3K56me1	0.5709	0.1312
H3K79me0	0.1624	-0.3163
H3K79me1	0.366	-0.2078
H3K79me2	0.2621	-0.2563

*Supplementary Table 3:
 JetSet probes associated with the OXPHOS genes that are enriched in PyMT MICs
 vs. Non-MICs that are used to stratify patients' probability for distant relapse.*

Jet Set Probes
209303_at
202026_at
201597_at
244293_at
227808_at
238974_at
209248_at
202941_at
212600_s_at
203606_at
203371_s_at
201227_s_at
202233_s_at
218226_s_at
217773_s_at
222992_s_at
223296_at
223048_at
218563_at
203621_at
202298_at
203613_s_at
221677_s_at
217491_x_at
203190_at
1553367_a_at
203478_at
200086_s_at
222521_x_at

217720_at
201304_at
208969_at
218200_s_at
228142_at
218160_at
202000_at
206353_at
225638_at
229443_at
202077_at
202785_at
201256_at
230426_at
227143_s_at
200059_s_at
201816_s_at
208909_at
244763_at
201822_at
201172_x_at
218408_at
201403_s_at
223448_x_at
201106_at
214297_at
201527_at
202447_at
202110_at
203880_at
218027_at
203465_at

201754_at
201441_at
207843_x_at
201931_at
218357_s_at
214170_x_at
200078_s_at
209620_s_at
226030_at
203517_at
218316_at
201619_at
211595_s_at
217874_at
201135_at
200947_s_at
220753_s_at
201007_at
201599_at
238765_at
202825_at
222474_s_at
200657_at
203814_s_at
202282_at
203658_at
212434_at
219162_s_at
202070_s_at
226463_at
221504_s_at
208678_at

219348_at
208845_at
201243_s_at

EXPERIMENTAL PROCEDURES

Mice

MMTV-PyMT mice in the FVB/N background and the $\text{rag2}^{-/-}\gamma\text{c}^{-/-}$ mice in the NMRI background were obtained from JAX and were described previously^{336,337}. DEREK mice in the BALB/c background were used as GFP-tolerant recipients and were obtained by backcrossing DEREK mice in the C57BL/6J background³³⁸ to wildtype BALB/c mice for at least 10 generations. Wildtype FVB mice were bred inhouse, and wildtype BALB/c mice were purchased from Charles River Laboratories. All animal procedures were in accordance with Swiss legislation on animal experimentation.

Cell lines

The murine cancer cell line 4T1 was obtained from ATCC, the human cancer cell lines MDA-MB-231 and BT549 were a kind gift from Dr. Paloma Ordonez Moran (University of Nottingham), and the human cancer cell lines, BT20 and HCC1806, were a kind gift from Prof. Cathrin Brisken (EPFL). Cell lines were maintained in Dulbecco's Modified Eagle Medium (Gibco #31966021) supplemented with 10% fetal bovine serum (FBS; Sigma-Aldrich), 20 mM HEPES buffered to pH 7.4 (HEPES), and penicillin-streptomycin (pen/strep; Gibco #15140122).

Tumor cell isolation from spontaneous PyMT tumors

MMTV-PyMT mice were sacrificed at approximately 12-18 weeks of age for tumor cell isolation. Tumors were minced then digested with 37.5 $\mu\text{g}/\text{ml}$ Liberase TH (Roche #5401151001), 37.5 $\mu\text{g}/\text{ml}$ Liberase TM (Roche #5401127001), and 25 $\mu\text{g}/\text{ml}$ DNase (Roche #11284932001) in DMEM/F12 (Gibco #31331028) supplemented with HEPES and pen/strep for 1 hour at 37°C. Cells were washed once in 4°C 1x PBS supplemented with 0.5% BSA and 2 mM EDTA, then were passed through a 70 μm strainer, then washed an additional two times in DMEM/F12 supplemented with HEPES and pen/strep. At this point, cells were stained for flow cytometry or lysed for RNA isolation. Otherwise, cells were seeded onto collagen-coated plates with DMEM/F12 supplemented with 2% FBS, HEPES, pen/strep, 20 ng/ml hEGF (Gibco #PHG0313), and 10 $\mu\text{g}/\text{ml}$ hInsulin (Sigma-Aldrich #I9278-5ML).

In vitro treatments

Galactose supplementation. For PyMT cells, after overnight seeding in complete media as outlined above, media was changed to glucose- and glutamine-free DMEM (Gibco #A1443001) supplemented with 2% FBS, HEPES, pen/strep, 1x GlutaMAX (Gibco # 35050061), hEGF, hInsulin, 0.5x MEM Non-Essential Amino Acids Solution, and 20 mM galactose or 20 mM glucose. Cells were incubated in this medium for 36-72 hours prior to trypsinization for flow cytometry. For 4T1 cells, after overnight seeding in complete media as outlined above, media was changed to glucose- and glutamine-free DMEM (Gibco #A1443001) supplemented with 10% FBS, HEPES, pen/strep, 1x GlutaMAX (Gibco # 35050061), and 20 mM galactose or 20 mM glucose. Cells were incubated in this medium for 48 hours prior to trypsinization for TVIs.

Inhibitor treatments. After overnight seeding, media was changed to media containing inhibitors of interest the next day. PyMT cells were incubated with the treatments for 72 hours and 4T1 cells and human cell lines were incubated with the treatments for 48 hours. Inhibitor concentrations were identified by maximal effective concentration or half-maximal lethal dose. Below are the list of inhibitors, catalog numbers, and concentrations used for the two cell lines.

Treatment	Catalog Number	PyMT	4T1
Oligomycin	Sigma-Aldrich #75351	1 μ M	1 μ M
Acetate	Sigma-Aldrich # S5636-250G	5 mM	5 mM
Fluoroacetate	Toronto Research Chemicals #S960143	5 mM	5 mM
Etomoxir	Sigma-Aldrich #E1905	40 μ M	50 μ M
ATGListatin	SAGECHEM Limited	20 μ M	40 μ M
T863	Cayman Chemical #25807	10 μ M	20 μ M
PF-06424439	Cayman Chemical #17680	20 μ M	40 μ M
SB204990	Tocris Bioscience #4962	30 μ M	50 μ M
JQ1	Sigma-Aldrich #SML0974	50 nM	500 nM
C646	Cayman Chemical #10549	1 μ M	n/a

Flow Cytometry

PyMT CSC frequency. Biotin-conjugated antibodies used for lineage depletion are Ter119 (Biolegend #116203, clone Ter119), CD31 (Biolegend #102503, clone

Mec13.3), and CD45 (Biolegend #103104, clone 30-F11). PyMT CSCs are then identified by staining for CD24 (Biolegend #101807, clone MI/69) and CD90.1 (Biolegend #202526, clone OX-7).

ALDEFLUOR Assay. Staining was performed according to manufacturer's instructions (STEMCELL Technologies #01700). Briefly, cells were incubated with ALDEFLUOR reagent with or without DEAB for 30 minutes at 37°C. Cells were washed with the provided assay buffer and kept on ice during acquisition.

Mitochondrial Probes. Cells were stained with 20 nM MitoSpy Red CMXRos (Biolegend #424801) in media for mitochondrial membrane potential in live cells and 200 nM in fixed cells at 37°C. Cells were stained with 50 nM MitoSpy Green FM (Biolegend #424806) for mitochondrial mass in live cells at 37°C.

Lipid Storage. Cells were stained according to a previously described protocol³³⁹. In brief, cells were washed twice with 1x PBS then were stained with 2 µm BODIPY 493/503 (Invitrogen #D3922) in 1x PBS for 15 minutes at 37°C. Cells were no longer subjected to FBS after staining.

Lipid Uptake. Cells were stained according to a previously described protocol³⁴⁰. In brief, attached cells were incubated with 37°C 2 µm BODIPY FL C12 (Invitrogen #D3822) in 0.1% Fatty-Acid Free BSA (Sigma-Aldrich #126609) in 1x HBSS (Gibco #14175095) for 30 seconds to 5 minutes. Staining was quenched by addition of 4°C 0.2% BSA in 1x PBS.

Histone Marks. Cells in suspension were first stained for viability using LIVE/DEAD Fixable Dead Cell Stain Kit (Invitrogen #L23105). Cells were then fixed and permeabilized using the Foxp3/Transcription Factor Staining Kit (eBioscience #00-5523-00) according to the manufacturer's protocol. Cells were then stained with antibodies against H3K27ac (CST #8173, clone D5E4) or Total H3 (Novus Biologicals #NBP2-59277, clone 1B1B2) at room temperature for 1 hour, then stained with anti-rabbit secondary antibody at room temperature for 1 hour.

Cell death. Cells were stained for Annexin V (Biolegend #640905) according to manufacturer's protocol and DAPI. Living cells were considered as Annexin V negative and DAPI negative.

Proliferation. Cells were stained using CellTrace Violet Proliferation Kit (Invitrogen #C34557) prior to plating and were measured 36 hours later. If not otherwise specified, viability was measured by DAPI staining.

ROS Measurements. Cells in suspension were stained using 5µm of freshly prepared DCFDA for 20 mins prior to antibody staining.

Measurements were analyzed using the FlowJo software v10.7.2.

Seahorse Assays

Tumorsphere Generation. Single cells were seeded into polyHEMA coated plates³⁴¹ with DMEM/F12 supplemented with 2% FBS, HEPES, pen/strep, 20 ng/ml hEGF, 10 µg/ml hInsulin, and 4 ng/ml of Heparin. Cells were cultured for 96 hours prior to trypsinization and plating for 4-6 hours for measurements.

Mito Stress Test. Cells were grown on Seahorse XF96 cell culture dishes for a minimum of 4 hours prior to media change. For the assay, cells were maintained in 1x KHB media supplemented with pen/strep, 20 ng/ml hEGF, 10 µg/ml hInsulin, and 0.5 mM L-Carnitine (Sigma-Aldrich #C0158), as described by the manufacturer's protocol. OCR and ECAR were measured every 6 minutes, and treatments were administered every 30 minutes. Glucose to 10 mM final concentration was injected first, followed by oligomycin (Sigma-Aldrich #495455-10MG) to 1 µM final concentration, then FCCP (Sigma-Aldrich #C2920-10MG) to 2 µM final concentration, then finally Rotenone (Sigma-Aldrich #R8875-1G) and Antimycin A (Sigma-Aldrich #A8674-25MG) to a final concentration of 0.5 µM each.

Mito Fuel Flex Test. Cells were grown on Seahorse XF96 cell culture dishes for a minimum of 4 hours prior to media change. For the assay, cells were maintained in DMEM/F12 supplemented with 2% FBS, pen/strep, and HEPES. OCR was measured every 6 minutes, and treatments were administered every 30 minutes. Final concentrations for drug injections were 40 µM for etomoxir (Sigma-Aldrich #E1905-5MG), 10 µM for BPTES (Sigma-Aldrich #SML0601-5MG), and 20µM for UK5099 (Sigma-Aldrich #PZ0160-5MG).

Proliferation Assay

Cells were treated for 48 to 72 hours prior to trypsinization and plating for proliferation. If KDs were used, sufficient KD was first confirmed via qPCR prior to plating for proliferation. For each measurement, MTT reagent was added to a final concentration of 0.5 mg/mL for 3.5 to 4 hours. Media was aspirated from the plates, and MTT solvent (Isopropanol + 4 mM HCl + 0.1% NP40) was added. After 5

minutes on a benchtop shaker, the absorbance was read using a spectrophotometer (TECAN) at 590 nm wavelength.

Metabolomics Measurements

Adherent cells were washed twice in 1x PBS prior to snap freezing in liquid nitrogen. Cells were scraped in a 2:2:1 ratio of methanol, acetonitrile, and water supplemented with 0.1M formic acid then homogenized in the Cryolys Precellys 24 sample Homogenizer (Bertin Technologies, Rockville, MD, US) with ceramic beads. Homogenized extracts were centrifuged and the resulting supernatant was collected and dried in a vacuum concentrator (LabConco, Missouri, US). Dried sample extracts were resuspended with 80% MeOH containing the internal standards and injected into the HILIC-MS/MS system. Extracted samples were analyzed by Hydrophilic Interaction Liquid Chromatography coupled to tandem mass spectrometry (HILIC - MS/MS)^{342,343} in negative ionization mode using a 6495 triple quadrupole system (QqQ) interfaced with 1290 UHPLC system (Agilent Technologies). Chromatographic separation was carried out on a SeQuant ZIC-pHILIC column (100 mm, 2.1 mm I.D. and 5 μ m particle size, Merck, Damstadt, Germany). Raw LC-MS/MS data was processed using the Agilent Quantitative analysis software (version B.07.00, MassHunter Agilent technologies). For absolute quantification, calibration curves and the stable isotope-labelled internal standards (IS) were used to determine the response factor. Linearity of the standard curves was evaluated for each metabolite using a 10-point range; in addition, peak area integration was manually curated and corrected when necessary. Concentrations were normalized to protein content measured by BCA assay (Thermo Scientific #23225) following the metabolite extraction.

Western Blotting

Cells were washed twice in 1x PBS supplemented with 5 mM sodium butyrate, then lysed with 1x PBS supplemented with 1% Triton X, 5 mM sodium butyrate, anti-protease inhibitors (100 μ M AEBSF, 10 μ M bestatin, 10 μ M E64, 10 μ M leupeptin, 10 μ M pepstatin A, 1 mM DTT), and anti-phosphatase inhibitors (2.5 mM sodium pyrophosphate, 1 mM β -glycerophosphate, 1 mM sodium orthovanadate, 2.5 mM sodium fluoride). Histones were precipitated using 0.2 N HCl overnight then quantified by BCA assay. Proteins were separated by electrophoresis, transferred to

PVDF membranes, then blocked with 5% BSA prior to overnight incubation with primary antibodies (H3K27ac: CST #8173, Total H3: CST #3638) at 4°C. Immunoreactive bands were visualized using HRP-conjugated secondary antibodies (Anti-Rabbit: Jackson Immunosearch #711-035-152, Anti-Mouse: Promega #W4021) and the detection reagent WesternBright Sirius HRP substrate (Advansta #K-12043-D10). For protein normalization, PVDF membranes were stripped with 2% SDS, 62.5 mM Tris HCl pH6.8, and 0.8% β -mercaptoethanol, washed extensively, then reprobed.

RNA Isolation and Sequencing

Primary PyMT cells were plated overnight, then sorted the next day for Lin-CD24+CD90+ and Lin-CD24+CD90- cells. Cells were directly collected into lysis buffer, and RNA isolation was subsequently performed with the Qiagen RNeasy Mini Kit (Qiagen #74104) according to the manufacturer's protocol. RNA quality was assessed using the Agilent DNF-472T33 HS RNA (15 nt) Kit (Agilent Technologies) on fragment analyzer (Qiaxcel). Library preparation was performed using the TruSeq mRNA stranded method (Illumina), then quality was checked using TapeStation TS4200 (Agilent). Libraries were then sequenced on a NextSeq500 sequencer (Illumina) for 75 cycles at 40 million reads per sample. Raw sequencing reads were aligned against the mouse transcriptome (GRCm38/mm10 release) and the quantification was done at the gene level using the Bowtie2/samtools pipeline. This data is deposited in GEO and can be accessed under GSE236222.

4T1 cells were plated overnight, then treated for 48 hours. Cells were harvested by trypsinization, and the cell pellet was resuspended in lysis buffer. For sorted 4T1 cells, cells were stained for 30 mins with 20 nM MitoSpy Red CMXRos, trypsinized, sorted for high and low MMP (5% each population), spun down, and resuspended in lysis buffer. RNA isolation was then performed using the High Pure RNA Isolation Kit (Roche #11828665001) according to the manufacturer's protocol. RNA Quality was assessed by TapeStation TS4200, then libraries were prepared using the Illumina Stranded mRNA Prep Kit. Library quality was then assessed by TapeStation TS4200, then sequenced on the NextSeq500 (Illumina) for 75 cycles at 40 million reads per sample. Raw sequencing reads were aligned against the mouse transcriptome (GRCm38/mm10 release) and the quantification was done at the gene

level using STAR³⁴⁴. This data is deposited in GEO and can be accessed under GSE220991 and GSE236185.

Gene Set Enrichment Analysis. Count matrices were normalized to total library size, filtered for genes expressed by at least half of the samples, then were subjected to unbiased gene set enrichment analysis using the GSEA software v4.2.3^{345–348}.

Analysis was performed against the Hallmark Gene Set collection and the Gene Ontology Gene Set collection with 1000 gene set permutations. Gene set enrichment was considered significant after Signal2Noise gene ranking at a false discovery rate under 0.05 for sets containing at least 3 replicates per condition (PyMT MICs vs. non-MICs and 4T1 cells treated with vehicle vs. acetate). For the high vs. low MMP dataset, gene set enrichment was considered significant at a false discover rate under 0.25 after log2 Ratio of Classes gene ranking.

Real time qPCR

Complementary DNA was synthesized using the Maxima H Minus Reverse Transcriptase (Thermo Scientific #EP0752) and oligodT priming. Quantitative PCR was performed using the PowerUp SYBR Green Master Mix (Applied Biosystems #A25741) on a QuantStudio 6 Flex Real Time PCR Machine (Applied Biosystems). Below are the primers used for each of the genes discussed. Primers that were designed using the PrimerBank database are annotated with the appropriate primer ID^{349–351}; primers of our own design are annotated as “n/a”.

Target Gene	MGH Primer ID	Forward Primer	Reverse Primer
<i>mHprt</i>	n/a	TGTATACCTAATCATTATG CCGAGG	CAGGTCAGCAAAGAACT TATAGC
<i>mRpl19</i>	n/a	CTGATCAAGGATGGGCTG AT	GGCAGTACCCTTCCTCTT CC
<i>mRpl22</i>	6677775a 1	AGCAGGTTTTGAAGTTCAC CC	CAGCTTTCCCATTCACCT TGA
<i>mYwha z</i>	6756041a 1	GAAAAGTTCTTGATCCCCA ATGC	TGTGACTGGTCCACAATT CCTT

<i>mPolr2</i> <i>m</i>	30519919 a1	TTGCCCGACAAAGGTA AAA AGA	TGTCTATTGAGGAACAGT CAGGA
<i>mAcly</i>	18204829 a1	ACCCTTTCACTGGGGATCA CA	GACAGGGATCAGGATTT CCTTG
<i>mAcss</i> <i>1</i>	18034773 a1	GTTTGGGACACTCCTTACC ATAC	AGGCAGTTGACAGACAC ATTC
<i>mAcss</i> <i>2</i>	31980996 a1	AAACACGCTCAGGGAAAAT CA	ACCGTAGATGTATCCCC CAGG
<i>mCpt1a</i>	n/a	TGCCTCTATGTGGTGTCCA A	ACAACCTCCATGGCTCA GAC
<i>mCpt2</i>	16213891 4c1	CAGCACAGCATCGTACCC A	TCCCAATGCCGTTCTCAA AAT
<i>mDrp1</i>	71061454 c1	CCTCAGATCGTCGTAGTG GGA	GTTCTCTGGGAAGAAG GTCC
<i>mActa2</i>	6671507a 1	GTCCCAGACATCAGGGAG TAA	TCGGATACTTCAGCGTC AGGA
<i>mPostn</i>	7657429a 1	CCTGCCCTTATATGCTCTG CT	AAACATGGTCAATAGGC ATCACT
<i>mltga5</i>	n/a	ATGGCTCAGACATCCACTC C	GGTCATCTAGCCCATCT CCA
<i>mltgb3</i>	7949057a 1	CCACACGAGGCGTGA ACT C	CTTCAGGTTACATCGGG GTGA
<i>mltgb6</i>	10946686 a1	CAACTATCGGCCAACTCAT TGA	GCAGTTCTTCATAAGCG GAGAT
<i>mCol1a</i> <i>1</i>	n/a	CTGCACGAGTCACACCGG AA	AGGCAGGGCCAATGTCT AGT
<i>mCol12</i> <i>a1</i>	6680960a 1	AAGTTGACCCACCTTCCGA C	GGTCCACTGTTATTCTGT AACCC
<i>mMmp</i> <i>3</i>	6754714a 1	ACATGGAGACTTTGTCCCT TTTG	TTGGCTGAGTGGTAGAG TCCC
<i>mMmp</i> <i>10</i>	n/a	TTTTAAAGGAAGTCAGTTC TGGG	ATGTCTTGTCTCATCAAA TCTCC

<i>mScub</i> e3	52138545 c1	CATCTGCCAGAATACCCCA CG	GTCCTCCCGTTCACACT CATC
<i>mSparc</i>	n/a	GCATCAAGGAGCAGGACA TCAA	ACGGTGAGCTTATGCAA CTCC
<i>mTwist</i> 2	n/a	CTACAGCAAGAAATCGAG CG	GGCCTCGTTGAGCGACT
<i>hTBP</i>	n/a	CGAAACGCCGAATATAATC CCA	GACTGTTCTTCACTCTTG GCTC
<i>hACLY</i>	38569422 c2	ATCGGTTCAAGTATGCTCG GG	GACCAAGTTTTCCACGA CGTT
<i>hACSS</i> 2	33472445 4c1	AAAGGAGCAACTACCAACA TCTG	GCTGAACTGACACACTT GGAC

Lentivirus Production for miR-mediated KDs

Lentiviruses were generated in 293T cells using 3rd generation packaging vectors. Viral particles were concentrated by ultracentrifugation for 2 hours and 30 minutes at 22,000 rpm. Titration was performed in 293Ts. Cells were then infected overnight with lentiviruses in the presence of 8 µg/ml polybrene. MicroRNA sequences for KDs are listed below:

Target Gene	Sense	Anti-sense
GFP	CCAGCCACAACGTCTATATCA	TGATATAGACGTTGTGGCTGT
<i>mCherry</i>	TCGAGTTCATCTACAAGGTGA	TCACCTTGTAGATGAACTCGC
<i>mAclY</i>	GAAGCCAGACCAGTTAATCAA	TTGATTAAGTGGTCTGGCTTG
<i>mAcss1</i>	GACAGTGGTATTTGCTGGCTT	AAGCCAGCAAATACCACTGTG
<i>mAcss2</i>	TCCAAGGAATTTACTGGAAA	TTTCCAGTAAAATTCCTTGGC
<i>mCpt1a</i>	TCCGATCATGGTTAACAGCAA	TTGCTGTTAACCATGATCGGC
<i>mCpt2</i>	GAGAGCTCAGACAGAAGTTGA	TCAACTTCTGTCTGAGCTCTG
<i>mDrp1</i>	ACAGATCAGAGAACTTATTCT	AGAATAAGTTCTCTGATCTGA
<i>hACLY</i>	CAGTCACAATCTTTGTCCGAA	TTCGGACAAAGATTGTGACTT
<i>hACSS2</i>	CAGCTTGGAGATAAAGTTGCT	AGCAACTTTATCTCCAAGCTT

ChIP-Seq

Chromatin immunoprecipitation was performed using the SimpleChIP Enzymatic Chromatin IP Kit (CST #9003) according to the manufacturer's protocol. Briefly, adherent cells were washed then fixed in 1x PBS supplemented with 1% methanol-free PFA (Thermo Scientific #28908). The reaction was quenched with 1X glycine, cells were pelleted, then stored at -80°C. Cells were lysed, and chromatin was sheared by adding 0.5 ul Micrococcal nuclease for 20 minutes at 37°C. Nuclei were then lysed by sonication. After addition of 7.5% of human spike-in, sheared mouse chromatin was incubated overnight at 4°C with 1:100 H3K27ac antibody (CST #8173). Protein G magnetic beads were used to pull down antibody-bound fragments then eluted at 65°C for 30 minutes. Reverse crosslinking was done with NaCl and Proteinase K then purified with columns.

Libraries were prepared using the NEBNext Ultra II DNA Prep Kit (NEB #E765S) according to the manufacturer's protocol then quality was assessed on the TapeStation TS4200. Libraries were then sequenced on NovaSeq6000 in a PE60 run with an average sequencing depth of 40 million reads per sample with Illumina protocol #1000000106351 v03.

Raw sequences were pre-processed and aligned to a merged GRCh38 and GRCmm10 reference genome through the nf-core/chipseq v1.2.2 workflow³⁵². Scaling factors for the mouse library were computed by normalizing to the size of the human spike-in library. BigWig files were generated using the BamCoverage tool from deepTools v3.5.1 then tracks were plotted using pyGenomeTracks v3.7³⁵³. The heatmap was generated using the computeMatrix (scaled mode; gene regions were scaled to 5000bp) and plotHeatmap function from deepTools. The plotted EMT genes comes from the union of genes present in HALLMARK_EPITHELIAL_MESENCHYMAL_TRANSITION and GOBP_EPITHELIAL_TO_MESENCHYMAL_TRANSITION available from the Molecular Signature Database. The BED file can be found in **Supplementary Table 1**. The data is deposited in GEO and can be accessed under GSE236223.

Lipid Droplet Measurements

Immunostaining on fresh frozen tissue was performed on 5 µm sections after 1 hour fixation with 4% paraformaldehyde and a 10-minute permeabilization with 0.1% Triton X-100. Primary antibody staining was done for 1 hour. Sections were then stained for 30 minutes with Oil Red O then washed extensively with water. Nuclei

were stained with DAPI, then mounted using Fluoromount G (SouthernBiotech #0100-01).

Images were analyzed by QuPath v0.4.2. Areas containing tumor cells were selected manually by annotating areas that were GFP positive and had enlarged nuclei. Lipid droplets and nuclei were detected by setting a size and intensity threshold using the pre-trained 2D_versatile_fluo 2D_paper_dsb2018 model from StarDist^{354,355}.

Experimental Metastasis Assay

Tumor cells were treated with inhibitors or supplements for 48 hours for 4T1, BT20, and MDA-MB-231 or 72 hours for PyMT cells. Cells were trypsinized, washed three times in cold 1x HBSS, then resuspended in 100 μ L of 1x HBSS. 5×10^5 PyMT cells were injected into each wildtype FVB/N recipient mice, 5×10^4 4T1 cells were injected into each wildtype Balb/c, DEREg, or Rag2^{-/-} γ c^{-/-} recipient mice, 3×10^5 BT20 cells were injected into each Rag2^{-/-} γ c^{-/-} mice, and 5×10^4 MDA-MB-231 cells were injected into each Rag2^{-/-} γ c^{-/-} mice. Mice were euthanized at a fixed time point –Day 35 for PyMT, Day 14 for 4T1 (Day 8 if injected into Rag2^{-/-} γ c^{-/-} recipients), and Day 28 for BT20, and MDA-MB-231. Lung lobes were separated and macrometastases were counted using a brightfield stereomicroscope. If cells were expressing GFP, GFP+ nodules were counted by flattening each lung lobe between two microscope slides then taking images using a fluorescent stereomicroscope (Nikon SMZ18 stereomicroscope). Images were then analyzed using Fiji v2.9.0 by size and intensity threshold and using the “analyze particles” function. All animal procedures were in accordance with Swiss legislation on animal experimentation.

Orthotopic Experiments

3.5×10^5 PyMT cells were resuspended in 30 μ L of 2mg/ml collagen I (Gibco #A1048301) and injected into the fourth mammary pad of wildtype FVB/N recipient mice. Tumor size was determined by caliper measurements and calculated using the formula: $V = (D \cdot d^2) / 2$, where d is the shorter and D is the longer tumor axis. Tumors were resected once they reached 1000mm³. Thirty days after tumor resection, mice were euthanized, and the number of spontaneous lung metastases were counted. All animal procedures were in accordance with Swiss legislation on animal experimentation.

CCLC Dataset Analysis

Chromatin profiling and metastasis potential datasets were downloaded from the CCLC depmap portal. Mean metastatic potential was calculated by averaging metastatic potential across the 5 different sites of metastatic colonization. Pearson coefficients and p-values for the correlations between scaled abundances of histone marks and mean metastatic potential were calculated using the `pearsonr` function from the SciPy Stats package (v1.10.1; **Supplementary Table 2**)³⁵⁶. Plots were then generated using the `mark_point` function of Altair (v4.2.2)³⁵⁷.

Kaplan-Meier

Kaplan-Meier plots for relapse-free survival were generated using the breast cancer cohort (mRNA gene chip) or the TCGA cohort (mRNA RNA-seq, breast cancer patients from the pan-cancer cohort) using `KM-plotter`³⁵⁸. Patients were stratified based on either the median or quartile cut-offs. For the microarray cohort, JetSet best probe sets were used for the genes of interest. The OXPHOS signature was generated from the genes that were identified as enriched from the HALLMARK_OXIDATIVE_PHOSPHORYLATION and GOBP_OXIDATIVE_PHOSPHORYLATION by GSEA in the sorted PyMT MICs compared to the non-MICs (**Supplementary Table 3**). Mean expression of all genes was used as input to stratify the patients.

Statistical Analysis and Data Availability

Processing and data analysis of microscopy images were performed in Fiji or QuPath. Flow cytometry files were analyzed using FlowJo. Experimental data are presented as mean +/- SEM and statistical computations were performed using GraphPad Prism9 or SciPy stats. Statistical significance was assessed by two-tailed unpaired Student's t test, two-tailed paired ratio t-test, or ordinary one-way ANOVA, data were considered significant at $p \leq 0.05$. High throughput data can be accessed under the GEO SuperSeries GSE220992.

REFERENCES

1. Surveillance Research Program National Cancer Institute. SEER*Explorer: An interactive website for SEER cancer statistics.
2. Hudock, N. L. *et al.* Future trends in incidence and long-term survival of metastatic cancer in the United States. *Commun. Med.* **3**, 1–7 (2023).
3. Harbeck, N. *et al.* Breast cancer. *Nat. Rev. Dis. Prim.* **5**, (2019).
4. Ganesh, K. & Massagué, J. Targeting metastatic cancer. *Nat. Med.* **27**, 34–44 (2021).
5. Lambert, A. W., Pattabiraman, D. R. & Weinberg, R. A. Emerging Biological Principles of Metastasis. *Cell* **168**, 670–691 (2016).
6. Massagué, J. & Obenauf, A. C. Metastatic colonization by circulating tumour cells. *Nature* **529**, 298–306 (2016).
7. Graziani, V., Rodriguez-Hernandez, I., Maiques, O. & Sanz-Moreno, V. The amoeboid state as part of the epithelial-to-mesenchymal transition programme. *Trends Cell Biol.* **32**, 228–242 (2022).
8. Friedl, P. & Wolf, K. Tumour-cell invasion and migration: Diversity and escape mechanisms. *Nat. Rev. Cancer* **3**, 362–374 (2003).
9. Hotary, K., Li, X. Y., Allen, E., Stevens, S. L. & Weiss, S. J. A cancer cell metalloprotease triad regulates the basement membrane transmigration program. *Genes Dev.* **20**, 2673–2686 (2006).
10. Levental, K. R. *et al.* Matrix Crosslinking Forces Tumor Progression by Enhancing Integrin Signaling. *Cell* **139**, 891–906 (2009).
11. Wang, W. *et al.* Single cell behavior in metastatic primary mammary tumors correlated with gene expression patterns revealed by molecular profiling. *Cancer Res.* **62**, 6278–6288 (2002).
12. Taftaf, R. *et al.* ICAM1 initiates CTC cluster formation and trans-endothelial migration in lung metastasis of breast cancer. *Nat. Commun.* **12**, 1–15 (2021).
13. Locard-Paulet, M. *et al.* Phosphoproteomic analysis of interacting tumor and endothelial cells identifies regulatory mechanisms of transendothelial migration. *Sci. Signal.* **9**, 1–17 (2016).
14. Gligorijevic, B. *et al.* N-WASP-mediated invadopodium formation is involved in intravasation and lung metastasis of mammary tumors. *J. Cell Sci.* **125**, 724–734 (2012).
15. Chabottaux, V. *et al.* Membrane-type 4 matrix metalloproteinase (MT4-MMP)

- induces lung metastasis by alteration of primary breast tumour vascular architecture. *J. Cell. Mol. Med.* **13**, 4002–4013 (2009).
16. Wyckoff, J. B. *et al.* Direct visualization of macrophage-assisted tumor cell intravasation in mammary tumors. *Cancer Res.* **67**, 2649–2656 (2007).
 17. Aceto, N. *et al.* Circulating tumor cell clusters are oligoclonal precursors of breast cancer metastasis. *Cell* **158**, 1110–1122 (2014).
 18. Lee, H. J. *et al.* Fluid shear stress activates YAP1 to promote cancer cell motility. *Nat. Commun.* **8**, 1–14 (2017).
 19. Xin, Y. *et al.* Mechanics and Actomyosin-Dependent Survival/Chemoresistance of Suspended Tumor Cells in Shear Flow. *Biophys. J.* **116**, 1803–1814 (2019).
 20. Schafer, Z. T. *et al.* Antioxidant and oncogene rescue of metabolic defects caused by loss of matrix attachment. *Nature* **461**, 109–113 (2009).
 21. Jiang, L. *et al.* Reductive carboxylation supports redox homeostasis during anchorage-independent growth. *Nature* **532**, 255–258 (2016).
 22. Nieswandt, B., Hafner, M., Echtenacher, B. & Männel, D. N. Lysis of tumor cells by natural killer cells in mice is impeded by platelets. *Cancer Res.* **59**, 1295–1300 (1999).
 23. Chambers, A. F., Groom, A. C. & MacDonald, I. C. Dissemination and growth of cancer cells in metastatic sites. *Nat. Rev. Cancer* **2**, 563–572 (2002).
 24. Al-Mehdi, A. B. *et al.* Intravascular origin of metastasis from the proliferation of endothelium-attached tumor cells: a new model for metastasis. *Nat. Med.* **6**, 100–102 (2000).
 25. Kienast, Y. *et al.* Real-time imaging reveals the single steps of brain metastasis formation. *Nat. Med.* **16**, 116–122 (2010).
 26. Schumacher, D., Strilic, B., Sivaraj, K. K., Wettschureck, N. & Offermanns, S. Platelet-Derived Nucleotides Promote Tumor-Cell Transendothelial Migration and Metastasis via P2Y2 Receptor. *Cancer Cell* **24**, 130–137 (2013).
 27. Tichet, M. *et al.* Tumour-derived SPARC drives vascular permeability and extravasation through endothelial VCAM1 signalling to promote metastasis. *Nat. Commun.* **6**, 1–15 (2015).
 28. Weis, S., Cui, J., Barnes, L. & Cheresh, D. Endothelial barrier disruption by VEGF-mediated Src activity potentiates tumor cell extravasation and metastasis. *J. Cell Biol.* **167**, 223–229 (2004).
 29. Wong, C. W. *et al.* Apoptosis: An early event in metastatic inefficiency. *Cancer Res.* **61**, 333–338 (2001).

30. Naumov, G. N. *et al.* Persistence of solitary mammary carcinoma cells in a secondary site: A possible contributor to dormancy. *Cancer Res.* **62**, 2162–2168 (2002).
31. Correia, A. L. *et al.* Hepatic stellate cells suppress NK cell-sustained breast cancer dormancy. *Nature* **594**, 566–571 (2021).
32. Bidwell, B. N. *et al.* Silencing of *Irf7* pathways in breast cancer cells promotes bone metastasis through immune escape. *Nat. Med.* **18**, 1224–1231 (2012).
33. Eyles, J. *et al.* Tumor cells disseminate early, but immunosurveillance limits metastatic outgrowth, in a mouse model of melanoma. *J. Clin. Invest.* **120**, 2030–2039 (2010).
34. Dykxhoorn, D. M. *et al.* miR-200 enhances mouse breast cancer cell colonization to form distant metastases. *PLoS One* **4**, 1–14 (2009).
35. Chaffer, C. L. *et al.* Mesenchymal-to-epithelial transition facilitates bladder cancer metastasis: Role of fibroblast growth factor receptor-2. *Cancer Res.* **66**, 11271–11278 (2006).
36. Malanchi, I. *et al.* Interactions between cancer stem cells and their niche govern metastatic colonization. *Nature* **481**, 85–89 (2012).
37. Oskarsson, T. *et al.* Breast cancer cells produce tenascin C as a metastatic niche component to colonize the lungs. *Nat. Med.* **17**, 867–874 (2011).
38. Luzzi, K. J. *et al.* Multistep nature of metastatic inefficiency: Dormancy of solitary cells after successful extravasation and limited survival of early micrometastases. *Am. J. Pathol.* **153**, 865–873 (1998).
39. Simeonov, K. P. *et al.* Single-cell lineage tracing of metastatic cancer reveals selection of hybrid EMT states. *Cancer Cell* **39**, 1150–1162.e9 (2021).
40. Batlle, E. & Clevers, H. Cancer stem cells revisited. *Nat. Med.* **23**, 1124–1134 (2017).
41. Yang, J. *et al.* Guidelines and definitions for research on epithelial–mesenchymal transition. *Nat. Rev. Mol. Cell Biol.* **21**, 341–352 (2020).
42. Thiery, J. P., Acloque, H., Huang, R. Y. J. & Nieto, M. A. Epithelial–Mesenchymal Transitions in Development and Disease. *Cell* **139**, 871–890 (2009).
43. Mani, S. A. *et al.* The Epithelial–Mesenchymal Transition Generates Cells with Properties of Stem Cells. *Cell* **133**, 704–715 (2008).
44. Lüönd, F. *et al.* Distinct contributions of partial and full EMT to breast cancer malignancy. *Dev. Cell* **56**, 3203–3221.e11 (2021).

45. Fischer, K. R. *et al.* Epithelial-to-mesenchymal transition is not required for lung metastasis but contributes to chemoresistance. *Nature* **527**, 472–476 (2015).
46. Zheng, X. *et al.* Epithelial-to-mesenchymal transition is dispensable for metastasis but induces chemoresistance in pancreatic cancer. *Nature* **527**, 525–530 (2015).
47. Kudo-Saito, C., Shirako, H., Takeuchi, T. & Kawakami, Y. Cancer Metastasis Is Accelerated through Immunosuppression during Snail-Induced EMT of Cancer Cells. *Cancer Cell* **15**, 195–206 (2009).
48. Dongre, A. *et al.* Epithelial-to-mesenchymal transition contributes to immunosuppression in breast carcinomas. *Cancer Res.* **77**, 3982–3989 (2017).
49. Pastushenko, I. *et al.* Identification of the tumour transition states occurring during EMT. *Nature* **556**, 463–468 (2018).
50. Puram, S. V. *et al.* Single-Cell Transcriptomic Analysis of Primary and Metastatic Tumor Ecosystems in Head and Neck Cancer. *Cell* **171**, 1611–1624.e24 (2017).
51. Brown, M. S. *et al.* Phenotypic heterogeneity driven by plasticity of the intermediate EMT state governs disease progression and metastasis in breast cancer. *Sci. Adv.* **8**, 1–19 (2022).
52. Aiello, N. M. *et al.* EMT Subtype Influences Epithelial Plasticity and Mode of Cell Migration. *Dev. Cell* **45**, 681–695.e4 (2018).
53. Dongre, A. & Weinberg, R. A. New insights into the mechanisms of epithelial–mesenchymal transition and implications for cancer. *Nat. Rev. Mol. Cell Biol.* **20**, 69–84 (2019).
54. Celià-Terrassa, T. & Kang, Y. Metastatic niche functions and therapeutic opportunities. *Nat. Cell Biol.* **20**, 868–877 (2018).
55. Kaplan, R. N. *et al.* VEGFR1-positive haematopoietic bone marrow progenitors initiate the pre-metastatic niche. *Nature* **438**, 820–827 (2005).
56. Huang, Y. *et al.* Pulmonary vascular destabilization in the premetastatic phase facilitates lung metastasis. *Cancer Res.* **69**, 7529–7537 (2009).
57. Murgai, M. *et al.* KLF4-dependent perivascular cell plasticity mediates pre-metastatic niche formation and metastasis. *Nat. Med.* **23**, 1176–1190 (2017).
58. Clevers, H. Wnt/ β -Catenin Signaling in Development and Disease. *Cell* **127**, 469–480 (2006).
59. Macias, H. & Hinck, L. Mammary gland development. *Wiley Interdiscip. Rev.*

- Dev. Biol.* **1**, 533–557 (2012).
60. Shackleton, M. *et al.* Generation of a functional mammary gland from a single stem cell. *Nature* **439**, 84–88 (2006).
 61. Guo, W. *et al.* Slug and Sox9 cooperatively determine the mammary stem cell state. *Cell* **148**, 1015–1028 (2012).
 62. Barker, N. *et al.* Identification of stem cells in small intestine and colon by marker gene Lgr5. *Nature* **449**, 1003–1007 (2007).
 63. Fumagalli, A. *et al.* Plasticity of Lgr5-Negative Cancer Cells Drives Metastasis in Colorectal Cancer. *Cell Stem Cell* **26**, 569-578.e7 (2020).
 64. Li, J. *et al.* Metastasis and immune evasion from extracellular cGAMP hydrolysis. *Cancer Discov.* **11**, 1212–1227 (2021).
 65. Malladi, S. *et al.* Metastatic Latency and Immune Evasion through Autocrine Inhibition of WNT. *Cell* **165**, 45–60 (2016).
 66. Pommier, A. *et al.* Unresolved endoplasmic reticulum stress engenders immune-resistant, latent pancreatic cancer metastases. *Science (80-.).* **360**, eaao4908 (2018).
 67. Jaiswal, S. *et al.* CD47 Is Upregulated on Circulating Hematopoietic Stem Cells and Leukemia Cells to Avoid Phagocytosis. *Cell* **138**, 271–285 (2009).
 68. Wang, H. Bin *et al.* Rise of PD-L1 expression during metastasis of colorectal cancer: Implications for immunotherapy. *J. Dig. Dis.* **18**, 574–581 (2017).
 69. Sun, X. *et al.* Tumour DDR1 promotes collagen fibre alignment to instigate immune exclusion. *Nature* **599**, 673–678 (2021).
 70. Tauriello, D. V. F. *et al.* TGF β drives immune evasion in genetically reconstituted colon cancer metastasis. *Nature* **554**, 538–543 (2018).
 71. Thomas, D. A. & Massagué, J. TGF- β directly targets cytotoxic T cell functions during tumor evasion of immune surveillance. *Cancer Cell* **8**, 369–380 (2005).
 72. Clever, D. *et al.* Oxygen Sensing by T Cells Establishes an Immunologically Tolerant Metastatic Niche. *Cell* **166**, 1117-1131.e14 (2016).
 73. Hu, Z., Li, Z., Ma, Z. & Curtis, C. Multi-cancer analysis of clonality and the timing of systemic spread in paired primary tumors and metastases. *Nat. Genet.* **52**, 701–708 (2020).
 74. Yang, D. *et al.* Lineage tracing reveals the phylogenetics, plasticity, and paths of tumor evolution. *Cell* **185**, 1905-1923.e25 (2022).
 75. Priestley, P. *et al.* Pan-cancer whole-genome analyses of metastatic solid

- tumours. *Nature* **575**, 210–216 (2019).
76. Reiter, J. G. *et al.* An analysis of genetic heterogeneity in untreated cancers. *Nat. Rev. Cancer* **19**, 639–650 (2019).
 77. Reiter, J. G. *et al.* Minimal functional driver gene heterogeneity among untreated metastases. *Science (80-.)*. **361**, 1033–1037 (2018).
 78. Jacob, L. S. *et al.* Metastatic competence can emerge with selection of preexisting oncogenic alleles without a need of new mutations. *Cancer Res.* **75**, 3713–3719 (2015).
 79. Lawson, D. A. *et al.* Single-cell analysis reveals a stem-cell program in human metastatic breast cancer cells. *Nature* **526**, 131–135 (2015).
 80. Lebleu, V. S. *et al.* PGC-1 α mediates mitochondrial biogenesis and oxidative phosphorylation in cancer cells to promote metastasis. *Nat. Cell Biol.* **16**, 992–1003 (2014).
 81. Denny, S. K. *et al.* Nfib Promotes Metastasis through a Widespread Increase in Chromatin Accessibility. *Cell* **166**, 328–342 (2016).
 82. Segelle, A. *et al.* Histone marks regulate the epithelial-to-mesenchymal transition via alternative splicing. *Cell Rep.* **38**, (2022).
 83. Javaid, S. *et al.* Dynamic chromatin modification sustains epithelial-mesenchymal transition following inducible expression of snail-1. *Cell Rep.* **5**, 1679–1689 (2013).
 84. Chaffer, C. L. *et al.* Poised chromatin at the ZEB1 promoter enables breast cancer cell plasticity and enhances tumorigenicity. *Cell* **154**, 61–74 (2013).
 85. Flavahan, W. A., Gaskell, E. & Bernstein, B. E. Epigenetic plasticity and the hallmarks of cancer. *Science (80-.)*. **357**, eaal2380 (2017).
 86. Obradović, M. M. S. *et al.* Glucocorticoids promote breast cancer metastasis. *Nature* **567**, 540–544 (2019).
 87. Rothwell, P. M. *et al.* Effect of daily aspirin on risk of cancer metastasis: A study of incident cancers during randomised controlled trials. *Lancet* **379**, 1591–1601 (2012).
 88. Labelle, M., Begum, S. & Hynes, R. O. Direct Signaling between Platelets and Cancer Cells Induces an Epithelial-Mesenchymal-Like Transition and Promotes Metastasis. *Cancer Cell* **20**, 576–590 (2011).
 89. Dumont, N. *et al.* Breast fibroblasts modulate early dissemination, tumorigenesis, and metastasis through alteration of extracellular matrix characteristics. *Neoplasia (United States)* **15**, 249–262 (2013).

90. Betancur, P. A. *et al.* A CD47-associated super-enhancer links pro-inflammatory signalling to CD47 upregulation in breast cancer. *Nat. Commun.* **8**, (2017).
91. Neelakantan, D. *et al.* Cooperativity between EMT and non-EMT cells promotes breast cancer metastasis via paracrine GLI activation. *Nat. Commun.* 1–14 (2017) doi:10.1038/ncomms15773.
92. Marusyk, A. *et al.* Non-cell-autonomous driving of tumour growth supports sub-clonal heterogeneity. *Nature* **514**, 54–58 (2014).
93. Dontu, G. *et al.* In vitro propagation and transcriptional profiling of human mammary stem / progenitor cells. *Genes Dev.* **17**, 1253–1270 (2003).
94. Ponti, D. *et al.* Isolation and in vitro propagation of tumorigenic breast cancer cells with stem/progenitor cell properties. *Cancer Res.* **65**, 5506–5511 (2005).
95. Joeckel, E. *et al.* High calcium concentration in bones promotes bone metastasis in renal cell carcinomas expressing calcium-sensing receptor. *Mol. Cancer* **13**, 1–11 (2014).
96. Eyre, R. *et al.* Patient-derived mammosphere and xenograft tumour initiation correlates with progression to metastasis. *J. Mammary Gland Biol. Neoplasia* **21**, 99–109 (2016).
97. Katt, M. E., Placone, A. L., Wong, A. D., Xu, Z. S. & Searson, P. C. In vitro tumor models: Advantages, disadvantages, variables, and selecting the right platform. *Front. Bioeng. Biotechnol.* **4**, (2016).
98. Pascual, G. *et al.* Targeting metastasis-initiating cells through the fatty acid receptor CD36. *Nature* **541**, 41–45 (2017).
99. Sikandar, S. S. *et al.* Identification of a minority population of LMO2+ breast cancer cells that integrate into the vasculature and initiate metastasis. *Sci. Adv.* **8**, eabm3548 (2022).
100. Hebert, J. D., Neal, J. W. & Winslow, M. M. Dissecting metastasis using preclinical models and methods. *Nat. Rev. Cancer* **23**, 391–407 (2023).
101. van Staveren, W. C. G. *et al.* Human cancer cell lines: Experimental models for cancer cells in situ? For cancer stem cells? *Biochim. Biophys. Acta - Rev. Cancer* **1795**, 92–103 (2009).
102. Liu, H. *et al.* Cancer stem cells from human breast tumors are involved in spontaneous metastases in orthotopic mouse models. *Proc. Natl. Acad. Sci. U. S. A.* **107**, 18115–18120 (2010).
103. Hermann, P. C. *et al.* Distinct Populations of Cancer Stem Cells Determine Tumor Growth and Metastatic Activity in Human Pancreatic Cancer. *Cell Stem Cell* **1**, 313–323 (2007).

104. Zhang, S. *et al.* CD133+CXCR4+ colon cancer cells exhibit metastatic potential and predict poor prognosis of patients. *BMC Med.* **10**, 1–14 (2012).
105. Kim, S. & Wysocka, J. Deciphering the multi-scale, quantitative cis-regulatory code. *Mol. Cell* **83**, 373–392 (2023).
106. Madsen, J. G. S. *et al.* Highly interconnected enhancer communities control lineage-determining genes in human mesenchymal stem cells. *Nat. Genet.* **52**, 1227–1238 (2020).
107. Koch, F. *et al.* Transcription initiation platforms and GTF recruitment at tissue-specific enhancers and promoters. *Nat. Struct. Mol. Biol.* **18**, 956–963 (2011).
108. Lin, C., Garruss, A. S., Luo, Z., Guo, F. & Shilatifard, A. The RNA Pol II elongation factor Ell3 marks enhancers in ES cells and primes future gene activation. *Cell* **152**, 144–156 (2013).
109. Sur, I. & Taipale, J. The role of enhancers in cancer. *Nat. Rev. Cancer* **16**, 483–493 (2016).
110. ar-Rushdi, A. *et al.* Differential Expression of the Translocated and the Untranslocated c-myc Oncogene in Burkitt Lymphoma. *Science (80-.).* **222**, 390–393 (1983).
111. Taub, R. *et al.* Activation and somatic mutation of the translocated c-myc gene in Burkitt lymphoma cells. *Cell* **36**, 339–348 (1984).
112. Bannister, A. J. & Kouzarides, T. Regulation of chromatin by histone modifications. *Cell Res.* **21**, 381–395 (2011).
113. Korolev, N., Vorontsova, O. V. & Nordenskiöld, L. Physicochemical analysis of electrostatic foundation for DNA-protein interactions in chromatin transformations. *Prog. Biophys. Mol. Biol.* **95**, 23–49 (2007).
114. Filippakopoulos, P. *et al.* Histone recognition and large-scale structural analysis of the human bromodomain family. *Cell* **149**, 214–231 (2012).
115. Bhagwat, A. S. *et al.* BET Bromodomain Inhibition Releases the Mediator Complex from Select cis-Regulatory Elements. *Cell Rep.* **15**, 519–530 (2016).
116. Zegerman, P., Canas, B., Pappin, D. & Kouzarides, T. Histone H3 lysine 4 methylation disrupts binding of nucleosome remodeling and deacetylase (NuRD) repressor complex. *J. Biol. Chem.* **277**, 11621–11624 (2002).
117. Cao, R. *et al.* Role of histone H3 lysine 27 methylation in polycomb-group silencing. *Science (80-.).* **298**, 1039–1043 (2002).
118. Torres-Perez, J. V., Irfan, J., Febrianto, M. R., Di Giovanni, S. & Nagy, I. Histone post-translational modifications as potential therapeutic targets for pain management. *Trends Pharmacol. Sci.* **42**, 897–911 (2021).

119. Jenuwein, T. & Allis, C. D. Translating the histone code. *Science (80-.)*. **293**, 1074–1080 (2001).
120. Strahl, B. D. & Allis, C. D. The language of covalent histone modifications. *Nature* **403**, 41–45 (2000).
121. Cano-Rodriguez, D. *et al.* Writing of H3K4Me3 overcomes epigenetic silencing in a sustained but context-dependent manner. *Nat. Commun.* **7**, (2016).
122. Santos-Rosa, H. *et al.* Active genes are tri-methylated at K4 of histone H3. *Nature* **419**, 407–411 (2002).
123. Lachner Monika, O'Carroll Do-nal, Rea Stephen, Mechtler Karl & Jenuwein Thomas. Methylation of histone H3 lysine 9 creates a binding site for HP1 proteins. *Nature* **410**, 116–120 (2001).
124. Bannister, A. J. *et al.* Selective recognition of methylated lysine 9 on histone H3 by the HP1 chromo domain. *Nature* **410**, 120–124 (2001).
125. Sankar, A. *et al.* Histone editing elucidates the functional roles of H3K27 methylation and acetylation in mammals. *Nat. Genet.* **54**, 754–760 (2022).
126. Pengelly, A. R., Copur, Ö., Jäckle, H., Herzig, A. & Müller, J. A Histone Mutant Reproduces the Phenotype Caused by Loss of Histone-Modifying Factor Polycomb. *Science (80-.)*. **339**, 698–699 (2013).
127. Kizer, K. O. *et al.* A Novel Domain in Set2 Mediates RNA Polymerase II Interaction and Couples Histone H3 K36 Methylation with Transcript Elongation. *Mol. Cell. Biol.* **25**, 3305–3316 (2005).
128. Gates, L. A. *et al.* Acetylation on histone H3 lysine 9 mediates a switch from transcription initiation to elongation. *J. Biol. Chem.* **292**, 14456–14472 (2017).
129. Creighton, M. P. *et al.* Histone H3K27ac separates active from poised enhancers and predicts developmental state. *Proc. Natl. Acad. Sci. U. S. A.* **107**, 21931–21936 (2010).
130. Hnisz, D. *et al.* Super-enhancers in the control of cell identity and disease. *Cell* **155**, 934–947 (2013).
131. Raisner, R. *et al.* Enhancer Activity Requires CBP/P300 Bromodomain-Dependent Histone H3K27 Acetylation. *Cell Rep.* **24**, 1722–1729 (2018).
132. Jin, Q. *et al.* Distinct roles of GCN5/PCAF-mediated H3K9ac and CBP/p300-mediated H3K18/27ac in nuclear receptor transactivation. *EMBO J.* **30**, 249–262 (2011).
133. Seto, E. & Yoshida, M. Erasers of histone acetylation: The histone deacetylase enzymes. *Cold Spring Harb. Perspect. Biol.* **6**, 1–26 (2014).

134. Kooistra, S. M. & Helin, K. Post-translational modifications: Molecular mechanisms and potential functions of histone demethylases. *Nat. Rev. Mol. Cell Biol.* **13**, 297–311 (2012).
135. Baylin, S. B. & Jones, P. A. Epigenetic determinants of cancer. *Cold Spring Harb. Perspect. Biol.* **8**, 1–35 (2016).
136. Shah, M. A., Denton, E. L., Arrowsmith, C. H., Lupien, M. & Schapira, M. A global assessment of cancer genomic alterations in epigenetic mechanisms. *Epigenetics and Chromatin* **7**, 1–15 (2014).
137. McCabe, M. T. *et al.* EZH2 inhibition as a therapeutic strategy for lymphoma with EZH2-activating mutations. *Nature* **492**, 108–112 (2012).
138. Zingg, D. *et al.* The epigenetic modifier EZH2 controls melanoma growth and metastasis through silencing of distinct tumour suppressors. *Nat. Commun.* **6**, 1–17 (2015).
139. Kleer, C. G. *et al.* EZH2 is a marker of aggressive breast cancer and promotes neoplastic transformation of breast epithelial cells. *Proc. Natl. Acad. Sci. U. S. A.* **100**, 11606–11611 (2003).
140. Varambally, S. *et al.* The polycomb group protein EZH2 is involved in progression of prostate cancer. *Nature* **419**, 624–629 (2002).
141. Kim, K. H. & Roberts, C. W. M. Targeting EZH2 in cancer. *Nat. Med.* **22**, 128–134 (2016).
142. Viré, E. *et al.* The Polycomb group protein EZH2 directly controls DNA methylation. *Nature* **439**, 871–874 (2006).
143. Straussman, R. *et al.* Developmental programming of CpG island methylation profiles in the human genome. *Nat. Struct. Mol. Biol.* **16**, 564–571 (2009).
144. Tian, J. *et al.* Targeting the unique methylation pattern of androgen receptor (AR) promoter in prostate stem/progenitor cells with 5-aza-2'-deoxycytidine (5-AZA) leads to suppressed prostate tumorigenesis. *J. Biol. Chem.* **287**, 39954–39966 (2012).
145. Tam, W. L. & Weinberg, R. A. The epigenetics of epithelial-mesenchymal plasticity in cancer. *Nat. Med.* **19**, 1438–1449 (2013).
146. Chatterjee, A., Rodger, E. J. & Eccles, M. R. Epigenetic drivers of tumourigenesis and cancer metastasis. *Semin. Cancer Biol.* **51**, 149–159 (2018).
147. Warburg, O. On the Origin of Cancer Cells. *Science (80-.)*. **123**, 309–314 (1956).
148. Hanahan, D. & Weinberg, R. A. Hallmarks of cancer: The next generation. *Cell*

- 144**, 646–674 (2011).
149. Martínez-Reyes, I. & Chandel, N. S. Cancer metabolism: looking forward. *Nat. Rev. Cancer* **21**, 669–680 (2021).
 150. Finley, L. W. S. What is cancer metabolism? *Cell* **186**, 1670–1688 (2023).
 151. Sounni, N. E. *et al.* Blocking lipid synthesis overcomes tumor regrowth and metastasis after antiangiogenic therapy withdrawal. *Cell Metab.* **20**, 280–294 (2014).
 152. Ying, H. *et al.* Oncogenic kras maintains pancreatic tumors through regulation of anabolic glucose metabolism. *Cell* **149**, 656–670 (2012).
 153. Krall, A. S., Xu, S., Graeber, T. G., Braas, D. & Christofk, H. R. Asparagine promotes cancer cell proliferation through use as an amino acid exchange factor. *Nat. Commun.* **7**, 1–13 (2016).
 154. Hayes, J. D., Dinkova-Kostova, A. T. & Tew, K. D. Oxidative Stress in Cancer. *Cancer Cell* **38**, 167–197 (2020).
 155. Mitsuishi, Y. *et al.* Nrf2 Redirects Glucose and Glutamine into Anabolic Pathways in Metabolic Reprogramming. *Cancer Cell* **22**, 66–79 (2012).
 156. Li, D. & Li, Y. The interaction between ferroptosis and lipid metabolism in cancer. *Signal Transduct. Target. Ther.* **5**, 1–10 (2020).
 157. Meng, T., Fukada, T. & Tonks, N. K. Reversible Oxidation and Inactivation of Protein Tyrosine Phosphatases In Vivo. *Mol. Cell* **9**, 387–399 (2002).
 158. Kwon, J. *et al.* Reversible oxidation and inactivation of the tumor suppressor PTEN in cells stimulated with peptide growth factors. *Proc. Natl. Acad. Sci. U. S. A.* **101**, 16419–16424 (2004).
 159. Bozza, P. T., Bakker-Abreu, I., Navarro-Xavier, R. A. & Bandeira-Melo, C. Lipid body function in eicosanoid synthesis: An update. *Prostaglandins Leukot. Essent. Fat. Acids* **85**, 205–213 (2011).
 160. Accioly, M. T. *et al.* Lipid bodies are reservoirs of cyclooxygenase-2 and sites of prostaglandin-E2 synthesis in colon cancer cells. *Cancer Res.* **68**, 1732–1740 (2008).
 161. Letouzé, E. *et al.* SDH Mutations Establish a Hypermethylator Phenotype in Paraganglioma. *Cancer Cell* **23**, 739–752 (2013).
 162. Sciacovelli, M. *et al.* Fumarate is an epigenetic modifier that elicits epithelial-to-mesenchymal transition. *Nature* **537**, 544–547 (2016).
 163. Xu, W. *et al.* Oncometabolite 2-hydroxyglutarate is a competitive inhibitor of α -ketoglutarate-dependent dioxygenases. *Cancer Cell* **19**, 17–30 (2011).

164. Hay, N. Reprogramming glucose metabolism in cancer: Can it be exploited for cancer therapy? *Nat. Rev. Cancer* **16**, 635–649 (2016).
165. Altman, B. J., Stine, Z. E. & Dang, C. V. From Krebs to clinic: Glutamine metabolism to cancer therapy. *Nat. Rev. Cancer* **16**, 619–634 (2016).
166. Carracedo, A., Cantley, L. C. & Pandolfi, P. P. Cancer metabolism: Fatty acid oxidation in the limelight. *Nat. Rev. Cancer* **13**, 227–232 (2013).
167. Liou, G.-Y. Y., Storz, P., Liou, M.-Y. & Storz, P. Reactive oxygen species in cancer. *Free Radic. Res.* **44**, 479–496 (2010).
168. Iurlaro, R., León-Annicchiarico, C. L. & Muñoz-Pinedo, C. Regulation of cancer metabolism by oncogenes and tumor suppressors. in *Methods in Enzymology* vol. 542 59–80 (2014).
169. Guo, J. Y. *et al.* Activated Ras requires autophagy to maintain oxidative metabolism and tumorigenesis. *Genes Dev.* **25**, 460–470 (2011).
170. Son, J. *et al.* Glutamine supports pancreatic cancer growth through a KRAS-regulated metabolic pathway. *Nature* **496**, 101–105 (2013).
171. Dupuy, F. *et al.* PDK1-dependent metabolic reprogramming dictates metastatic potential in breast cancer. *Cell Metab.* **22**, 577–589 (2015).
172. Hardie, D. G., Ross, F. A. & Hawley, S. A. AMPK: A nutrient and energy sensor that maintains energy homeostasis. *Nat. Rev. Mol. Cell Biol.* **13**, 251–262 (2012).
173. Cai, Z. *et al.* Phosphorylation of PDHA by AMPK Drives TCA Cycle to Promote Cancer Metastasis. *Mol. Cell* **80**, 263-278.e7 (2020).
174. Elia, I. *et al.* Breast cancer cells rely on environmental pyruvate to shape the metastatic niche. *Nature* **568**, 117–121 (2019).
175. Rossi, M. *et al.* PHGDH heterogeneity potentiates cancer cell dissemination and metastasis. *Nature* **605**, 747–753 (2022).
176. Christopher W Pugh & Peter J Ratcliffe. Regulation of angiogenesis by hypoxia: role of the HIF system. *Nat. Med.* **9**, 677–684 (2003).
177. Yang, M. H. *et al.* Direct regulation of TWIST by HIF-1 α promotes metastasis. *Nat. Cell Biol.* **10**, 295–305 (2008).
178. Zhang, W. *et al.* HIF-1 α promotes epithelial-mesenchymal transition and metastasis through direct regulation of ZEB1 in colorectal cancer. *PLoS One* **10**, 1–16 (2015).
179. Mathieu, J. *et al.* HIF induces human embryonic stem cell markers in cancer cells. *Cancer Res.* **71**, 4640–4652 (2011).

180. Hanna, S. C. *et al.* HIF1 α and HIF2 α independently activate SRC to promote melanoma metastases. *J. Clin. Invest.* **123**, 2078–2093 (2013).
181. Liao, D., Corle, C., Seagroves, T. N. & Johnson, R. S. Hypoxia-inducible factor-1 α is a key regulator of metastasis in a transgenic model of cancer initiation and progression. *Cancer Res.* **67**, 563–572 (2007).
182. Zhou, X., Guo, X., Chen, M., Xie, C. & Jiang, J. HIF-3 α promotes metastatic phenotypes in pancreatic cancer by transcriptional regulation of the RhoC-ROCK1 signaling pathway. *Mol. Cancer Res.* **16**, 124–134 (2018).
183. Kanarek, N. *et al.* Histidine catabolism is a major determinant of methotrexate sensitivity. *Nature* **559**, 632–636 (2018).
184. Dai, Z., Ramesh, V. & Locasale, J. W. The evolving metabolic landscape of chromatin biology and epigenetics. *Nat. Rev. Genet.* **21**, 737–753 (2020).
185. Reid, M. A., Dai, Z. & Locasale, J. W. The impact of cellular metabolism on chromatin dynamics and epigenetics. *Nat. Cell Biol.* **19**, 1298–1306 (2017).
186. Carey, B. W., Finley, L. W. S., Cross, J. R., Allis, C. D. & Thompson, C. B. Intracellular α -ketoglutarate maintains the pluripotency of embryonic stem cells. *Nature* **518**, 413–416 (2015).
187. Moussaieff, A. *et al.* Glycolysis-mediated changes in acetyl-CoA and histone acetylation control the early differentiation of embryonic stem cells. *Cell Metab.* **21**, 392–402 (2015).
188. Ulanovskaya, O. A., Zuhl, A. M. & Cravatt, B. F. NNMT promotes epigenetic remodeling in cancer by creating a metabolic methylation sink. *Nat. Chem. Biol.* **9**, 300–306 (2013).
189. Mentch, S. J. *et al.* Histone Methylation Dynamics and Gene Regulation Occur through the Sensing of One-Carbon Metabolism. *Cell Metab.* **22**, 861–873 (2015).
190. Arnold, M. *et al.* Current and future burden of breast cancer: Global statistics for 2020 and 2040. *Breast* **66**, 15–23 (2022).
191. Ewertz, M. *et al.* Effect of obesity on prognosis after early-stage breast cancer. *J. Clin. Oncol.* **29**, 25–31 (2011).
192. Holmes, M. D., Chen, W. Y., Feskanich, D., Kroenke, C. H. & Colditz, G. A. Physical Activity and Survival After Breast Cancer Diagnosis. *J. Am. Med. Assoc.* **293**, 2479–2486 (2005).
193. Pierce, J. P. *et al.* Lifetime cigarette smoking and breast cancer prognosis in the after breast cancer pooling project. *J. Natl. Cancer Inst.* **106**, 1–8 (2014).
194. Koboldt, D. C. *et al.* Comprehensive molecular portraits of human breast

- tumours. *Nature* **490**, 61–70 (2012).
195. Sørli, T. *et al.* Repeated observation of breast tumor subtypes in independent gene expression data sets. *Proc. Natl. Acad. Sci. U. S. A.* **100**, 8418–8423 (2003).
 196. De Ruijter, T. C., Veeck, J., De Hoon, J. P. J., Van Engeland, M. & Tjan-Heijnen, V. C. Characteristics of triple-negative breast cancer. *J. Cancer Res. Clin. Oncol.* **137**, 183–192 (2011).
 197. Gudjonsson, T., Adriance, M. C., Sternlicht, M. D., Petersen, O. W. & Bissell, M. J. Myoepithelial Cells: Their Origin and Function in Breast Morphogenesis and Neoplasia. *J. Mammary Gland Biol. Neoplasia* **10**, 261–272 (2005).
 198. Abe, O. *et al.* Relevance of breast cancer hormone receptors and other factors to the efficacy of adjuvant tamoxifen: Patient-level meta-analysis of randomised trials. *Lancet* **378**, 771–784 (2011).
 199. Slamon, D. J. *et al.* Use of Chemotherapy plus a Monoclonal Antibody against HER2 for Metastatic Breast Cancer That Overexpresses HER2. *N. Engl. J. Med.* **344**, 783–792 (2001).
 200. Bianchini, G., Balko, J. M., Mayer, I. A., Sanders, M. E. & Gianni, L. Triple-negative breast cancer: Challenges and opportunities of a heterogeneous disease. *Nat. Rev. Clin. Oncol.* **13**, 674–690 (2016).
 201. Ben-porath, I. *et al.* An embryonic stem cell-like gene expression signature in poorly differentiated aggressive human tumors. *Nat. Genet.* **40**, 499–507 (2008).
 202. Ma, F. *et al.* Enriched CD44+/CD24- population drives the aggressive phenotypes presented in triple-negative breast cancer (TNBC). *Cancer Lett.* **353**, 153–159 (2014).
 203. Honeth, G. *et al.* The CD44+/CD24-phenotype is enriched in basal-like breast tumors. *Breast Cancer Res.* **10**, 1–12 (2008).
 204. Dong, C. *et al.* Loss of FBP1 by snail-mediated repression provides metabolic advantages in basal-like breast cancer. *Cancer Cell* **23**, 316–331 (2013).
 205. Camarda, R. *et al.* Inhibition of fatty acid oxidation as a therapy for MYC-overexpressing triple-negative breast cancer. *Nat. Med.* **22**, 427–432 (2016).
 206. Wang, T. *et al.* JAK/STAT3-Regulated Fatty Acid β -Oxidation Is Critical for Breast Cancer Stem Cell Self-Renewal and Chemoresistance. *Cell Metab.* **27**, 136-150.e5 (2017).
 207. Andrzejewski, S. *et al.* PGC-1 α Promotes Breast Cancer Metastasis and Confers Bioenergetic Flexibility against Metabolic Drugs. *Cell Metab.* **26**, 778-787.e5 (2017).

208. Lee, K. min *et al.* MYC and MCL1 Cooperatively Promote Chemotherapy-Resistant Breast Cancer Stem Cells via Regulation of Mitochondrial Oxidative Phosphorylation. *Cell Metab.* **26**, 633-647.e7 (2017).
209. Nguyen, Q. H. *et al.* Profiling human breast epithelial cells using single cell RNA sequencing identifies cell diversity. *Nat. Commun.* **9**, 1–12 (2018).
210. Karaayvaz, M. *et al.* Unravelling subclonal heterogeneity and aggressive disease states in TNBC through single-cell RNA-seq. *Nat. Commun.* **9**, (2018).
211. Grosselin, K. *et al.* High-throughput single-cell ChIP-seq identifies heterogeneity of chromatin states in breast cancer. *Nat. Genet.* **51**, (2019).
212. Kondo, H. *et al.* Single-cell resolved imaging reveals intra-tumor heterogeneity in glycolysis, transitions between metabolic states, and their regulatory mechanisms. *Cell Rep.* **34**, 108750 (2021).
213. Bensaad, K. *et al.* TIGAR, a p53-Inducible Regulator of Glycolysis and Apoptosis. *Cell* **126**, 107–120 (2006).
214. Rathmell, J. C. *et al.* Akt-Directed Glucose Metabolism Can Prevent Bax Conformation Change and Promote Growth Factor-Independent Survival. *Mol. Cell. Biol.* **23**, 7315–7328 (2003).
215. Gao, X. *et al.* Dietary methionine influences therapy in mouse cancer models and alters human metabolism. *Nature* **572**, 397–401 (2019).
216. Gupta, G. P. & Massagué, J. Cancer Metastasis: Building a Framework. *Cell* **127**, 679–695 (2006).
217. Pesenti, C. *et al.* The genetic landscape of human glioblastoma and matched primary cancer stem cells reveals intratumour similarity and intertumour heterogeneity. *Stem Cells Int.* **2019**, 2617030 (2019).
218. Klevebring, D. *et al.* Sequencing of breast cancer stem cell populations indicates a dynamic conversion between differentiation states in vivo. *Breast Cancer Res.* **16**, 1–7 (2014).
219. Yasuda, T., Ishimoto, T. & Baba, H. Conflicting metabolic alterations in cancer stem cells and regulation by the stromal niche. *Regen. Ther.* **17**, 8–12 (2021).
220. Bergers, G. & Fendt, S.-M. The metabolism of cancer cells during metastasis. *Nat. Rev. Cancer* **21**, 162–180 (2021).
221. Mendelsohn, B. A. *et al.* A high-throughput screen of real-time ATP levels in individual cells reveals mechanisms of energy failure. *PLoS Biol.* **16**, e2004624 (2018).
222. Kim, R. J. *et al.* High aldehyde dehydrogenase activity enhances stem cell features in breast cancer cells by activating hypoxia-inducible factor-2 α .

- Cancer Lett.* **333**, 18–31 (2013).
223. Davis, R. T. *et al.* Transcriptional diversity and bioenergetic shift in human breast cancer metastasis revealed by single-cell RNA sequencing. *Nat. Cell Biol.* **22**, 310–320 (2020).
 224. Williamson, J. R. Glycolytic Control Mechanisms. *J. Biol. Chem.* **242**, 4476–4485 (1967).
 225. Izzo, L. *et al.* The carnitine shuttle links mitochondrial metabolism to histone acetylation and lipogenesis. *Sci. Adv.* **9**, eadf0115 (2023).
 226. Zhao, S. *et al.* ATP-Citrate Lyase Controls a Glucose-to-Acetate Metabolic Switch. *Cell Rep.* **17**, 1037–1052 (2016).
 227. Ghandi, M. *et al.* Next-generation characterization of the Cancer Cell Line Encyclopedia. *Nature* **569**, 503–508 (2019).
 228. Jin, X. *et al.* A metastasis map of human cancer cell lines. *Nature* **588**, 331–336 (2020).
 229. Diehn, M. *et al.* Association of reactive oxygen species levels and radioresistance in cancer stem cells. *Nature* **458**, 780–783 (2009).
 230. Tasdogan, A. *et al.* Metabolic heterogeneity confers differences in melanoma metastatic potential. *Nature* **577**, 115–120 (2020).
 231. Nagdas, S. *et al.* Drp1 Promotes KRas-Driven Metabolic Changes to Drive Pancreatic Tumor Growth. *Cell Rep.* **28**, 1845-1859.e5 (2019).
 232. Beziaud, L. *et al.* IFN γ -induced stem-like state of cancer cells as a driver of metastatic progression following immunotherapy. *Cell Stem Cell* **30**, 818-831.e6 (2023).
 233. Tan, A. S. *et al.* Mitochondrial genome acquisition restores respiratory function and tumorigenic potential of cancer cells without mitochondrial DNA. *Cell Metab.* **21**, 81–94 (2015).
 234. Dong, L. F. *et al.* Horizontal transfer of whole mitochondria restores tumorigenic potential in mitochondrial DNA-deficient cancer cells. *Elife* **6**, e22187 (2017).
 235. Wellen, K. E. *et al.* ATP-Citrate Lyase Links Cellular Metabolism to Histone Acetylation. *Science (80-.)*. **324**, 1076–1081 (2009).
 236. McDonnell, E. *et al.* Lipids Reprogram Metabolism to Become a Major Carbon Source for Histone Acetylation. *Cell Rep.* **17**, 1463–1472 (2016).
 237. Loo, S. Y. *et al.* Fatty acid oxidation is a druggable gateway regulating cellular plasticity for driving metastasis in breast cancer. *Sci. Adv.* **7**, (2021).

238. Barth, T. K. & Imhof, A. Fast signals and slow marks: the dynamics of histone modifications. *Trends Biochem. Sci.* **35**, 618–626 (2010).
239. Bailey, A. P. *et al.* Antioxidant Role for Lipid Droplets in a Stem Cell Niche of *Drosophila*. *Cell* **163**, 340–353 (2015).
240. Mahendralingam, M. J. *et al.* Mammary epithelial cells have lineage-rooted metabolic identities. *Nat. Metab.* **3**, 665–681 (2021).
241. Gao, X. *et al.* Acetate functions as an epigenetic metabolite to promote lipid synthesis under hypoxia. *Nat. Commun.* **7**, 1–14 (2016).
242. Bose, S., Ramesh, V. & Locasale, J. W. Acetate Metabolism in Physiology, Cancer, and Beyond. *Trends Cell Biol.* **29**, 695–703 (2019).
243. Nuutinen, H., Lindros, K., Hekali, P. & Salaspuro, M. Elevated blood acetate as indicator of fast ethanol elimination in chronic alcoholics. *Alcohol* **2**, 623–626 (1985).
244. Perry, R. J. *et al.* Acetate mediates a microbiome-brain- β -cell axis to promote metabolic syndrome. *Nature* **534**, 213–217 (2016).
245. Wang, S. *et al.* Ethanol promotes mammary tumor growth and angiogenesis: The involvement of chemoattractant factor MCP-1. *Breast Cancer Res. Treat.* **133**, 1037–1048 (2012).
246. Sundaram, S. & Yan, L. High-fat diet enhances mammary tumorigenesis and pulmonary metastasis and alters inflammatory and angiogenic profiles in MMTV-PyMT mice. *Anticancer Res.* **36**, 6279–6287 (2016).
247. Sivanand, S. *et al.* Nuclear Acetyl-CoA Production by ACLY Promotes Homologous Recombination. *Mol. Cell* **67**, 252-265.e6 (2017).
248. Masui, K. *et al.* Glucose-dependent acetylation of Rictor promotes targeted cancer therapy resistance. *Proc. Natl. Acad. Sci. U. S. A.* **112**, 9406–9411 (2015).
249. Liu, X. *et al.* Acetate Production from Glucose and Coupling to Mitochondrial Metabolism in Mammals. *Cell* **175**, 502-513.e13 (2018).
250. Massagué, J. & Ganesh, K. Metastasis-initiating cells and ecosystems. *Cancer Discov.* **11**, 971–994 (2021).
251. Cavalli, L. R., Varella-Garcia, M. & Liang, B. C. Diminished tumorigenic phenotype after depletion of mitochondrial DNA. *Cell Growth Differ.* **8**, 1189–1198 (1997).
252. Park, J. H. *et al.* Fatty Acid Oxidation-Driven Src Links Mitochondrial Energy Reprogramming and Oncogenic Properties in Triple-Negative Breast Cancer. *Cell Rep.* **14**, 2154–2165 (2016).

253. Wright, H. J. *et al.* CDCP1 drives triple-negative breast cancer metastasis through reduction of lipid-droplet abundance and stimulation of fatty acid oxidation. *Proc. Natl. Acad. Sci.* **114**, E6556–E6565 (2017).
254. Bartman, C. R. *et al.* Slow TCA flux and ATP production in primary solid tumours but not metastases. *Nature* **614**, 349–357 (2023).
255. Rios Garcia, M. *et al.* Acetyl-CoA Carboxylase 1-Dependent Protein Acetylation Controls Breast Cancer Metastasis and Recurrence. *Cell Metab.* **26**, 842-855.e5 (2017).
256. Altea-Manzano, P. *et al.* A palmitate-rich metastatic niche enables metastasis growth via p65 acetylation resulting in pro-metastatic NF- κ B signaling. *Nat. Cancer* **4**, 344–364 (2023).
257. Unni, A. M. *et al.* Hyperactivation of ERK by multiple mechanisms is toxic to RTK-RAS mutation-driven lung adenocarcinoma cells. *Elife* **7**, e33718 (2018).
258. Albuquerque, C. *et al.* The ‘just-right’ signaling model: APC somatic mutations are selected based on a specific level of activation of the β -catenin signaling cascade. *Hum. Mol. Genet.* **11**, 1549–1560 (2002).
259. Zhang, J. & Zhong, Q. Histone deacetylase inhibitors and cell death. *Cell. Mol. Life Sci.* **71**, 3885–3901 (2014).
260. Leslie, N. R. *et al.* Redox regulation of PI 3-kinase signalling via inactivation of PTEN. *EMBO J.* **22**, 5501–5510 (2003).
261. Schreck, R., Rieber, P. & Baeuerle, P. A. Reactive oxygen intermediates as apparently widely used messengers in the activation of the NF- κ B transcription factor and HIV-1. *EMBO J.* **10**, 2247–2258 (1991).
262. Liao, Z., Chua, D. & Tan, N. S. Reactive oxygen species: A volatile driver of field cancerization and metastasis. *Mol. Cancer* **18(1)**, 1–10 (2019).
263. Porporato, P. E. *et al.* A mitochondrial switch promotes tumor metastasis. *Cell Rep.* **8**, 754–766 (2014).
264. Weinberg, F. *et al.* Mitochondrial metabolism and ROS generation are essential for Kras-mediated tumorigenicity. *Proc. Natl. Acad. Sci. U. S. A.* **107**, 8788–8793 (2010).
265. Goh, J. *et al.* Mitochondrial targeted catalase suppresses invasive breast cancer in mice. *BMC Cancer* **11**, 1–12 (2011).
266. Arnold, P. K. *et al.* A non-canonical tricarboxylic acid cycle underlies cellular identity. *Nature* **603**, 477–481 (2022).
267. Luengo, A. *et al.* Increased demand for NAD⁺ relative to ATP drives aerobic glycolysis. *Mol. Cell* **81**, 691-707.e6 (2021).

268. Martínez-Reyes, I. *et al.* TCA Cycle and Mitochondrial Membrane Potential Are Necessary for Diverse Biological Functions. *Mol. Cell* **61**, 199–209 (2016).
269. Liesa, M. & Shirihai, O. S. Mitochondrial dynamics in the regulation of nutrient utilization and energy expenditure. *Cell Metab.* **17**, 491–506 (2013).
270. Parida, P. K. *et al.* Limiting mitochondrial plasticity by targeting DRP1 induces metabolic reprogramming and reduces breast cancer brain metastases. *Nat. Cancer* **4**, 893–907 (2023).
271. Civenni, G. *et al.* Epigenetic Control of Mitochondrial Fission Enables Self-Renewal of Stem-like Tumor Cells in Human Prostate Cancer. *Cell Metab.* **30**, 303-318.e6 (2019).
272. Tran, T. Q. *et al.* α -Ketoglutarate attenuates Wnt signaling and drives differentiation in colorectal cancer. *Nat. cancer* **1**, 345–358 (2020).
273. Stephens, F. B., Constantin-teodosiu, D. & Greenhaff, P. L. New insights concerning the role of carnitine in the regulation of fuel metabolism in skeletal muscle. *J. Physiol.* **581**, 431–444 (2007).
274. Madiraju, P., Pande, S. V., Prentki, M. & Madiraju, S. R. M. Mitochondrial acetylcarnitine provides acetyl groups for nuclear histone acetylation. *Epigenetics* **4**, 399–403 (2009).
275. Ortega, E. *et al.* Transcription factor dimerization activates the p300 acetyltransferase. *Nature* **562**, 538–544 (2018).
276. Hogg, S. J. *et al.* BET-Bromodomain Inhibitors Engage the Host Immune System and Regulate Expression of the Immune Checkpoint Ligand PD-L1. *Cell Rep.* **18**, 2162–2174 (2017).
277. Li, G. *et al.* Intersection of immune and oncometabolic pathways drives cancer hyperprogression during immunotherapy. *Cancer Cell* **41**, 304-322.e7 (2023).
278. Policarpi, C., Munafò, M., Tsagkris, S., Carlini, V. & Hackett, J. A. Systematic Epigenome Editing Captures the Context-dependent Instructive Function of Chromatin Modifications. *bioRxiv* 2022.09.04.506519 (2022)
doi:10.1101/2022.09.04.506519.
279. Tufegdžić Vidaković, A. *et al.* Context-Specific Effects of TGF- β /SMAD3 in Cancer Are Modulated by the Epigenome. *Cell Rep.* **13**, 2480–2490 (2015).
280. Marsolier, J. *et al.* H3K27me3 conditions chemotolerance in triple-negative breast cancer. *Nat. Genet.* **54**, 459–468 (2022).
281. McDonald, O. G. *et al.* Epigenomic reprogramming during pancreatic cancer progression links anabolic glucose metabolism to distant metastasis. *Nat. Genet.* **49**, 367–376 (2017).

282. Ye, C. & Tu, B. P. Sink into the Epigenome: Histones as Repositories That Influence Cellular Metabolism. *Trends Endocrinol. Metab.* **29**, 626–637 (2018).
283. McBrian, M. A. *et al.* Histone Acetylation Regulates Intracellular pH. *Mol. Cell* **49**, 310–321 (2013).
284. Li, X. *et al.* Nucleus-Translocated ACS2 Promotes Gene Transcription for Lysosomal Biogenesis and Autophagy. *Mol. Cell* **66**, 684–697.e9 (2017).
285. Zaugg, K. *et al.* Carnitine palmitoyltransferase 1C promotes cell survival and tumor growth under conditions of metabolic stress. *Genes Dev.* **25**, 1041–1051 (2011).
286. Hatzivassiliou, G. *et al.* ATP citrate lyase inhibition can suppress tumor cell growth. *Cancer Cell* **8**, 311–321 (2005).
287. Li, J. *et al.* Lipid Desaturation Is a Metabolic Marker and Therapeutic Target of Ovarian Cancer Stem Cells. *Cell Stem Cell* **20**, 303–314.e5 (2017).
288. Li, Y. *et al.* Fatty acid oxidation protects cancer cells from apoptosis by increasing mitochondrial membrane lipids. *Cell Rep.* **39**, 110870 (2022).
289. Zhao, W. *et al.* Candidate antimetastasis drugs suppress the metastatic capacity of breast cancer cells by reducing membrane fluidity. *Cancer Res.* **76**, 2037–2049 (2016).
290. Mullen, P. J., Yu, R., Longo, J., Archer, M. C. & Penn, L. Z. The interplay between cell signalling and the mevalonate pathway in cancer. *Nat. Rev. Cancer* **16**, 718–731 (2016).
291. Wang, D. & Dubois, R. N. Eicosanoids and cancer. *Nat. Rev. Cancer* **10**, 181–193 (2010).
292. Yao, C.-H. *et al.* Identifying off-target effects of etomoxir reveals that carnitine palmitoyltransferase I is essential for cancer cell proliferation independent of β -oxidation. *PLOS Biol.* **16**, e2003782 (2018).
293. Dhakal, B. *et al.* Perhexiline: Old Drug, New Tricks? A Summary of Its Anti-Cancer Effects. *Molecules* **28(8)**, 1–19 (2023).
294. Granchi, C. ATP citrate lyase (ACLY) inhibitors: An anti-cancer strategy at the crossroads of glucose and lipid metabolism. *Eur. J. Med. Chem.* **157**, 1276–1291 (2018).
295. Wei, J. *et al.* An allosteric mechanism for potent inhibition of human ATP-citrate lyase. *Nature* **568**, 566–570 (2019).
296. Yap, T. A. *et al.* Complex I inhibitor of oxidative phosphorylation in advanced solid tumors and acute myeloid leukemia: phase I trials. *Nat. Med.* **29**, 115–126 (2023).

297. Luft, D., Schmülling, R. M. & Eggstein, M. Lactic Acidosis in Biguanide-Treated Diabetics. *Diabetologia* **14**, 75–87 (1978).
298. Sheng, Z. H. & Cai, Q. Mitochondrial transport in neurons: Impact on synaptic homeostasis and neurodegeneration. *Nat. Rev. Neurosci.* **13**, 77–93 (2012).
299. Goodwin, P. J. *et al.* Effect of Metformin vs Placebo on Invasive Disease-Free Survival in Patients with Breast Cancer: The MA.32 Randomized Clinical Trial. *Jama* **327**, 1963–1973 (2022).
300. Dolgin, E. A drug to block fat intake and combat cancer spread. *Nature* (2021) doi:<https://doi.org/10.1038/d41586-021-01667-8>.
301. Perets, R. *et al.* Phase 1 first-in-human trial of MTB-9655, the first oral inhibitor of ACSS2, in patients with advanced solid tumors. *J. Clin. Oncol.* **40**, e20609–e20609 (2022).
302. Falchook, G. *et al.* First-in-human study of the safety, pharmacokinetics, and pharmacodynamics of first-in-class fatty acid synthase inhibitor TVB-2640 alone and with a taxane in advanced tumors. *EClinicalMedicine* **34**, 100797 (2021).
303. Alistar, A. *et al.* Safety and tolerability of the first-in-class agent CPI-613 in combination with modified FOLFIRINOX in patients with metastatic pancreatic cancer: a single-centre, open-label, dose-escalation, phase 1 trial. *Lancet Oncol.* **18**, 770–778 (2017).
304. Philip, P. A. *et al.* Phase 3, multicenter, randomized study of CPI-613 with modified FOLFIRINOX (mFFX) versus FOLFIRINOX (FFX) as first-line therapy for patients with metastatic adenocarcinoma of the pancreas (AVENGER500). *J. Clin. Oncol.* **40**, 4023–4023 (2022).
305. Lang, L. *et al.* Blockade of glutamine-dependent cell survival augments antitumor efficacy of CPI-613 in head and neck cancer. *J. Exp. Clin. Cancer Res.* **40**, 1–14 (2021).
306. Secretan, B. L. *et al.* Body Fatness and Cancer — Viewpoint of the IARC Working Group. *N. Engl. J. Med.* **375**, 794–798 (2016).
307. Goncalves, M. D. *et al.* High-fructose corn syrup enhances intestinal tumor growth in mice. *Science (80-.)*. **363**, 1345–1349 (2019).
308. Kim, J. *et al.* Ketohexokinase-A acts as a nuclear protein kinase that mediates fructose-induced metastasis in breast cancer. *Nat. Commun.* **11**, 1–20 (2020).
309. Bousquenaud, M., Fico, F., Solinas, G., Rüegg, C. & Santamaria-Martínez, A. Obesity promotes the expansion of metastasis-initiating cells in breast cancer. *Breast Cancer Res.* **20**, 1–11 (2018).
310. Taylor, S. R., Falcone, J. N., Cantley, L. C. & Goncalves, M. D. Developing

- dietary interventions as therapy for cancer. *Nat. Rev. Cancer* **22**, 452–466 (2022).
311. Pomatto-Watson, L. C. D. *et al.* Daily caloric restriction limits tumor growth more effectively than caloric cycling regardless of dietary composition. *Nat. Commun.* **12**, 1–17 (2021).
 312. Caffa, I. *et al.* Fasting-mimicking diet and hormone therapy induce breast cancer regression. *Nature* **583**, 620–624 (2020).
 313. Salvadori, G. *et al.* Fasting-mimicking diet blocks triple-negative breast cancer and cancer stem cell escape. *Cell Metab.* **33**, 2247-2259.e6 (2021).
 314. Lee, C. *et al.* Fasting cycles retard growth of tumors and sensitize a range of cancer cell types to chemotherapy. *Sci. Transl. Med.* **4**, 124ra27 (2012).
 315. Goodwin, P. J. *et al.* The LISA randomized trial of a weight loss intervention in postmenopausal breast cancer. *npj Breast Cancer* **6**, (2020).
 316. de Groot, S. *et al.* Fasting mimicking diet as an adjunct to neoadjuvant chemotherapy for breast cancer in the multicentre randomized phase 2 DIRECT trial. *Nat. Commun.* **11**, 1–9 (2020).
 317. Chlebowski, R. T. *et al.* Association of Low-Fat Dietary Pattern with Breast Cancer Overall Survival: A Secondary Analysis of the Women’s Health Initiative Randomized Clinical Trial. *JAMA Oncol.* **4**, e181212 (2018).
 318. Chlebowski, R. T. *et al.* Dietary fat reduction and breast cancer outcome: Interim efficacy results from the women’s intervention nutrition study. *J. Natl. Cancer Inst.* **98**, 1767–1776 (2006).
 319. Kalaany, N. Y. & Sabatini, D. M. Tumours with PI3K activation are resistant to dietary restriction. *Nature* **458**, 725–731 (2009).
 320. Soldati, L. *et al.* The influence of diet on anti-cancer immune responsiveness. *J. Transl. Med.* **16**, 1–18 (2018).
 321. Dahlin, J. L. *et al.* Assay interference and off-target liabilities of reported histone acetyltransferase inhibitors. *Nat. Commun.* **8**, 1–14 (2017).
 322. Hu, Z. *et al.* Histone deacetylase inhibitors promote breast cancer metastasis by elevating NEDD9 expression. *Signal Transduct. Target. Ther.* **8**, 1–13 (2023).
 323. Lin, K. T. *et al.* HDAC inhibitors augmented cell migration and metastasis through induction of PKCs leading to identification of low toxicity modalities for combination cancer therapy. *Clin. Cancer Res.* **18**, 4691–4701 (2012).
 324. Hu, X. ting *et al.* HDAC2 inhibits EMT-mediated cancer metastasis by downregulating the long noncoding RNA H19 in colorectal cancer. *J. Exp. Clin.*

- Cancer Res.* **39**, 1–14 (2020).
325. Luu, T. H. *et al.* A phase II trial of vorinostat (suberoylanilide hydroxamic acid) in metastatic breast cancer: A California cancer consortium study. *Clin. Cancer Res.* **14**, 7138–7142 (2008).
 326. Vansteenkiste, J. *et al.* Early phase II trial of oral vorinostat in relapsed or refractory breast, colorectal, or non-small cell lung cancer. *Invest. New Drugs* **26**, 483–488 (2008).
 327. Suraweera, A., O’Byrne, K. J. & Richard, D. J. Combination therapy with histone deacetylase inhibitors (HDACi) for the treatment of cancer: Achieving the full therapeutic potential of HDACi. *Front. Oncol.* **8**, 1–15 (2018).
 328. Jiang, Z. *et al.* Tucidinostat plus exemestane for postmenopausal patients with advanced, hormone receptor-positive breast cancer (ACE): a randomised, double-blind, placebo-controlled, phase 3 trial. *Lancet Oncol.* **20**, 806–815 (2019).
 329. Andrikopoulou, A., Liontos, M., Koutsoukos, K., Dimopoulos, M. A. & Zagouri, F. The emerging role of BET inhibitors in breast cancer. *Breast* **53**, 152–163 (2020).
 330. Yang, L. *et al.* Repression of BET activity sensitizes homologous recombination-proficient cancers to PARP inhibition. *Sci. Transl. Med.* **9**, eaal1645 (2017).
 331. Shi, J. *et al.* Disrupting the Interaction of BRD4 with Diacetylated Twist Suppresses Tumorigenesis in Basal-like Breast Cancer. *Cancer Cell* **25**, 210–225 (2014).
 332. Shorstova, T., Foulkes, W. D. & Witcher, M. Achieving clinical success with BET inhibitors as anti-cancer agents. *Br. J. Cancer* **124**, 1478–1490 (2021).
 333. Anderson, R. L. *et al.* A framework for the development of effective anti-metastatic agents. *Nat. Rev. Clin. Oncol.* **16**, 185–204 (2019).
 334. Fizazi, K. *et al.* Denosumab versus zoledronic acid for treatment of bone metastases in men with castration-resistant prostate cancer: A randomised, double-blind study. *Lancet* **377**, 813–822 (2011).
 335. Furlow, B. US FDA advisory panel rejects early denosumab therapy. *Lancet Oncol.* **13**, e94 (2012).
 336. Davie, S. A. *et al.* Effects of FVB/NJ and C57Bl/6J strain backgrounds on mammary tumor phenotype in inducible nitric oxide synthase deficient mice. *Transgenic Res.* **16**, 193–201 (2007).
 337. Overwijk, W. W. *et al.* Tumor regression and autoimmunity after reversal of a functionally tolerant state of self-reactive CD8⁺ T cells. *J. Exp. Med.* **198**, 569–

- 580 (2003).
338. Lahl, K. *et al.* Selective depletion of Foxp3⁺ regulatory T cells induces a scurfy-like disease. *J. Exp. Med.* **204**, 57–63 (2007).
 339. Qiu, B. & Simon, M. BODIPY 493/503 Staining of Neutral Lipid Droplets for Microscopy and Quantification by Flow Cytometry. *Bio-Protocol* **6**, 1–6 (2016).
 340. Dubikovskaya, E., Chudnovskiy, R., Karateev, G., Park, H. M. & Stahl, A. Measurement of long-chain fatty acid uptake into adipocytes. *Methods Enzymol.* **538**, 107–134 (2014).
 341. Kuroda, Y. *et al.* Isolation, culture and evaluation of multilineage-differentiating stress-enduring (Muse) cells. *Nat. Protoc.* **8**, 1391–1415 (2013).
 342. Gallart-Ayala, H. *et al.* A global HILIC-MS approach to measure polar human cerebrospinal fluid metabolome: Exploring gender-associated variation in a cohort of elderly cognitively healthy subjects. *Anal. Chim. Acta* **1037**, 327–337 (2018).
 343. Medina, J. *et al.* Single-step extraction coupled with targeted hilic-ms/ms approach for comprehensive analysis of human plasma lipidome and polar metabolome. *Metabolites* **10**, 1–17 (2020).
 344. Dobin, A. *et al.* STAR: Ultrafast universal RNA-seq aligner. *Bioinformatics* **29**, 15–21 (2013).
 345. Liberzon, A. *et al.* The Molecular Signatures Database Hallmark Gene Set Collection. *Cell Syst.* **1**, 417–425 (2015).
 346. Liberzon, A. *et al.* Molecular signatures database (MSigDB) 3.0. *Bioinformatics* **27**, 1739–1740 (2011).
 347. Subramanian, A. *et al.* Gene set enrichment analysis: A knowledge-based approach for interpreting genome-wide expression profiles. *Proc. Natl. Acad. Sci. U. S. A.* **102**, 15545–15550 (2005).
 348. Mootha, V. K. *et al.* PGC-1 α -responsive genes involved in oxidative phosphorylation are coordinately downregulated in human diabetes. *Nat. Genet.* **34**, 267–273 (2003).
 349. Wang, X. & Seed, B. A PCR primer bank for quantitative gene expression analysis. *Nucleic Acids Res.* **31**, 1–8 (2003).
 350. Spandidos, A., Wang, X., Wang, H. & Seed, B. PrimerBank: A resource of human and mouse PCR primer pairs for gene expression detection and quantification. *Nucleic Acids Res.* **38**, 792–799 (2009).
 351. Spandidos, A. *et al.* A comprehensive collection of experimentally validated primers for Polymerase Chain Reaction quantitation of murine transcript

- abundance. *BMC Genomics* **9**, 1–17 (2008).
352. Ewels, P. A. *et al.* The nf-core framework for community-curated bioinformatics pipelines publish. *Nat. Biotechnol.* **38**, 276–278 (2020).
 353. Lopez-Delisle, L. *et al.* pyGenomeTracks: reproducible plots for multivariate genomic datasets. *Bioinformatics* **37**, 422–423 (2021).
 354. Weigert, M., Schmidt, U., Haase, R., Sugawara, K. & Myers, G. Star-convex polyhedra for 3D object detection and segmentation in microscopy. *Proc. - 2020 IEEE Winter Conf. Appl. Comput. Vision, WACV 2020* 3655–3662 (2020) doi:10.1109/WACV45572.2020.9093435.
 355. Schmidt, U., Weigert, M., Broaddus, C. & Myers, G. Cell Detection with Star-Convex Polygons. in *Medical Image Computing and Computer Assisted Intervention -- MICCAI 2018* (eds. Frangi, A. F., Schnabel, J. A., Davatzikos, C., Alberola-López, C. & Fichtinger, G.) 265–273 (Springer International Publishing, 2018).
 356. Virtanen, P. *et al.* SciPy 1.0: fundamental algorithms for scientific computing in Python. *Nat. Methods* **17**, 261–272 (2020).
 357. VanderPlas, J. *et al.* Altair: Interactive Statistical Visualizations for Python. *J. Open Source Softw.* **3**, 1057 (2018).
 358. Györfy, B. *et al.* An online survival analysis tool to rapidly assess the effect of 22,277 genes on breast cancer prognosis using microarray data of 1,809 patients. *Breast Cancer Res. Treat.* **123**, 725–731 (2010).

CURRICULUM VITAE

MEGAN YOUNG

PHD MOLECULAR LIFE SCIENCES, ONCOLOGY

Quartier de la Levratte 22, 1260 Nyon. +41 (0) 78 648 0350. cm816young@gmail.com

EDUCATION

PHD, SWISS FEDERAL INSTITUTE OF TECHNOLOGY (ÉPFL)
MOLECULAR LIFE SCIENCES *Lausanne, Switzerland*

Cancer Biology Swiss Institute for Experimental Cancer Research (ISREC)
Jun 2017 - Now Swiss Cancer Center Lèman

BACHELOR OF SCIENCE, SIMON FRASER UNIVERSITY
BIOLOGY *Burnaby, Canada*

Cells, Molecules, and Physiology Graduated Honours with Distinction, Co-Operative Education
Sep 2010 – Apr 2016 Overall GPA: 85%, Upper-Level GPA: 95%

SPECIALIZATION PROGRAM, BAMFIELD MARINE SCIENCES CENTRE
MARINE BIOLOGY *Bamfield, Canada*

Marine Ecology and Physiology On-site and hands-on intensive specialization in marine biology
Sep 2013 – Dec 2013

ACADEMIC RESEARCH EXPERIENCE

HÜLSKEN LAB SWISS FEDERAL INSTITUTE OF TECHNOLOGY (ÉPFL)
PhD Student *Lausanne, Switzerland*

Metabolism of Metastasis Project: Deciphering the metabolic dependencies and their
Jun 2017 - Now mechanism-of-action in metastasis-initiating cells in breast cancer

TUVESON LAB COLD SPRING HARBOR LABORATORY
Research Technician II *Cold Spring Harbor, USA*

Precision Medicine in Project: Establishment, maintenance, banking, and characterization
Pancreas Cancer of patient- derived organoids (PDOs) for high-throughput therapeutics
Jun 2016 – May 2017 screens.

- BAMJI LAB UNIVERSITY OF BRITISH COLUMBIA**
Honours Project Vancouver, Canada
 Neurobiology Project: Characterization of autism spectrum disorder-associated
 Jan 2016 – Apr 2016 genetic variants in hippocampal neurons
- MEDIA R&D STEMCELL TECHNOLOGIES**
Co-op Student / Intern Vancouver, Canada
 Organoid-Specific Media Project: Development and optimization of media for establishment
 May 2015 – Dec 2015 and long-term culture of intestinal PDOs
- BREDEN LAB SIMON FRASER UNIVERSITY**
Research Technician I Burnaby, Canada
 Evolution and Project: The population genetics and evolution of long-wave sensitive
 Population Genetics opsin genes in Central and South American guppies
 May 2013 – Apr 2015
- RINTOUL LAB SIMON FRASER UNIVERSITY**
Directed Studies Burnaby, Canada
 Rare Optic Neuropathies Project: Live-imaging of mitochondrial motility with confocal
 Jan 2015 – Apr 2015 microscopy
- MOORE LAB SIMON FRASER UNIVERSITY**
Directed Studies Burnaby, Canada
 Microbiology Project: Elucidating the role of siderophore secretion in the virulence
 Sep 2014 – Dec 2014 of a pathogenic fungi
- MARINE BIOLOGY BAMFIELD MARINE SCIENCES CENTRE**
FALL PROGRAM Bamfield, Canada
Directed Studies Project: Determining the effect of increased nitrogen levels and
 Marine Sciences temperature on the physiology of an invasive tunicate
 Sep 2013 – Dec 2013

**During this period, won scholarships and financial awards totalling to a value of 27,000 CAD

TECHNICAL SKILLS

TISSUE CULTURE	<ul style="list-style-type: none">• Primary human and mouse organoid culture	<ul style="list-style-type: none">• Monolayer Cell Culture• Lentivirus production
IN VIVO & PATHOLOGY	<ul style="list-style-type: none">• Tumor initiation assays (orthotopic, subcutaneous)• Metastasis assays (tail, spleen)• Systemic drug administration (intraperitoneal, oral gavage)	<ul style="list-style-type: none">• <i>In vivo</i> bioluminescence• Necropsies• Tissue harvesting• Sectioning (frozen, paraffin)• Immunostaining
MOLECULAR BIOLOGY	<ul style="list-style-type: none">• DNA, RNA, protein isolation• Expression profiling• Chromatin immunoprecipitation	<ul style="list-style-type: none">• Cloning• PCR (and variations)• Gel electrophoresis
BIOLOGICAL ASSAYS	<ul style="list-style-type: none">• Metabolic flux experiments• High-throughput drug screening	<ul style="list-style-type: none">• ELISAs• Flow cytometry• Fluorescence Microscopy
SOFTWARE	<ul style="list-style-type: none">• Python (Numpy, Pandas, Matplotlib, SciPy, Scanpy, etc.)• R (Tidyverse, DESeq2)• Cluster computing	<ul style="list-style-type: none">• Microsoft Office (Word, Powerpoint, Excel)• Adobe Creative Suite (Illustrator, Photoshop, InDesign)
SOFT SKILLS	<ul style="list-style-type: none">• Project management• Critical thinking & strategy• Organizational skills• Data science & research	<ul style="list-style-type: none">• Leadership• Mentoring & teaching• Communications• Teamwork & coordination

SCIENCE COMMUNICATION EXPERIENCE

Teaching Assistant **SCHOOL OF LIFE SCIENCES (ÉPFL)**

Jun 2017 – Now **Lausanne, Switzerland**

Assisted and taught the following courses: Introduction to Biology, Cellular and Molecular Biology, and Practical Laboratory Skills for Life Sciences

Elementary & High **TUTOR DOCTOR**

School Tutor **North Vancouver, Canada**

May 2015 – Apr 2016

- Guided students through their math & science curricula and mentored students' time management and organizational skills using the academic game plan

Outreach & Tours **TRIUMF**

Assistant **Vancouver, Canada**

Jan 2012 – Aug 2012

- Conducted educational tours of a particle and nuclear physics lab to the general public and generated web content to promote events aimed at improving the accessibility of science research to the public

CERTIFICATIONS

Federation of European Laboratory
Animal Science Associations **INTRODUCTORY COURSE IN LABORATORY ANIMAL
SCIENCES**

- Theory & Practical (Module I)

National Institutes of Health **PROTECTING HUMAN RESEARCH PARTICIPANTS
COURSE**

Canadian Council on Animal Care **ANIMAL USER TRAINING COURSE**

Professional Association of
Diving Instructors **OPEN WATER DIVING
DRYSUIT SPECIALTY**

Vehicle License **DRIVER'S LICENSE
PLEASURE CRAFT OPERATOR CARD**

PRESENTATIONS & POSTERS

- **Young CM**, Huelsken J (2021) Metastasizing breast cancer cells rely on acetyl-coa for colonization of the lung. **EMBO | EMBL Symposium: Metabolism Meets Epigenetics**
- **Young CM**, Santamaria-Martínez A, Huelsken J (2021) Metastasizing breast cancer cells rely on acetyl-coa for colonization of the lung. **ISREC-SCCL Symposium: Hallmarks of Cancer - 21 Years On**
- **Young CM**, Santamaria-Martínez A, Huelsken J (2018) Metabolism of breast cancer cells and opportunities for therapy. **Faculty and Staff Retreat of the Swiss Cancer Centre Léman**

PEER-REVIEWED PUBLICATIONS

- **Young CM**, Beziud L, Dessen P, Madurga-Alonso A, Santamaria-Martínez A, Huelsken J (in review) Metabolic dependencies of metastasis-initiating cells in breast cancer.
- Beziud L, **Young CM**, Norkin M, Madurga-Alonso A, Huelsken J (2023) Immunotherapy-induced plasticity of cancer cells as a driver of progression. **Cell Stem Cell**, **30:6**, 818-831.e6
- Tiriác H, Belleau P, Engle DD, Plenker D, Deschenes A, Somerville T, Froeling FEM, Burkhart RA, Denroche RE, Jang GH, Miyabayashi K, **Young CM**, ..., Tuveson DA (2018) Organoid profiling identifies common responders to chemotherapy in pancreatic cancer. **Cancer Discovery**, **8:9**, 1112–1129.
- Roe JS, Hwang CI, Somerville TDD, Milazzo JP, Lee EJ, Da Silva B, Maiorino L, Tiriác H, **Young CM**, Miyabayashi K, Filippini D, Creighton B, Burkhart RA, Buscaglia JM, Kim EJ, Grem JL, Lazenby AJ, Grunkemeyer JA, Hollingsworth MA, Grandgenett PM, Egeblad M, Park Y, Tuveson DA, Vakoc CR (2017) Enhancer Reprogramming Promotes Pancreatic Cancer Metastasis. **Cell**, **170:5**, 875–888.e20.
- Buscaglia JM, Bucobo JC, Tiriác H, Tzimas D, Grewal S, LaComb J, RoweHL L, Nagula S, Wu M, Kim J, Sasson A, Li E, **Young CM**, Tuveson DA (2017) 111 Successful Creation of Pancreatic Cancer Organoids By Means of Eus-Guided Fine- Needle Biopsy (EUS-FNB) for Personalized Cancer Treatment. **Gastrointestinal Endoscopy**, **85:5**.
- Sandkam B, **Young CM**, Breden FMW, Bourne GR, Breden F (2015) Color vision varies more among populations than among species of live-bearing fish from South America. **BMC Evolutionary Biology**, **15:225**.
- Sandkam B, **Young CM**, Breden F (2015) Beauty in the eyes of the beholders: colour vision is tuned to mate preference in the Trinidadian guppy (*Poecilia reticulata*). **Molecular Ecology**, **24**, 596-609.